

Functional surfaces through biomimetic block copolymer membranes

Inauguraldissertation

zur

Erlangung der Würde eines Doktors der Philosophie
vorgelegt der
Philosophisch-Naturwissenschaftlichen Fakultät
der Universität Basel



von

Smahan Toughraï
aus Frankreich

Basel, 2015

Original document stored on the publication server of the University of Basel edoc.unibas.ch

This work is licenced under the agreement „Attribution Non-Commercial No Derivatives – 3.0 Switzerland“ (CC BY-NC-ND 3.0 CH). The complete text may be reviewed here: creativecommons.org/licenses/by-nc-nd/3.0/ch/deed.en

Genehmigt von der Philosophisch-Naturwissenschaftlichen Fakultät
auf Antrag von

Prof. Dr. Wolfgang Meier

Prof. Dr. Nico Bruns

Prof. Dr. Marcus Textor

Basel, den 9. Dezember 2014

Prof. Dr. Jörg Schibler

Dekan



Namensnennung-Keine kommerzielle Nutzung-Keine Bearbeitung 3.0 Schweiz
(CC BY-NC-ND 3.0 CH)

Sie dürfen: Teilen — den Inhalt kopieren, verbreiten und zugänglich machen

Unter den folgenden Bedingungen:



Namensnennung — Sie müssen den Namen des Autors/Rechteinhabers in der von ihm festgelegten Weise nennen.



Keine kommerzielle Nutzung — Sie dürfen diesen Inhalt nicht für kommerzielle Zwecke nutzen.



Keine Bearbeitung erlaubt — Sie dürfen diesen Inhalt nicht bearbeiten, abwandeln oder in anderer Weise verändern.

Wobei gilt:

- **Verzichtserklärung** — Jede der vorgenannten Bedingungen kann **aufgehoben** werden, sofern Sie die ausdrückliche Einwilligung des Rechteinhabers dazu erhalten.
- **Public Domain (gemeinfreie oder nicht-schützbarer Inhalte)** — Soweit das Werk, der Inhalt oder irgendein Teil davon zur Public Domain der jeweiligen Rechtsordnung gehört, wird dieser Status von der Lizenz in keiner Weise berührt.
- **Sonstige Rechte** — Die Lizenz hat keinerlei Einfluss auf die folgenden Rechte:
 - Die Rechte, die jedermann wegen der Schranken des Urheberrechts oder aufgrund gesetzlicher Erlaubnisse zustehen (in einigen Ländern als grundsätzliche Doktrin des **fair use** bekannt);
 - Die **Persönlichkeitsrechte** des Urhebers;
 - Rechte anderer Personen, entweder am Lizenzgegenstand selber oder bezüglich seiner Verwendung, zum Beispiel für **Werbung** oder Privatsphärenschutz.
- **Hinweis** — Bei jeder Nutzung oder Verbreitung müssen Sie anderen alle Lizenzbedingungen mitteilen, die für diesen Inhalt gelten. Am einfachsten ist es, an entsprechender Stelle einen Link auf diese Seite einzubinden.

Quelle: <http://creativecommons.org/licenses/by-nc-nd/3.0/ch/> Datum: 13.01.2015

“Science is the poetry of reality”

Richard Dawkins

Table of contents

Acknowledgements	13
Abbreviations and symbols	15
Abstract	17
1. Introduction	19
1.1. General aspects of cell membranes	19
1.2. Amphiphilic block copolymers	21
1.2.1. Self-assembly behaviors of amphiphilic block copolymers	21
1.2.2. Atom transfer radical polymerization (ATRP).....	27
1.3. Solid-supported block copolymer membranes	32
1.4. References	35
2. Scope of the thesis	45
2.1. Aim and motivation	45
2.2. Strategies and approaches	45
2.3. References	48
3. Self-organization behavior of methacrylate-based reduction-sensitive amphiphilic triblock copolymers in solution	49
3.1. Introduction	49
3.2. Results and discussion	51
3.2.1. Formation of micelles	51
3.2.2. Formation of nanoparticles	62
3.3. Conclusions and outlook	69
3.4. References	70
4. Solid-supported amphiphilic block copolymer membranes using Langmuir techniques	73
4.1. Introduction	73
4.2. Results and discussion	75
4.2.1. Monolayers at the air-water interface	75
4.2.2. Langmuir transfer techniques.....	76
4.2.3. Characterization of the block copolymer membranes on the surface.....	78
4.2.4. Interaction of channel proteins with the polymeric bilayer	82
4.3. Conclusions and outlook	88
4.4. References	89
5. Functionalization of gold surfaces with amphiphilic block copolymer brushes using surface-initiated ATRP	93

5.1. Introduction	93
5.2. Results and discussion.....	95
5.2.1. Synthesis strategy of the triblock copolymers.....	95
5.2.2. Initiator self-assembled monolayer on gold surfaces	96
5.2.3. Characterization of the polymer brushes	100
5.2.4. Influence of the grafting density on the block copolymer brushes	106
5.2.5. Influence of channel proteins on the block copolymer brushes	109
5.3. Conclusions and outlook	116
5.4. References	117
6. General conclusions and outlook	121
7. Experimental Part	123
7.1. Materials.....	123
7.2. Self-organization behavior of methacrylate-based redox-sensitive amphiphilic triblock copolymers in solution	123
7.2.1. Synthesis and characterization of block copolymers.....	123
7.2.2. Preparation of self-assembled structures	126
7.2.3. Reduction of the disulfide bond	127
7.2.4. Thiol quantification using ThioGlo-5.....	127
7.2.5. Fluorescence kinetics.....	127
7.2.6. Encapsulation efficiency.....	128
7.2.7. Fluorescence correlation spectroscopy (FCS).....	128
7.3. Solid-supported amphiphilic block copolymer membranes using Langmuir techniques	128
7.3.1. Gold substrates preparation.....	128
7.3.2. Bilayer preparation using Langmuir-Blodgett/Langmuir-Schaefer transfers	129
7.3.3. Measurement methods of the bilayer.....	129
7.3.4. Bilayer incubation with channel proteins analyzed by in-situ ATR-FTIR.....	131
7.3.5. Incubation of bilayers with channel protein using Biobeads	131
7.3.6. Electrical measurements with channel proteins	131
7.4. Functionalization of gold surfaces with amphiphilic block copolymer brushes using surface-initiated ATRP	132
7.4.1. Preparation of initiator functionalized substrates.....	132
7.4.2. Growth of polymer brushes from immobilized initiator SAMs.....	132
7.4.3. Measurement methods of initiator SAMs and the polymer brushes	133
7.4.4. Influence of the channel proteins on block copolymer brushes	136
7.5. References	137
8. Curriculum Vitae and list of publications	139

Acknowledgements

First of all, I would like to thank *Prof. Dr. Wolfgang Meier* for having given me the opportunity to do my thesis in his group. Also, I am deeply grateful for his trust to let me conduct such an interesting and multidisciplinary project.

A big thank you goes to my PhD supervisor *Prof. Dr. Nico Bruns* for his daily support during my thesis, his useful advice, his patience to answer all my questions, and for the time involved in the thesis corrections.

I would also like to thank my co-referee *Prof. Dr. Marcus Textor* for this time and his interest in my thesis subject.

I would like to warmly thank *Prof. Dr. Cornelia Palivan* for accepting to take over the presidency of the exam and also for her friendship and precious advice regarding both scientific and personal discussions.

Financial support by the *Swiss National Science Foundation*, in particular the National Research Program *NRP 62* is gratefully acknowledged.

I would like to gratefully thank all the former and current “*Meier group*” members for the warm welcoming, the nice working atmosphere, their helpfulness and availability regarding technical matters and scientific discussion, and for all the social events organized, especially the Science Slam Basel.

My special thanks go now to *Dr. Violeta Malinova*, *Dr. Raffaello Masciadri*, *Dr. Ekaterina Rakhmatullina* and *Dr. Serena Belegri* for all their advice that helped me to start this thesis well. Particularly *Violeta* for the Skype evenings spent together and for giving me confidence in my work during doubts moments; and *Raffaello* for the lunch times spent talking about science and beyond. Also, thanks to *Dr. Gesine Gunkel-Grabole*, *Justyna Kowal* and *Dr. Xiaoyan Zhang* for all the scientific and technical discussions related to surface chemistry.

Thanks to all the following people for their introduction of all the characterization techniques I learned during my thesis: *Prof. Dr. Nico Bruns* (polymer synthesis, glovebox, GPC), *PD Dr. Daniel Häussinger* (NMR), *Dr. Kasper Renggli* and *Dr. Daniela Vasquez* (light scattering), *Dr. Pascal Tanner* (fluorimetry), *Dr. Xiaoyan Zhang* (Langmuir transfer techniques, channel protein insertion methods, EIS), *Alina Darjan* (Langmuir-Blodgett), *Dr. Wangyang Fu* (EIS), *Dr. Agnieszka Jagoda* (BAM), *Dr. Serena Belegri* (ellipsometry), *Dr. Thomas Schuster* (AFM).

Many thanks to *Gabriele Persy* for her help in TEM and GPC measurements, for the pleasant moments spent together as an office neighbour, and during all the university events. Also, thanks to *Dr. Pascal Tanner* for his time and efforts spent in FCS measurements and discussion of the results. For protein insertion experiments, I would like to thank *Patric Baumann* and *Fabian Itel* for having provided me the channel proteins. In addition, I would like to acknowledge *Dr. Mohamed Chami* for having performed cryo-TEM experiments and *Nicolas Touchard* for his help and assistance in the preparation of graphics.

This thesis would not be successfully accomplished without the contribution of all those scientific collaborators:

- Department of Physics, University of Basel: thanks to *Dr. Hans-Peter Lang* for his help with the preparation of gold substrates; *Dr. Laurent Marot* for XPS measurements; and to *Prof. Dr. Christian Schönenberger* for the access to the impedance spectroscopy set-up in his laboratory.
- Department of Microsystems Engineering IMTEK Freiburg: thanks a lot to *Dr. Katrin Moosman* and *Dr. C.K. Pandiyarajan* for their help and nice time spent with the SPR measurements.
- Department of Physical Chemistry, University of Geneva: a big thank you goes to *Prof. Dr. Thomas Bürgi* for his time and patience with the PM-IRRAS measurements and interpretation of the data, and for the access to in-situ ATR-FTIR equipment. Thanks to *Harekrishna Ghosh* for having conducted all the in-situ ATR-FTIR measurements.
- Paul Scherrer Institute: many thanks to *Dr. Thomas Geue* and *Dr. Panos Korelis* for their availability performing neutron reflectivity experiments at PSI, and for the nice atmosphere that made my stay at PSI very comfortable.

My special thanks go to all the students I supervised during this thesis: *Fabienne Thommen* and *Alexandra Wiesler*, *Riina Häkkinen*, *Jan Burri*, *Jean-Laurent Perin*, *Thomas Nijs*. They all did a great job and I really appreciate their help.

Many thanks to *Danni Tischhauser* and *Maya Greuter* for their time, help and reliability in all administrative issues; *Grischa Martin* und *Philipp Knöpfel* for their friendship and technical help in the institute.

Special thanks to *Philippe Gaillard* for having joined this thesis journey at the later stages of my PhD. You were revealed to be such a wonderful support, nice fellow and my best friend ever.

Last but not least, I would like to thank my family, in particular my parents *Ahmed and Badia Toughrai* and my young sister *Soukaiina* for their unconditional support during my whole career path.

Abbreviations and symbols

ABA1	PHEMA ₂₅ - <i>b</i> -(PBMA ₂₅ -S-S-PBMA ₂₅)- <i>b</i> -PHEMA ₂₅
ABA2	PHEMA ₁₃ - <i>b</i> -(PBMA ₂₀ -S-S-PBMA ₂₀)- <i>b</i> -PHEMA ₁₃
AFM	Atomic Force Microscopy
α -HL	Alpha-hemolysin
AqpZ	Aquaporin Z
ATR-FTIR	Attenuated Total Reflectance Fourier Transform Infrared Spectroscopy
ATRP	Atom Transfer Radical Polymerization
Au	Gold
B1	Br-PBMA ₂₅ -S-S-PBMA ₂₅ -Br
B2	Br-PBMA ₂₀ -S-S-PBMA ₂₀ -Br
BAM	Brewster Angle Microscopy
BMA	n-Butyl methacrylate
BodiPy	Boron-Dipyrromethene (4,4-difluoro-3a,4a-diaza- <i>s</i> -indacene)
CMC	Critical Micellar Concentration
Da	Dalton
DEE	Diethyl Ether
DLS	Dynamic Light Scattering
DMF	Dimethylformamide
ϵ	Dielectric Permittivity
EIS	Electrochemical Impedance Spectroscopy
FCS	Fluorescence Correlation Spectroscopy
Ge	Germanium
GPC	Gel Permeation Chromatography
HEMA	2-Hydroxyethyl methacrylate
LB	Langmuir-Blodgett (transfer)
LS	Langmuir-Schaefer (transfer)
MCT	Mercury Cadmium Telluride
M_n	Number Average Molecular Weight
M_w	Weight Average Molecular Weight
ν	Frequency (nu)

NMR	Nuclear Magnetic Resonance
Octyl-POE	n-Octyl-oligo-oxyethylene
OmpF	Outer Membrane Protein F
PBMA	Poly (butyl methacrylate)
PBS	Phosphate Buffered Saline
PDI	Polydispersity Index
PHEMA	Poly (2-hydroxyethyl methacrylate)
PMDETA	N,N,N',N'',N'''- Pentamethyldiethylenetriamine
PM-IRRAS	Polarization Modulation Infrared Reflection Absorption Spectroscopy
PTFE	Polytetrafluoroethylene
R _g	Radius of Gyration
R _h	Hydrodynamic Radius
RI	Refractive Index
SAM	Self-Assembled Monolayer
Si	Silicon (wafers)
SiO ₂	Silicon dioxide
SLS	Static Light Scattering
SPR	Surface Plasmon Resonance
TCEP	Tris (2-carboxyethyl) phosphine
TEM	Transmission Electron Microscopy
T _g	Glass Transition Temperature
THF	Tetrahydrofuran
ThioGlo-5	Methyl 9-maleimido-8-methoxy-2-oxo-2H-naphtho[2,3-b]pyran-3 carboxylate
TR	Transfer ratio
TSG	Template Stripped Gold
XPS	X-Ray Photoelectron Spectroscopy

Abstract

Fundamental scientific research was always interested by the concept of mimicking Nature because of the presence of remarkable designs. In particular, due to their importance in numerous cellular processes, biological membranes got great interest in biochemical and biophysical research. It is crucial to understand the membrane morphology, the role of individual membrane components, and also to correlate the membrane structure to its various functions. In addition to contributing to fundamental understanding, membranes are also highly attractive for industrial research and technological development. However, the complexity and fragility of natural membranes often limit their direct use. For that reason, the development of membrane models is indispensable. Suitable building blocks for model systems could be lipids or amphiphilic polymers.

The versatility of polymer chemistry allows the fine-tuning of biomimetic membranes in solution and on solid supports. Methacrylate-based amphiphilic triblock copolymers poly (2-hydroxyethyl methacrylate)-*b*-poly (butyl methacrylate)-*b*-poly (2-hydroxyethyl methacrylate) PHEMA-*b*-PBMA-*b*-PHEMA were designed in solution and on gold surfaces. By varying the hydrophilic to hydrophobic ratio as well as the chain length, the polymers self-assembled into nanoparticles and micelles in solution. The micelles were used to encapsulate and release hydrophobic model payloads, showing their potential use as intracellular drug delivery systems. Also, artificial planar membranes as mimics of natural membranes were synthesized directly from gold surfaces. Upon the variations in thickness and packing density, potential incorporation of membrane proteins was shown at a determined grafting density. Upon insertion of those proteins, this system may find its application as biosensing devices.

In solution, the nanostructures were characterized by using a wide range of methodologies including static and dynamic light scattering, transmission electron microscopy, ThioGlo detection, UV-vis spectroscopy, fluorescence spectroscopy and fluorescence correlation microscopy. On solid supports, atomic force microscopy and surface plasmon resonance along with neutron reflectivity were used to gain insights into morphology, homogeneity, grafting density and thickness of the layers. To demonstrate the planar membranes' biomimetic potential, they were incubated with different channel proteins: Outer Membrane Protein F, Aquaporin Z and alpha-hemolysin. Occurring interactions were detected by in-situ ATR-FTIR and electrochemical impedance spectroscopy. In summary, this thesis might impact fundamental membrane science as well as prospective biotechnological applications.

1. Introduction

1.1. General aspects of cell membranes

Biological membranes are essential for all living organisms, as they play a central role for the structure and function of cells. Their complex self-assembled structure and composition is a prerequisite for the multiple functions of these membranes. Biological membranes act as a barrier that protects the inner space of a cell from their external environment. For instance, in the human body, we encounter about 100 km² of membranes, barely 5 nm thick, forming the boundary of the cells and cell organelles, such as mitochondria, Golgi-apparatus, endoplasmic reticulum, or lysosomes.^[1] Apart from compartmentalizing and protecting cells and cell organelles from their environment, they are involved in a multitude of biochemical processes. Membrane-related functions comprise passive and active transport of ions between the intra- and extracellular space in order to maintain electrochemical gradients across the membrane. To fulfil all these functions, highly selective membrane permeability is required. Nature solved this by creating a composite material formed by a lipid matrix in which highly specialized and optimized proteins achieve the respective functions. These proteins have different functions, such molecular transport across the membrane (transporter), anchoring point of cytoskeletal or extracellular elements (linker), selective receptivity and signal transduction (receptor) or are involved in enzymatic reactions (enzyme). Cell membranes are also involved in many different specialized processes like cell recognition and adhesion or immune reactions. Furthermore, membranes are involved in dynamic processes such as cellular differentiation or cell migration.^[2] The structure of a cell membrane can be described by the “fluid mosaic model” proposed by Singer and Nicolson in 1972,^[3] depicted in *Figure 1-1*.

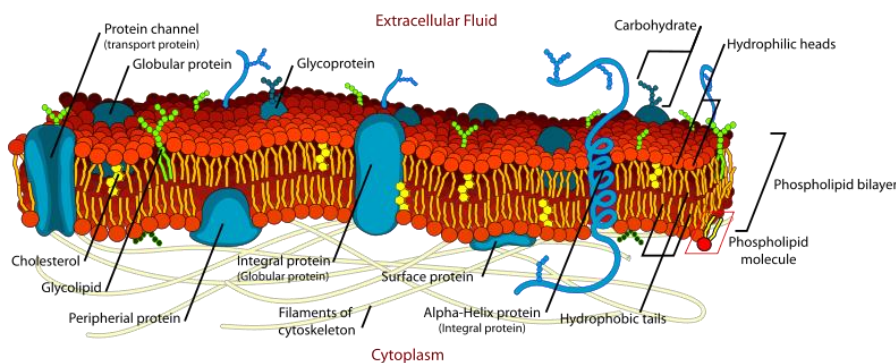


Figure 1-1: A fluid mosaic model of the cell membrane.^[4]

According to this model, the central structural element is the lipid bilayer. It is arranged in such a way, that the fatty acid chains face towards each other and form the hydrophobic membrane core, whereas the hydrophilic parts are exposed to the intra- and extracellular space, respectively.

This arrangement is driven by the lipid geometry and the hydrophobic effect.^[5-7] The two individual leaflets of the lipid bilayer are held together by (non-covalent) hydrophobic interactions. Steroids, *e.g.* cholesterol, are embedded in the lipid matrix, mainly to stabilize the structure. Membrane proteins can be embedded in the bilayer as integral proteins, or/and associated to one side of the bilayer as peripheral proteins.

Thus, the cell membrane can be formally considered as a two-dimensional solution of proteins in a viscous lipid bilayer solvent.^[3] The exact composition of biological membranes varies depending on the type and function of the cell or a membrane region.^[8]

Since the cell membrane with its vital functions is the most important interface in living organisms, modern research focuses on the investigation of its structure, properties, and functions. Membranes are valuable for addressing biophysical and biochemical questions such as studies of individual membrane-related processes, investigations of membrane components at a single-molecule level, or ligand-receptor binding. In pharmaceuticals, they are very important as therapeutic targets, since antibiotics or virus receptors interact with membranes. Furthermore, integral proteins are one of the key targets for drugs. However, due to their high hydrophobicity, investigations have to be performed in their natural environment, *i.e.* in a lipid membrane.^[1] The thorough investigation of integral proteins in lipid membranes is a fundamental step in drug design and development.^[9] Besides basic research, membranes are also highly attractive for industrial research. Membranes might be technologically interesting, *e.g.* for water purifications and desalination applications.^[10, 11] Moreover, they could act as platform for sensor devices, with potential applications in trace analysis or in biosensing.^[10, 12]

However, natural membranes as highly specialized and complex multi-component assemblies are not always suitable to investigate and understand distinct membranes functions. Furthermore, their complexity and their lack of long-term stability are disadvantageous for many technological and industrial processes. Therefore, the development of simplified biomimetic model membranes is necessary. In order to break down the complexity of natural membranes, model systems usually consist of only a few membrane components, mainly mimicking a characteristic feature of the membrane, *e.g.* the central bilayer structure.

Following Nature, commonly phospholipids are implemented as building blocks to create membrane mimics. Even though some reports on advanced lipid-based systems were already published,^[13-15] they still suffer from some drawbacks. Lipids are prone to oxidation, and chemical modification of lipids with functional groups is limited. Moreover, lipid membranes may not possess sufficient stability, mechanically and against air,^[16] which, depending on the conditions, limits their use for technological applications.

These drawbacks can be overcome by employing alternative building blocks, *i.e.* amphiphilic block copolymers. These polymers are already well-known in the field of materials science, surface coatings or tissue engineering.^[17-20] Recently, amphiphilic block copolymers also attracted considerable interest as

constituents for model membranes,^[21-24] and proved to be a suitable platform to study specific (membrane) proteins and protein-related processes in a non-natural environment.^[25-29] With an appropriate molar mass and hydrophilic to hydrophobic block ratio, amphiphilic block copolymers can adopt the bilayer structure in water.^[30, 31] Since the molecular weight of polymers can be considerably higher compared to lipids, the resulting membranes thickness can be also larger than the ones of lipid membranes, thus making polymer membranes mechanically more stable.^[32] Polymer synthesis allows for the adjustment of such parameters as block length, molecular weight, chemical composition, hydrophilic/hydrophobic balance, and molecular architecture. Hence, a broad range of possibilities are accessible to tailor customized block copolymer membranes.^[23, 33]

1.2. Amphiphilic block copolymers

1.2.1. Self-assembly behaviors of amphiphilic block copolymers

Block copolymers are macromolecules consisting of two or more polymer segments linked by covalent bonds or through an intermediate non-repeating unit known as a junction block.^[34] Block copolymers can be classified based on the arrangement and order of the homopolymer subunits which are normally marked as A, B, C etc. *Figure 1-2* depicts some examples of block copolymer architectures.

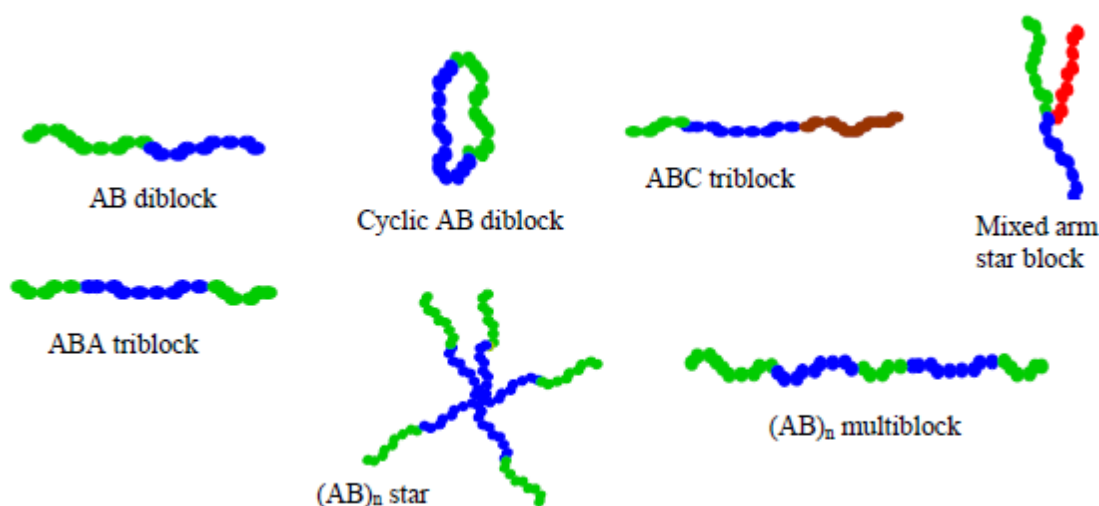


Figure 1-2: Different possible block copolymer architectures.^[35]

To be used in self-assembly, synthetic block copolymers must be constituted of two polymer segments having both long-range repulsive and short-range attractive forces.^[19] Such structures are called amphipathic, or amphiphilic (in the case of water) and resemble more conventional molecules such as surfactants or lipids. The basic principle of self-assembly is based on the poor solubility of one of the

blocks in a given solvent, while the second block has good solvent-solute interactions. In the case of water as solvent, although attractive forces between hydrophobic chains are weak, they will pack to segregate out of the aqueous environment, this both due to weak interactions with the water molecules, and to the large energy barrier that cause the disturbance of the water lattice surrounding them.^[7] In contrast, the hydrophilic chains are more soluble in water, due to strong solvent-solute interactions. Intuitively, one can deduce from this basic principle the most simple self-assembled structure induced by such forces, the micelle. In those self-assembled structures, the hydrophobic chains aggregate into a core to avoid contact with solvent molecules, while the hydrophilic chains interacting with solvent molecules form a corona at the surface. It should be noted that this example is only valid in the diluted state, where the critical micellar concentration (CMC) is extremely low for amphiphilic block copolymers when compared to low molecular weight surfactants. In this thesis, the behavior of the synthesized block copolymers was only studied in the diluted regime, where structures like micelles can be found.

In the next paragraph, a short theoretical background on the formation of self-assembled structures in aqueous solution and on solid supports generated by synthetic amphiphilic block copolymers will be given.

1.2.1.1. Self-assembly in solution

Amphiphilic (*amphi*: of both kinds; *philic*: having an affinity for) block copolymers consist of at least two polymer subunits, one of them with hydrophilic properties while the other has a hydrophobic character. Similar to low molecular weight amphiphiles (lipids, surfactants), amphiphilic block copolymers can self-assemble in block-selective solvents into a variety of structures such as micelles, vesicles, tubes, lyotropic liquid-crystal phases.^[36] *Figure 1-3* shows some examples of copolymer self-assemblies. The type of morphologies can be controlled by varying the copolymer composition, the initial copolymer concentration in the solution, the nature of the common solvent, the amount of water present in the medium, the temperature, the presence of additives such as ions, homopolymers, or surfactants and the polydispersity of the copolymer chains.^[37] The copolymer composition is mostly defined by the molecular weight and size of the homopolymer blocks which, in turn, determine the degree of block stretching.^[38] The latter is an important parameter and its value depends on the type of self-assemblies.^[39] The influence of the morphology on the concentration can be clearly seen in the phase diagram of particular copolymer systems. Shen and Eisenberg investigated the formation of PS-*co*-PAA vesicles as a function of the polymer concentration.^[40, 41] Generally, increasing the copolymer concentration or the amount of water content implies changes in aggregate morphology.^[41]

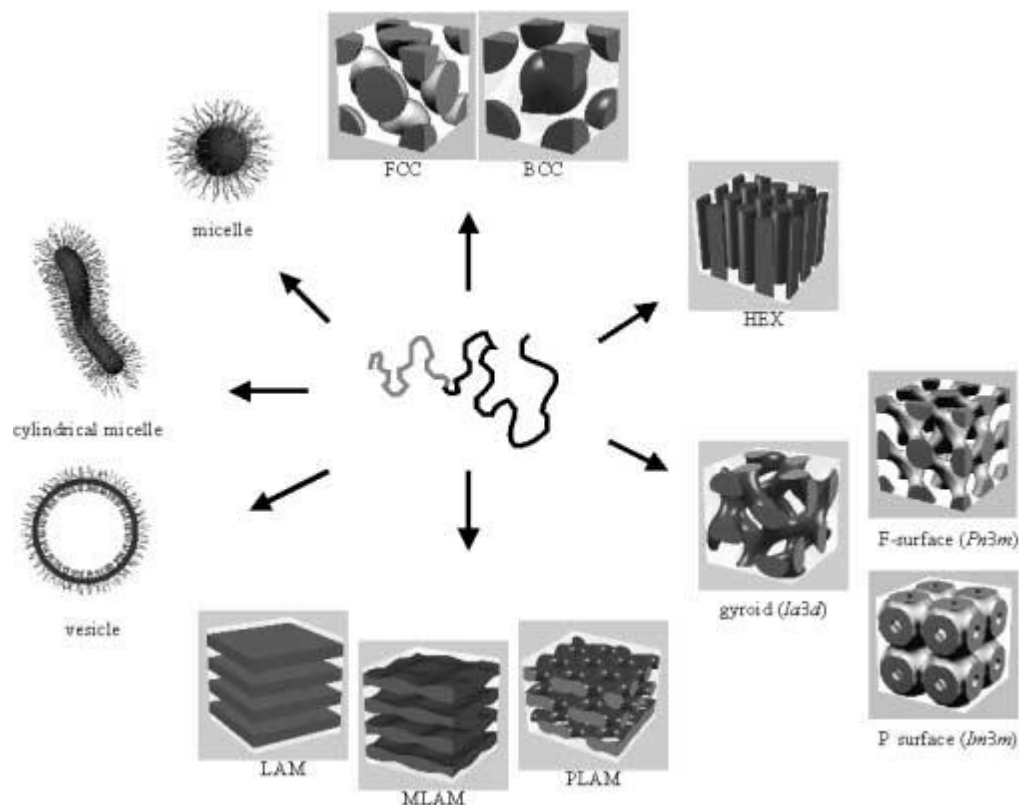


Figure 1-3: Examples of amphiphilic polymer self-assemblies^[19]

The choice of common solvent has also an effect on the morphologies of the resulting self-assemblies.^[42] The control of the morphology of block copolymer aggregates can be achieved not only with single but also with mixed solvents.^[43] The addition of water serves to modify the polymer-solvent interactions and to induce self-assembly and morphological changes.^[44-46] The same can be accomplished in a single solvent through variation of the applied temperature. Temperature that implied changes of the block copolymer self-assembly were reported for thermoresponsive polymer systems.^[47-51] The experimental aspects of the influence of ionic strength^[43], pH^[49, 52], added salt^[52-57] and homopolymers^[50, 58] were mainly investigated with polyelectrolyte-based amphiphilic block copolymer systems. The effect of the chain polydispersity on the aggregate morphology was reported by Terreau and coauthors with series of PS-*co*-PAA copolymers.^[59] They showed that the size of vesicles decreased as the PAA polydispersity index increased.

Generally, the self-assembling behavior of amphiphilic block copolymers can be affected by a variety of different factors. However, there are theories which provide guidelines for rationalizing the observed morphologies and might be used to predict the type of self-assembled structures.^[60, 61] From another point of view, the influence of the macromolecular composition or common solvent on the polymer self-assembly can be exploited to tailor the type and properties of the aggregates. One advantage of polymer self-assembly in comparison to lipids and surfactants is the possibility for macromolecular amphiphilic structures to be fine-tuned by introducing different functional groups in order to obtain self-assemblies with defined properties for specific applications.^[62] Other advantages include the possibility of

introducing additional mechanisms for colloidal stabilization, the control over the polymer critical micellar concentration (CMC),^[18] lower permeability and improved stability of the amphiphilic polymer membranes^[23, 63] which might be used for technological applications.

There is an ongoing debate as to know whether the aggregates formed upon self-assembly are kinetically frozen or equilibrium structures (thermodynamic).^[19] As of today, due to the incredible diversity in block copolymers, there is no universal theory able to predict which morphology will be adopted preferentially. However, several key parameters are well-known to influence the self-assembly and will be briefly reviewed here. Self-assembly of amphiphilic block copolymers has been described in two aspects. First, in terms of geometric constraints, that is directly related to the macromolecular features of the polymer chains. Also, thermodynamic considerations, such as minimization of the total free energy of the system, involve the decrease of interfacial tension at hydrophilic/hydrophobic interface and the entropy loss from polymer chains.^[64]

From a geometry perspective, the morphology is best described using the packing parameter p (*Equation 1*).^[65]

$$p = \frac{v}{al} \quad \text{Equation 1}$$

This parameter encompasses the volume of the hydrophobic block (v), the area covered by hydrophilic groups (a), and the length of the hydrophobic block (l). p can also be related to the radius of curvature through *Equation 2*:

$$p = 1 - Hl + \frac{Kl^2}{3} = 1 - \frac{1}{2} \left(\frac{1}{R1} + \frac{1}{R2} \right) + \frac{l^2}{3R1R2} \quad \text{Equation 2}$$

where K is the Gaussian curvature and H is the mean curvature, $R1$ and $R2$ are curvature radii.^[64] As can be deduced from Equation 2, p approaches unity for very large curvature radii, which is characteristic of vesicular shapes. Such a high curvature is the result of the preferential chain packing upon bilayer formation, driven by volume and steric constraints. As an example, this phenomenon was illustrated by Discher *et al.* for poly (ethylene oxide)-*b*-poly

(butadiene) (PEO-PBD) aggregates.^[66] In their work, they also define a convenient quantity, the hydrophilic to hydrophobic ratio f to characterize this phenomenon (*Equation 3*):

$$f = \frac{Mn \text{ (hydrophilic)}}{Mn \text{ (hydrophobic)}} \quad \text{Equation 3}$$

As a general rule, copolymers with ratios above 0.5 tend to form preferentially micelles, when copolymers with ratios less than 0.33 tend to form vesicles (see *Figure 1-4*). Although this ratio gives a good approximation, it may not be applicable to all systems.

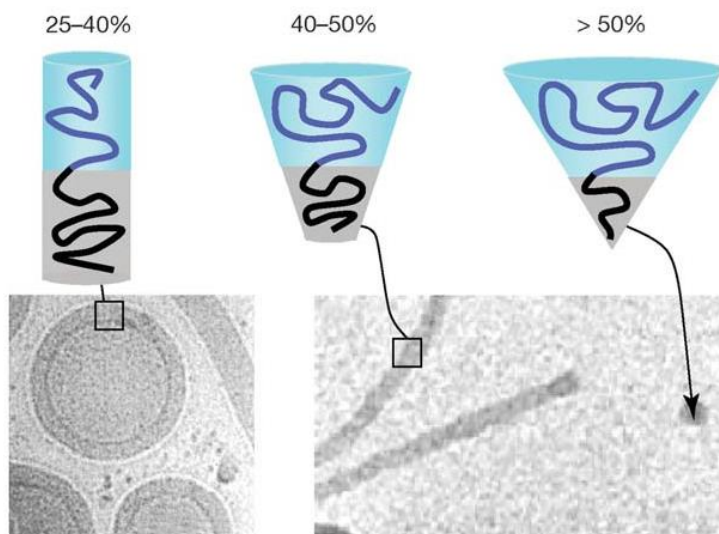


Figure 1-4: Schematics of block copolymer fractions with respective cryogenic transmission electron microscopy images showing vesicles or worm micelles and spherical micelles associated with different f ratios.^[66]

For all material scientists, the macromolecular architecture of amphiphilic block copolymers as well as their assembly at different length scales, time scales and levels of interaction make the use of these compounds very attractive. The most interesting examples of their potential applications are delivery of various substances,^[67] medical diagnostics,^[68] and reconstitution of biological molecules.^[26, 69, 70] Among different polymer self-assemblies, micelles and vesicles were mostly used in biotechnology so far. For instance, they serve as carriers of hydrophobic molecules (in the hydrophobic shell) as well as hydrophilic compounds (in the aqueous interior).^[71] The use of polymer micelles as drug delivery systems was pioneered by the group of Ringsdorf in 1984.^[72] Nowadays polymeric micelles are extensively studied as a promising nanoscopic drug carrier because of their attractive features to fulfill the requirements for selective drug delivery.^[39, 73-76] Most notably, the hydrophobic micellar core has a large capacity to accommodate hydrophobic drugs. Recently, polymeric micelles were also investigated as an oral drug delivery system,^[77, 78] but originally they were considered to be most suitable for intravenous administration.^[71] Extensive variety of drugs such as doxorubicin,^[79, 80] paclitaxel,^[81, 82] cisplatin,^[83, 84] indomethacin^[85, 86] and others were incorporated into polymer micelles and tested for drug delivery application. The drug loading and release by polymer micelles, the approaches to further improve the effectiveness of such polymer delivery systems are well described elsewhere.^[71, 87, 88] Also, polymer vesicular self-assemblies were used as drug carriers.^[89] More complex systems were achieved by insertion of natural proteins into vesicular membranes.^[90, 91]

1.2.1.2. Self-assembly of polymer brushes

The term “polymer brush” refers to an assembly of polymer chains chemically attached to a surface with one or a few anchor points. Tethering is high enough so that the macromolecular chains become crowded and are stretched away from the surface.^[92] The main parameters governing the conformation of the polymer brushes in solution are the quality of the solvent, the chain stiffness and the degree of polymerization. Moreover, the conformational behavior of the polymer chains will be a function of the grafting density (the distance between two anchoring points) and on the radius of gyration (the average size of the chains). Two cases are distinguished depending on the grafting density σ :^[92, 93]

- If the grafting density is larger than the radius of gyration ($\sigma > R_g$), each chain will be isolated from the surrounding chains. According to the strength of interactions between polymer segments and the surface, two cases must be distinguished. If the interaction between chains and surface is weak, a “mushroom” conformation is coined. On the other hand, if the chains are strongly adsorbed onto the surface, a “pancake” conformation is obtained. Conformation of the tethered polymer chains and those that are free in solution, are similar.
- If the grafting density is short ($\sigma < R_g$), the chains segments are close to each other, and try to minimize the segment-segment interactions by stretching away from the surface. This is the “brush” conformation. Conformation of tethered chains is significantly different to the one in solution.^[94]

The first description of such a brush system has been attempted by Alexander^[95] and de Gennes^[96] for monodisperse chains consisting of N segments, which are attached to non-adsorbing surface with an average distance of the anchor points d much smaller than the radius of gyration of the same unperturbed chains not in contact with the surface (*Figure 1-5*).^[97]

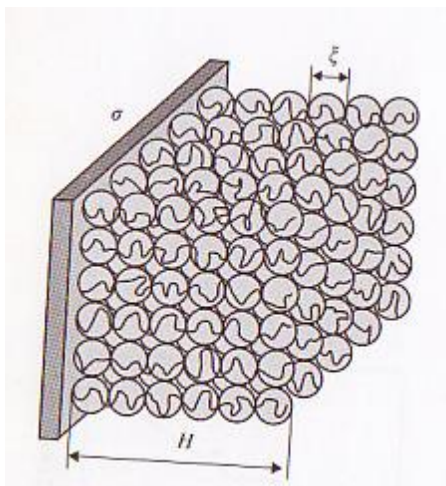


Figure 1-5: Schematic description of the Alexander-de Gennes model of polymer brushes.^[97]

Using Flory theory, a universal law establishes the radius gyration dependence on the number of monomer N :

$$R_g \sim N^\nu b$$

Where b is the radius of the monomer and ν reflects the quality of solvent.

The value of ν for good, theta and bad solvent of the tethered polymer chains is respectively 3/5, 1/2 and 1/3.

Previous theoretical treatments of polymer brushes have employed scaling arguments where each polymer was considered as a sequence of “blobs”.^[98] Using the concept of Alexander-de Gennes model, the size of a blob ξ is defined as:

$$\xi \sim 1/\sqrt{\sigma}$$

The number of monomers g in a blob is determined by:

$$g \sim \left(\frac{\xi}{b}\right)^{1/\nu} \sim \sigma^{1/(2\nu)} b^{1/\nu}$$

The number of correlation blobs per chain is N/g

$$N/g \sim N \sigma^{1/(2\nu)} b^{1/\nu}$$

The height of the brush is the size of a correlation blob times the number of these blobs per chain:

$$H \sim \xi N/g \sim N \sigma^{1/(2\nu)} b^{1/\nu}$$

The height H increases linearly with the number of monomers N per chain at constant grafting density.

1.2.2. Atom transfer radical polymerization (ATRP)

Current approaches for the synthesis of amphiphilic block copolymers usually require “living” polymerization techniques, such as anionic,^[99] cationic,^[100] or group transfer polymerization.^[101] Living polymerization approaches have the advantage of yielding polymers with narrow molecular weight distributions with predetermined degrees of polymerization that depend only on the molar ratio of monomer to initiator concentration and the conversion. However, when one of the components cannot be polymerized according to a living mechanism, macromonomer synthesis,^[102, 103] or capping with special end-groups for restarting, chain transfer or termination^[104, 105] are also possible. For most synthetic procedures, high purity of reactants, tedious isolation protocols or/and use of protecting group chemistry is required. However, for controlled living polymerization in general, these tight procedures are not necessary.

All synthetic approaches were discussed and reviewed in details by Hadjichristidis *et al.*,^[106] Taton *et al.*^[107] and in Förster *et al.*^[18] as well. However, in the next paragraphs, we will focus on the ATRP

technique, since this approach was used in this research work for the preparation of the amphiphilic block copolymers in solution and on surfaces.

1.2.2.1. Introduction to ATRP

In 1995, Matyjaszewski and Wang^[108, 109] independently from Sawamoto *et al.*^[110] developed this polymerization approach from redox catalyzed telomerization reactions^[111, 112] and atom transfer radical addition (ATRA).^[113] Atom transfer radical polymerization (ATRP) is one of the most successful methods to polymerize styrenes, methacrylates, acrylates and a variety of other monomers in a controlled fashion, yielding polymers with predetermined molecular weights and narrow polydispersities.^[114] This technique allows preserving of the polymer functionalities and modeling of the polymer chain architecture, thus resulting in multifunctional polymers of different compositions and architectures such as block copolymers, multiarmed stars or hyperbranched polymers.^[114]

1.2.2.2. Components of ATRP

ATRP is in many ways a complex reaction, which includes one or more (co)monomers, a transition metal complex in two or more oxidation states,^[115] which can be composed of various counter ions and ligands, an initiator with one or more radically transferable atoms or groups and can additionally include an optional solvent, suspending media and various additives. All of the components present in the reaction medium can, and often do, affect the ATRP equilibrium.^[116, 117] The initiator molecule is typically an alkyl halide (R-X). In all of the published literature on ATRP, this R-X molecule has been called the initiator. Even though in contrast to a standard free radical polymerization initiator, this molecule is an inherently thermally stable entity and is incorporated into the final polymer. The halide is most frequently a bromide or chloride, although iodide based initiators were reported.^[118] Examples of halogenated compounds that were used as initiators in ATRP are carbon tetrachloride and chloroform, benzyl halides and α -halo esters.^[119] The R-X molecule can be a mono functional initiator, a multifunctional initiator, *i.e.* it can either possess more than one initiating functionality or it can be used to introduce additional functionalities into the alpha-chain end; it can be a macroinitiator (a polymer containing initiator site), or initiators attached to a surface, either a particle, flat surface or fiber. The only requirement is the presence of the radical stabilizing substituents around the halogen group. Also, the initiation step must be faster than or equal to the propagation rate for a controlled polymerization.^[120] Several transition metals were applied in ATRP. Catalyst systems employing copper are mostly used for the polymerization; however a wide range of other metals can be applied for ATRP including iron,^[121, 122] ruthenium,^[110, 123] nickel,^[124, 125] molybdenum,^[126, 127] rhenium,^[128] rhodium,^[129] palladium,^[130] osmium^[131] and cobalt.^[132] But transition metals catalysts can be an issue in the synthesis of polymers for biomedical applications. To overcome this problem, Bruns *et al.* developed new systems of natural catalysts for ATRP called

ATRPases, made of hemoglobin^[133] and horseradish peroxidase.^[134] To fine-tune the catalyst systems, a variety of ligands were developed that attenuate solubility, selectivity and/or reactivity of catalysts. For example, the use of 4,4'-alkyl- substituted bipyridines resulted in the preparation of polymers with very low dispersity ($M_w/M_n < 1.1$).^[135] Furthermore, linear aliphatic amines,^[136] terpyridyl,^[137] and picolyl^[138] ligands provided catalysts that were more reactive than the 2,2'-bipyridyne (bpy) ligands originally employed for ATRP.^[108] Phosphine-based ligands are also applied in the ATRP catalyst systems.^[110, 121, 122] ATRP is well-suited for the polymerization of styrenes,^[139] methacrylates^[140-143] and acrylates.^[144-146] The power of this technique is its tolerance towards many functional groups of the monomer molecules. These functional monomers often contain donor atoms such as N or O, and have the potential to coordinate to the catalyst.^[147] However, sometimes a protected monomer is still required during the ATRP process because *e.g.* acid monomers can poison the catalysts by coordinating to the transition metal.^[148]

1.2.2.3. Mechanism of ATRP

ATRP is a catalytic process where a transition metal complex reversibly activates the dormant chains via a halogen atom transfer reaction^[108, 110, 137-139] (Figure 1-6).

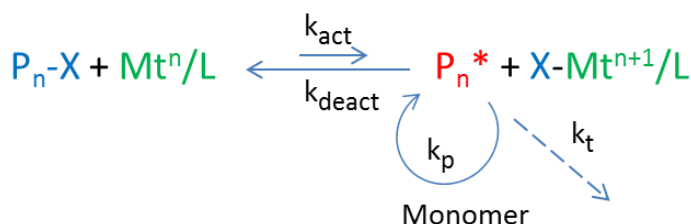


Figure 1-6: Mechanism of metal complex-mediated ATRP.^[152]

Thus, the transition metal catalyst (Mt^n/L) reacts with an alkyl halide initiator generating a radical and a transition metal complex by transfer of the halogen (X) to the catalyst. The bond between the alkyl and the halide is cleaved homolytically and a carbon-centered radical is formed on the alkyl.^[109]

The radical propagates by addition of monomer (M) is rapidly deactivated by reaction with the oxidized transition metal halide ($X-Mt^{n+1}/L$) to reform the original catalyst and an oligomeric alkyl halide. This process repeats itself with all chains growing in sequential steps, resulting in polymers with molecular weights defined by:

$$DP_n = \frac{\Delta[M]}{[I]_0}$$

where $[I]_0$ is the original concentration of initiator (alkyl halide) and DP the degree of polymerization. Narrow molecular weight distributions were considered for $M_w/M_n < 1.5$.

The activity of the catalyst is correlated to the equilibrium constant (K_{eq}) defined by the ratio $K_{eq}=k_{act}/k_{deact}$, where k_{act} and k_{deact} are activation and deactivation rate constants, respectively. In order to obtain a good control over the polymerization, the equilibrium must be strongly shifted towards the dormant species to limit termination between active species (k_t). Furthermore, deactivation of the active species must be fast enough, in comparison with propagation (k_p), to provide the same rate of growth for all chains and to lead to a controlled/"living" behavior.^[153] If deactivation is very slow or non-existent, the polymerization becomes uncontrolled.^[154] The reaction is termed controlled/"living" since termination reactions are not completely avoided.^[109, 149] Therefore, the ATRP should be carefully distinguished from ideal living polymerizations as defined by Szwarc.^[155] Taking into account the termination processes, the percentage of living chains capped by a halogen atom is less than 100%. Moreover, besides bimolecular termination, several side reactions may affect the chain-end functionality, which additionally reduce the number of living chains. Since a high portion of living chains is required for the preparation of well-defined block copolymers,^[156] an accurate control over the chain-end functionality must be provided. Lutz *et al.* reported a significant decrease of the amount of bromine-functionalized chains during the increase of the monomer conversion for bulk ATRP of styrene.^[157] The loss of functionality was divided into two steps: first, the functionality decreased linearly with the monomer conversion, and second, at very high conversions (> 90%, *i.e.* long reaction times), the functionality decreased faster with the conversion. The authors experimentally proved that the quenching of the ATRP at the latest 47 % of styrene conversion provided 92% of end-functional polymer chains which could further serve as macroinitiators for the subsequent polymerization steps. This is one of the crucial features of ATRP when applied for the synthesis of block copolymers. In order to reduce the fraction of termination reactions and slow down the propagation rate, a low level of oxidized transition metal halide is usually injected.^[158, 159]

1.2.2.4. Kinetics of ATRP

Based on the ATRP mechanism presented in *Figure 1-6*, two equations were proposed by Matyjaszewski *et al.*^[139] (*M-2*) and by Fischer^[160] (*F-2*) to describe the kinetics of ATRP.

$$K_{eq} = \frac{k_{act}}{k_{deact}} = \frac{[P_n][X-M_t^{n+1}-Y]}{[M_t^n-Y][P_n-X]} \quad (I)$$

$$\ln \frac{[M]_0}{[M]} = k_p K_{eq} [R - X] \frac{[M_t^n - Y]}{[X - M_t^{n+1} - Y]} t \quad (M-2)$$

$$\ln \frac{[M]_0}{[M]} = \frac{3}{2} k_p ([R - X]_0 [M_t^n - Y]_0)^{1/3} \frac{K_{eq}^{1/3}}{3k_t} t^{2/3} \quad (F-2)$$

Equation (*M-2*) is based on the assumption that the termination step can be neglected and a fast pre-equilibrium is established, thus the value of k_p is constant throughout the reaction. According to *M-2*, the propagation rate (R_p) corresponds to a first-order reaction with respect to monomer $[M]$, initiator $[R-X]$

and activator $[M_t^n-Y]$ concentrations. This equation explains the fact that the rate of ATRP in bulk is about four times greater than that conducted with 50 % in volume of monomer solutions.^[151] Thus, a reduction in the concentrations of both initiator and activator by a factor of two should result in a reduction of the overall rate by a factor of four. So far, the majority of the experimental results were analyzed according to Matyjaszewski's equation ($M-2$). Some data were in agreement with $M-2$ in terms of reaction orders for initiator and Cu(I),^[151, 161, 162] while some others deviated to various extents.^[163-165] The deviations were mostly assigned to the existence of "self-regulation" caused by the persistent radical effect in ATRP.^[166] On the basis of the existence of this persistent radical effect, Fischer derived a kinetic equation for the ATRP ($F-2$). This equation was also proven to be applicable in some living radical polymerization systems.^[167, 168] Zhang *et al.* experimentally verified both equations ($M-2$ and $F-2$) in Cu-mediated ATRP of methyl methacrylate.^[169] The results obtained showed that initially added Cu(II) had strong effects on the kinetics of the ATRP depending on the $[Cu(II)]_0/[Cu(I)]_0$ ratio. When $\leq 10\%$ of Cu(II) relative to Cu(I) was added at the beginning of the polymerization, the kinetics were described by Fischer's equation ($\ln([M]_0/[M]) \sim t^{2/3}$, $F-2$). The obtained reaction orders for initiator, Cu(I) and Cu(II) were close to or the same as those in Fischer's equation verifying the applicability of Fischer's equation in ATRP systems of lower activity. On the other hand, when $[Cu(II)]_0/[Cu(I)]_0 \geq 0.1$, the kinetics could be interpreted by Matyjaszewski's equation ($\ln([M]_0/[M]) \sim t$, $M-2$).

The polymerization rate was almost first order with respect to the concentration of the initiator and Cu(I) and inverse first order with respect to the concentration of Cu(II), suggesting that the "self-regulation" and radical termination becomes less important for ATRP process when enough Cu(II) is added at the beginning of the reaction. These results brought a great contribution to a better control of ATRP systems as well as an understanding of applicability of both kinetic equations for ATRP.

1.2.2.5. Surface-initiated ATRP

As mentioned before, the ATRP initiator molecule can be attached to a planar surface, spherical particles, fibers, etc. In this case, the polymerization proceeds from the surface and the final polymer chains are anchored on the support. Often, the control over the surface-initiated ATRP does not necessarily result from the application of conditions suitable for the ATRP in solution. Prucker and Ruhe showed that the main differences between surface and solution polymerizations occur because of changes in termination reactions.^[170] For some polymerizations from surfaces, termination is enhanced at elevated temperatures because of rapid initiation, and the rate of "thickening" can actually decrease with the reaction temperature.^[171] Several studies of surface-initiated ATRP proved that the growth in polymer film thicknesses decreases with time, suggesting significant termination.^[172-174] Matyjaszewski *et al.* simulated the growth of polymer chains by surface-initiated polymerization, considering the transfer of the monomer to the growing chains and changes in the polydispersity index with time.^[175] The authors

concluded that initiator coverage is a major factor in defining whether the growth in layer thickness depends linearly on the reaction time. Moreover, the effect of initiator density of monolayer adsorbed on surface clearly affects the configuration and the thickness of the brushes. Jones *et al.* reported the first systematic study of initiator density on surface-initiated polymerization. Indeed, they showed that the density of initiating sites strongly influences the chains growth rate and the morphology of the resulting polymer film.^[176] Si-ATRP of methyl methacrylate and glycidyl methacrylate were carried out from a mixed monolayer of two thiols (where the quantity of each thiol was known). Only one of these two thiols carries a bromoisobutyrate end-group and is able to surface-initiate the synthesis of the polymer chains. As mentioned previously, linear relationship between the initiator density and the thickness of the polymer brush has been established. Chilkoti *et al.* clearly show that protein repelling on poly (oligo (ethylene glycol) methyl methacrylate) brushes depends on both parameters: film thickness and polymer surface density.^[177] Authors show that the synthesis of low density brushes lead to the best coating against protein adsorption.

Later, Kim *et al.* showed that there is a specific catalyst concentration that yields a maximum film thickness for a given polymerization time.^[178] The optimal catalyst concentration depends on the particular ATRP system applied. They concluded that the polymerization at high catalyst concentration causes a high concentration of radicals and, therefore, rapid initial growth followed by early termination, whereas polymerization at low catalyst concentrations simply yields very little film growth. Interestingly, stirring of the solution also appears to enhance early termination processes. This was explained in terms of increased mobility of chain ends during stirring, which increases the possibility of radical coupling.^[178]

1.3. Solid-supported block copolymer membranes

Solid-supported biomimetic membranes were developed in the 1980s as membrane models to overcome the lack of stability of natural cell membranes.^[179] To create such artificial membranes, immobilization of polymeric nanostructures such as vesicles on surfaces as well as the formation of planar membranes can be performed. The immobilization on surfaces offers the ability to easily isolate and array vesicles individually^[180-182] or in groups,^[183] to apply a wide range of surface-sensitive techniques for the investigation of the vesicles^[180] and to create well-suited platforms for high-throughput experiments.^[184] However, most of the reported studies were performed on liposomes while anchoring of polymer vesicles on surfaces is rarely reported. The situation is similar with solid-supported planar membranes. For almost 20 years, phospholipid bilayers deposited onto solid substrates were the only used experimental cell-surface models and allowed gaining insights into immune reactions and cell adhesion.^[185-189] This resulted in membranes, only separated from the solid support by an ultrathin (1-2 nm) water film.^[190, 192] However, this concept suffers from a number of intrinsic difficulties. The mere physical coupling between the lipid

bilayer and the solid support eventually may lead to partial detachment of membrane constituents or replacement by other surface-active compounds.^[192]

Furthermore, as depicted in *Figure 1-7a*, the membrane-substrate distance is usually not large enough to avoid direct contact between incorporated membrane components (*e.g.* integral proteins) and the solid surface.^[193] Some of the proteins envisaged for basic biophysical studies or technological applications, however, possess functional units which stick out far from the bilayer.^[192] Strong interactions and/or frictional coupling between the substrate and incorporated proteins might lead to partial loss of functionality or even to complete protein denaturation.^[192]

Next generations of solid-supported membranes were therefore optimized in such a way that unfavorable contacts between the substrate and integral membrane components can be avoided. Two major concepts, depicted in *Figures 1-7b and 1-7c*, are used to achieve this improvement: lipid bilayers are either “cushioned” on polymer or polyelectrolyte films,^[190, 191, 193, 194] or covalently coupled to the substrate by anchor or spacer groups (and are often referred to as “tethered bilayer membranes”).^[192, 194, 195]

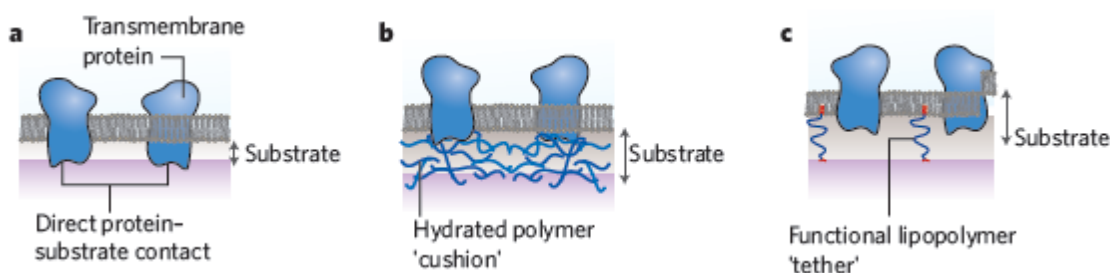


Figure 1-7: Solid-supported membranes. Solid-supported lipid membrane (a), lipid membrane that is supported using a polymer cushion (b) or lipopolymer tethers (c). Transmembrane proteins are marked as blue objects across the membranes.^[193]

Recent attempts involved the introduction of spacer units like peptides, oligomers, or polymers.^[13, 193, 195-198] In particular, the approach of covalent tethering is of central importance to this thesis. This concept guarantees a mechanically and chemically robust attachment of the artificial membranes to the solid support, while at the same time the membrane retains its fluid character.^[195] The covalent attachment of the polymer chains to the substrate can be achieved either by “grafting-to” or “grafting-from” techniques. The “grafting-to” procedure implies to anchor an end-functional polymer chain to the substrate containing suitable functional groups for covalent binding.^[199] Common preparation techniques for such membranes include dip- or spin-coating,^[200] layer-by-layer deposition,^[201] Langmuir film transfers,^[202-204] or vesicle and micelles spreading.^[205-207] This method usually leads to polymer membranes with low grafting density of the chains due to diffusion problems of large macromolecules reaching a substrate. The “grafting-from” technique overcomes this problem and results in preparation of thick, covalently tethered polymer brushes with a high grafting density.^[208] This method attracted a lot of attention since the “living” polymerization techniques were optimized for surface functionalization. The grafting of

amphiphilic triblock copolymer from gold substrates and subsequent analysis of the resulting brushes will be presented in this thesis.

Tethering polymer vesicles to solid surfaces can find their applications as smart and active surfaces.^[209] Two publications^[27, 210] made use of the specific and strong streptavidin-biotin binding assay to immobilize triblock copolymer vesicles on glass. Rosenkranz *et al.* employed this approach to investigate protein folding at a single molecule level. Proteins, encapsulated in triblock copolymer nanocontainers, could be individually observed for extended time periods.^[210] Moreover, this immobilization method proved its usefulness for studying enzymatic conversions on precisely patterned surfaces. Grzelakowski *et al.* encapsulated an enzyme in surface-bound hybrid protein-polymer nanoreactors.^[27] A fluorogenic substrate was introduced into the nanoreactors via a previously incorporated channel protein. By enzymatic conversion, it became insoluble and fluorescent, thus detectable by laser scanning microscopy. More recently, polymer nanoreactors immobilized on surfaces were shown to be used as local drug delivery and antifouling systems.^[211, 212] Langowska *et al.* designed and prepared vesicles based on a poly (2-methyloxazoline)-*block*-poly (dimethylsiloxane)-*block*-poly (2-methyloxazoline (PMOXA-*b*-PDMS-*b*-PMOXA) amphiphilic triblock copolymer encapsulating the enzyme penicillin acylase for local and controlled production of antibiotics.^[211] The latter system found its use as a self-defending system to fight bacterial adhesion by a controlled release of drugs for a long period of time.^[212]

Planar membranes anchored to a solid support were designed as active surfaces for potential applications in tissue engineering^[213, 214] or biosensing.^[215, 216] As templates for biological mineralization, amphiphilic poly (acrylic acid)-*block*-poly (*n*-butylacrylate) diblock copolymer films at the air-water interface as well as a system based on polymer-lipid mixed monolayers have been mineralized with calcium phosphate.^[213, 214] As sensing devices, laccase enzyme has been immobilized on an asymmetric amphiphilic triblock copolymers made of poly (ethylene glycol)-*block*-poly (γ -methyl- ϵ -caprolactone)-*block*-poly ((2-dimethylamino) ethyl methacrylate) (PEG₄₅-*b*-PMCL_x-*b*-PDMAEMA_y), with preservation of enzyme activity.^[215] Additionally, potential biosensor devices can be designed by the incorporation of biological moieties *i.e.* membrane proteins inside planar membranes. So far the closest achievements in this area are the successful insertion of channel proteins alpha-hemolysin (α -HL) and potassium channel protein MloK1 into polymeric bilayers created with Langmuir techniques.^[216, 217] Similarly, incorporation of proteins will be performed in this thesis. For this purpose, the system presented in the work of Rakhmatullina *et al.*^[218] will be optimized by controlling the packing density, as the polymers were synthesized using a “grafting-from” approach.

1.4. References

- [1] C. Steinem, A. Janshoff, *Chem. Unserer Zeit*, **2008**, *42*, 116-127.
- [2] B. Alberts, A. Johnson, J. Lewis, M. Raff, K. Roberts, P. Walter, *Molecular biology of the cell*, Garland Science, New York, **2002**.
- [3] S. J. Singer, G. L. Nicolson, *Science*, **1972**, *175*, 720-731.
- [4] <http://cellbiology.med.unsw.edu.au/units/science/lecture0803.htm>, accessed on November 23, **2014**.
- [5] J. N. Israelachvili, D. J. Mitchell, B. W. Ninham, *Biochim. Biophys. Acta, Biomembr.*, **1977**, *470*, 185-201.
- [6] R. Nagarajan, E. Ruckenstein, *Langmuir*, **1991**, *7*, 2934-2969.
- [7] C. Tanford, *Science*, **1978**, *200*, 1012-1018.
- [8] K. Simons, E. Ikonen, *Nature*, **1997**, *387*, 569-572.
- [9] C. Peetla, A. Stine, V. Labhasetwar, *Mol. Pharmaceutics*, **2009**, *6*, 1264-1276.
- [10] C. H. Nielsen, *Anal. Bioanal. Chem.*, **2009**, *395*, 697-718.
- [11] M. A. Shannon, P. W. Bohn, M. Elimelech, J. G. Georgiadis, B. J. Marinas, A. M. Mayes, *Nature*, **2008**, *452*, 301-310.
- [12] W. Knoll, F. Yu, T. Neumann, S. Schiller, R. Naumann, *Phys. Chem. Chem. Phys.*, **2003**, *5*, 5169-5175.
- [13] J. Spinke, J. Yang, H. Wolf, M. Liley, H. Ringsdorf, W. Knoll, *Biophys. J.*, **1992**, *63*, 1667-1671.
- [14] C. Steinem, A. Janshoff, W.-P. Ulrich, M. Sieber, H.-J. Galla, *Biochim. Biophys. Acta, Biomembr.*, **1996**, *1279*, 169-180.
- [15] I. K. Vockenroth, P. P. Atanasova, J. R. Long, A. T. A. Jenkins, W. Knoll, I. Koeper, *Biochim. Biophys. Acta, Biomembr.*, **2007**, *1768*, 1114-1120.
- [16] S. H. White, *Biophys. J.*, **1970**, *10*, 1127-1148.
- [17] S. Förster, *Top. Curr. Chem.*, **2003**, *226*, 1-28.
- [18] S. Förster, M. Antonietti, *Adv. Mater.*, **1998**, *10*, 195-217.
- [19] S. Förster, T. Plantenberg, *Angew. Chem. Int. Ed.*, **2002**, *41*, 688-714.
- [20] K. Kita-Tokarczyk, M. Junginger, S. Belegriou, A. Taubert, *Adv. Polym. Sci.*, **2011**, *242*, 151-201.
- [21] K. Kita-Tokarczyk, J. Grumelard, T. Haefele, W. Meier, *Polymer*, **2005**, *46*, 3540-3563.
- [22] K. Kita-Tokarczyk, W. Meier, *Chimia*, **2008**, *62*, 820.
- [23] A. Mecke, C. Dittrich, W. Meier, *Soft Matter*, **2006**, *2*, 751-759.

- [24] V. Malinova, S. Belegriinou, D. d. B. Ouboter, W. P. Meier, *Adv. Polym. Sci.*, **2010**, 224, 113-165.
- [25] A. Graff, C. Fraysse-Ailhas, C. G. Palivan, M. Grzelakowski, T. Friedrich, C. Vebert, G. Gescheidt, W. Meier, *Macromol. Chem. Phys.*, **2010**, 211, 229-238.
- [26] A. Graff, M. Sauer, P. Van Gelder, W. Meier, *Proc. Natl. Acad. Sci. USA*, **2002**, 99, 5064-5068.
- [27] M. Grzelakowski, O. Onaca, P. Rigler, M. Kumar, W. Meier, *Small*, **2009**, 5, 2545-2548.
- [28] M. Kumar, M. Grzelakowski, J. Zilles, M. Clark, W. Meier, *Proc. Natl. Acad. Sci. USA*, **2007**, 104, 20719-20724.
- [29] C. Nardin, W. Meier, *Rev. Mol. Biotechnol.*, **2002**, 90, 17-26.
- [30] D. E. Discher, A. Eisenberg, *Science*, **2002**, 297, 967-973.
- [31] K. Yu, A. Eisenberg, *Macromolecules*, **1998**, 31, 3509-3518.
- [32] H. Bermudez, A. K. Brannan, D. A. Hammer, F. S. Bates, D. E. Discher, *Macromolecules*, **2002**, 35, 8203-8208.
- [33] A. Taubert, A. Napoli, W. Meier, *Curr. Opin. Chem. Biol.*, **2004**, 8, 598-603.
- [34] IUPAC. "Glossary of Basic Terms in Polymer Science", *Pure Appl. Chem.*, **1996**, 68, 2287-2311.
- [35] E. Cabane, *photoresponsive polymersomes as smart, trigerrable nanocarriers*, PhD thesis, **2011**, University of Basel, Basel, Switzerland, p. 13.
- [36] I. W. Hamley, *Introduction to Block Copolymers In Developments in Block Copolymer Science and Technology*, Hamley I. W. Ed. ; Wiley **2004**.
- [37] P. L. Soo, A. Eisenberg, *J. Polym. Sci. B: Polym. Phys.*, **2004**, 42, 923-938.
- [38] L. Zhang, A. Eisenberg, *J. Am. Chem. Soc.*, **1996**, 118, 3168-3181.
- [39] C. Allen, D. Maysinger, A. Eisenberg, *Colloids Surf. B*, **1999**, 16, 3-27.
- [40] H. Shen, A. Eisenberg, *Macromolecules*, **2000**, 33, 2561-2572.
- [41] H. Shen, A. Eisenberg, *J. Phys. Chem. B*, **1999**, 103, 9473-9487.
- [42] Y. Yu, L. Zhang, A. Eisenberg, *Macromolecules*, **1998**, 31, 1144-1154.
- [43] Y. Yu, A. Eisenberg, *J. Am. Chem. Soc.*, **1997**, 119, 8383-8384.
- [44] S. Hauschild, U. Lipprandt, A. Rumpelcker, U. Borchert, A. Rank, R. Schubert, S. Förster, *Small*, **2005**, 1, 1177-1180.
- [45] H.-J. Choi, E. Brooks, C. D. Montemagno, *Nanotechnology*, **2005**, 16, 143-149.
- [46] J. Yang, D. Levy, W. Deng, P. Keller, M.-H. Li, *Chem. Commun.*, **2005**, 4345-4347.
- [47] Y. Yamamoto, K. Yasugi, A. Harada, Y. Nagasaki, K. Kataoka, *J. Controlled Release*, **2002**, 82, 359-371.

- [48] A.-L. Kjoniksen, A. Laukkanen, C. Galant, K. D. Knudsen, H. Tenhu, B. Nyström, *Macromolecules*, **2005**, *38*, 948-960.
- [49] C. M. Schilli, M. F. Zhang, E. Rizzardo, S. H. Thang, Y. K. Chong, K. Edwards, G. Karlsson, A. H. E. Müller, *Macromolecules*, **2004**, *37*, 7861-7866.
- [50] H. Shen, L. Zhang, A. Eisenberg, *J. Phys. Chem. B*, **1997**, *101*, 4697-4708.
- [51] I. Astafieva, X. F. Zhong, A. Eisenberg, *Macromolecules*, **1993**, *26*, 7339-7352.
- [52] H. Matsuoka, M. Matsutani, E. Mouri, K. Matsumoto, *Macromolecules*, **2003**, *36*, 5321-5330.
- [53] S. Förster, N. Hermsdorf, C. Böttcher, P. Lindner, *Macromolecules*, **2002**, *35*, 4096-4105.
- [54] T. Rager, W. H. Meyer, G. Wegner, K. Mathauer, W. Mächtle, W. Schrof, D. Urban, *Macromol. Chem. Phys.*, **1999**, *200*, 1681-1691.
- [55] H. Matsuoka, S. Maeda, P. Kaewsaiha, K. Matsumoto, *Langmuir*, **2004**, *20*, 7412-7421.
- [56] K. Matsumoto, T. Ishizuka, T. Harada, H. Matsuoka, *Langmuir*, **2004**, *20*, 7270-7282.
- [57] P. Kaewsaiha, K. Matsumoto, H. Matsuoka, *Langmuir*, **2005**, *21*, 9938-9945.
- [58] L. Zhang, A. Eisenberg, *J. Polym. Sci. B: Polym. Phys.*, **1999**, *37*, 1469-1484.
- [59] O. Terreau, L. Luo, A. Eisenberg, *Langmuir*, **2003**, *19*, 5601-5607.
- [60] F. Drolet, G. H. Fredrickson, *Phys. Re. Lett.*, **1999**, *83*, 4317-4320.
- [61] Y. Bohbot-Raviv, Z.-G. Wang, *Phys. Re. Lett.*, **2000**, *85*, 3428-3431.
- [62] D. M. Vriezema, M. C. Aragonés, J. A. A. W. Elemans, J. J. L. M. Cornelissen, A.E. Rowan, R. J. M. Nolte, *Chem. Rev.*, **2005**, *105*, 1445-1490.
- [63] B. M. Discher, Y. Y. Won, D. S. Ege, J. C. M. Lee, F. S. Bates, D. E. Discher, D. A. Hammer, *Science*, **1999**, *284*, 1143-1146.
- [64] M. Antionetti, S. Förster, *Advanced Materials*, **2003**, *15*, 1323-1333.
- [65] V. Guida, *Advances in Colloid and Interfaces Sci.*, **2010**, *161*, 77-88.
- [66] D. E. Discher, F. Ahmed, *Annual Review of Biomedical Engineering*, **2006**, *8*, 323-341.
- [67] F. Najafi, M. N. Sarbolouki, *Biomaterials*, **2003**, *24*, 1175-1182.
- [68] G. S. Kwon, *Crit. Rev. Ther. Drug*, **1998**, *15*, 481-512.
- [69] C. Nardin, T. Hirt, J. Leukel, W. Meier, *Langmuir*, **2000**, *16*, 1035-1041.
- [70] C. Nardin, J. Widmer, M. Winterhalter, W. Meier, *Eur. Phys. J. E*, **2001**, *4*, 403-410.
- [71] C. J. F. Rijcken, O. Soga, W. E. Hennink, C. F. van Nostrum, *J. Controlled Release*, **2007**, *120*, 131-148.

- [72] H. Bader, H. Ringsdorf, B. Schmidt, *Angew. Macromol. Chem.*, **1984**, 123/124, 457-485.
- [73] M. L. Adams, A. Lavasanifar, G. S. Kwon, *J. Pharm. Sci.*, **2003**, 92, 1343-1355.
- [74] A. Lavasanifar, J. Samuel, G. S. Kwon, *Adv. Drug Deliv. Rev.*, **2002**, 54, 169-190.
- [75] M. C. Jones, J.-C. Leroux, *Eur. J. Pharm. Biopharm.*, **1999**, 48, 101-111.
- [76] V. P. Torchilin, *J. Controlled Release*, **2001**, 73, 137-172.
- [77] F. Mathot, L. van Beijsterveldt, V. Preat, M. Brewster, A. Arien, *J. Controlled Release*, **2006**, 111, 47-55.
- [78] V. P. Sant, D. Smith, J.-C. Leroux, *J. Controlled Release*, **2005**, 104, 289-300.
- [79] M. Yokoyama, G. S. Kwon, T. Okano, Y. Sakurai, T. Seto, K. Kataoka, *Bioconjug. Chem.*, **1992**, 3, 295-301.
- [80] N. Rapoport, *Int. J. Pharm.*, **2004**, 277, 155-162.
- [81] X. Shuai, T. Merdan, A. K. Schaper, F. Xi, T. Kissel, *Bioconjug. Chem.*, **2004**, 15, 441-448.
- [82] R. T. Liggins, H. M. Burt, *Adv. Drug Deliv. Rev.*, **2002**, 54, 191-202.
- [83] N. Nishiyama, S. Okazaki, H. Cabral, M. Miyamoto, Y. Kato, Y. Sugiyama, K. Nishio, Y. Matsumara, K. Kataoka, *Cancer. Res.*, **2003**, 63, 8977-8983.
- [84] N. Nishiyama, Y. Kato, Y. Sugiyama, K. Kataoka, *Pharm. Res.*, **2001**, 18, 1035-1041.
- [85] W. J. Lin, L. W. Juang, C. C. Lin, *Pharm. Res.*, **2003**, 20, 668-673.
- [86] J. Djordjevic, M. Barch, K. E. Uhrich, *Pharm. Res.*, **2005**, 22, 24-32.
- [87] A. Rösler, G. W. M. Vandermeulen, H.-A. Klok, *Adv. Drug Deliv. Rev.*, **2001**, 53, 95-108.
- [88] R. Cheng, F. Feng, F. Meng, C. Deng, J. Feijen, Z. Zhong, *Journal of Controlled Release*, **2011**, 152, 2-12.
- [89] S. Cerritelli, D. Velluto, J. A. Hubbell, *Biomacromolecules*, **2007**, 8, 1966-1972.
- [90] W. Meier, C. Nardin, M. Winterhalter, *Angew. Chem. Int. Ed.*, **2000**, 39, 4599-4602.
- [91] M. Kumar, J. E. O. Habel, Y.-X. Shen, W. P. Meier, T. Walz, *J. Am. Chem. Soc.*, **2012**, 134, 18631-18637.
- [92] R. C. Advincula, W. J. Brittain, K. C. Caster, J. Rühle, *Polymer Brushes*, Wiley-CVH, **2004**.
- [93] R. A. L. Jones, R. W. Richards, *Polymers at Surfaces and Interfaces*, Cambridge University Press, Cambridge, **1999**.
- [94] R. R. Bhat, M. R. Tomlinson, T. Wu, J. Genzer, *Adv. Polym. Sci.*, **2006**, 198, 51-124.
- [95] S. Alexander, *J. Physique*, **1977**, 38, 977-981.
- [96] P.-G. de Gennes, *Macromolecules*, **1980**, 13, 1069-1075.

- [97] M. Rubinstein, R. H. Colby, *Polymer Physics*, Oxford University Press, **2003**.
- [98] S. T. Milner, T. A. Witten, M. E. Cates, *Macromolecules*, **1988**, *21*, 2610-2619.
- [99] M. Szwarc, *Adv. Polym. Sci.*, **1983**, *49*, 1-177.
- [100] J. P. Kennedy, B. Ivan, *Designed polymers by carbocationic macromolecular engineering*, Hanser Verlag, **1991**.
- [101] W. J. Brittain, *Rubber Chem. Technol.*, **1992**, *65*, 580-600.
- [102] Y. Tezuka, *Prog. Polym. Sci.*, **1992**, *17*, 471-514.
- [103] G. F. Meijs, E. Rizzardo, *J. Macromol. Sci. Rev.*, **1990**, *C30*, 305-377.
- [104] R. P. T. Chung, D. H. Solomon, *Prog. Org. Coat.*, **1992**, *21*, 227-254.
- [105] G. Riess, G. Hurtrez, P. Bahadur, In *Encyclopedia of polymer science and engineering*, 2nd Ed., Wiley, New York, **1985**.
- [106] N. Hadjichristidis, S. Pispas, G. Floudas, *Block Copolymers by Group Transfer Polymerization*, In *Block Copolymers*, Wiley, **2003**, p. 65.
- [107] D. Taton, Y. Gnanou, *Guidelines for Synthesizing Block Copolymers*, In *Block Copolymers in Nanoscience*, Wiley-VCH, **2007**, p. 9.
- [108] J.-S. Wang, K. Matyjaszewski, *J. Am. Chem. Soc.*, **1995**, *117*, 5614-5615.
- [109] J.-S. Wang, K. Matyjaszewski, *Macromolecules*, **1995**, *28*, 7901-7910.
- [110] M. Kato, M. Kamigaito, M. Sawamoto, T. Higashimura, *Macromolecules*, **1995**, *28*, 1721-1723.
- [111] B. Boutevin, C. Maubert, A. Mebkhout, Y. J. Pietrasanta, *J. Polym. Sci. A : Polym. Chem.*, **1981**, *19*, 499-509.
- [112] B. Boutevin, *J. Polym. Sci. A : Polym. Chem.*, **2000**, *38*, 3235-3243.
- [113] D. P. Curran, *Synthesis*, **1988**, 489-513.
- [114] V. Coessens, T. Pintauer, K. Matyjaszewski, *Prog. Polym. Sci.*, **2001**, *26*, 337-377.
- [115] K. Matyjaszewski, S. Coca, S. G. Gaynor, M. Wei, B. E. Woodworth, *Macromolecules*, **1998**, *31*, 5967-5969.
- [116] W. A. Braunecker, K. Matyjaszewski, *Prog. Polym. Sci.*, **2007**, *32*, 93-146.
- [117] N. V. Tsarevsky, W. A. Braunecker, K. Matyjaszewski, *J. Organomet. Chem.*, **2007**, *692*, 3212-3222.
- [118] K. Matyjaszewski, S. M. Jo, H.-J. Paik, D. A. Shipp, *Macromolecules*, **1999**, *32*, 6431-6438.
- [119] K. Matyjaszewski, J. Xia, *J. Chem. Rev.*, **2001**, *101*, 2921-2990.

- [120] K. Matyjaszewski, J. L. Wang, T. Grimaud, D. A. Shipp, *Macromolecules*, **1998**, *31*, 1527-1534.
- [121] K. Matyjaszewski, M. Wei, J. Xia, N. E. McDermott, *Macromolecules*, **1997**, *30*, 8161-8164.
- [122] T. Ando, M. Kamigaito, M. Sawamoto, *Macromolecules*, **1997**, *30*, 4507-4510.
- [123] F. Simal, A. Demonceau, A. F. Noels, *Angew. Chem. Int. Ed.*, **1999**, *38*, 538-540.
- [124] C. Granel, P. Dubois, R. Jerome, P. Teyssie, *Macromolecules*, **1996**, *29*, 8576-8582.
- [125] H. Uegaki, Y. Kotani, M. Kamigaito, M. Sawamoto, *Macromolecules*, **1997**, *30*, 2249-2253.
- [126] J. A. M. Brandts, P. van der Geijn, E. E. van Faassen, J. Boersma, G. van Koten, *J. Organomet. Chem.*, **1999**, *584*, 246-253.
- [127] E. Le Grogne, J. Claverie, R. Poli, *J. Am. Chem. Soc.*, **2001**, *123*, 9513-9524.
- [128] Y. Kotani, M. Kamigaito, M. Sawamoto, *Macromolecules*, **1999**, *32*, 2420-2424.
- [129] G. Moineau, C. Granel, P. Dubois, R. Jerome, P. Teyssie, *Macromolecules*, **1998**, *31*, 542-544.
- [130] P. Lecomte, I. Drapier, P. Dubois, P. Teyssie, R. Jerome, *Macromolecules*, **1997**, *30*, 7631-7633.
- [131] W. A. Braunecker, Y. Itami, K. Matyjaszewski, *Macromolecules*, **2005**, *38*, 9402-9404.
- [132] B. Wang, Y. Zhuang, X. Luo, S. Xu, X. Zhou, *Macromolecules*, **2003**, *36*, 9684-9686.
- [133] T. B. Silva, M. Spulber, M. K. Kocik, F. Seidi, H. Charan, M. Rother, S. J. Sigg, K. Renggli, G. Kali, N. Bruns, *Biomacromolecules*, **2013**, *14*, 2703-2712.
- [134] S. J. Sigg, F. Seidi, K. Renggli, T. B. Silva, G. Kali, N. Bruns, *Macromol. Rapid Commun.*, **2011**, *32*, 1710-1715.
- [135] K. Matyjaszewski, T. Patten, J. Xia, T. Abernathy, *Science*, **1996**, *272*, 866-868.
- [136] K. Matyjaszewski, J. H. Xia, *Macromolecules*, **1997**, *30*, 7697-7700.
- [137] G. Kickelbick, K. Matyjaszewski, *Macromol. Rapid Commun.*, **1999**, *20*, 341-346.
- [138] J. Xia, K. Matyjaszewski, *Macromolecules*, **1999**, *32*, 2434-2437.
- [139] K. Matyjaszewski, T. E. Patten, J. Xia, *J. Am. Chem. Soc.*, **1997**, *119*, 674-380.
- [140] K. L. Beers, S. Boo, S. G. Gaynor, K. Matyjaszewski, *Macromolecules*, **1999**, *32*, 5772-5776.
- [141] S. M. Kimani, S. C. Moratti, *J. Polym. Sci. A : Polym. Chem.*, **2005**, *43*, 1588-1598.
- [142] A. P. Narrainen, S. Pascual, D. M. Haddleton, *J. Polym. Sci. A : Polym. Chem.*, **2002**, *40*, 439-450.
- [143] E. Rakhmatullina, T. Braun, M. Chami, V. Malinova, W. Meier, *Langmuir*, **2007**, *23*, 12371-12379.
- [144] K. A. Davis, K. Matyjaszewski, *Macromolecules*, **2000**, *33*, 4039-4047.
- [145] G. Wang, D. Yan, *J. Appl. Polym. Sci.*, **2001**, *82*, 2381-2386.

- [146] P. Ravi, C. Wang, K. C. Tam, L. H. Gan, *Macromolecules*, **2003**, *36*, 173-179.
- [147] J. Lad, S. Harisson, G. Mantovani, D. M. Haddleton, *Dalton Trans.*, **2003**, 4175-4180.
- [148] H. Mori, A. H. E. Müller, *Prog. Polym. Sci.*, **2003**, *28*, 1403-1439.
- [149] T. E. Patten, K. Matyjaszewski, *Adv. Mater.*, **1998**, *10*, 901-915.
- [150] T. E. Patten, K. Matyjaszewski, *Acc. Chem. Res.*, **1999**, *32*, 895-903.
- [151] K. Matyjaszewski, *Chem. Eur. J.*, **1999**, *5*, 3095-3102.
- [152] http://www.cmu.edu/maty/development-atrp/understanding_mechanistic_parameters.html#understanding, accessed on November 23, **2014**.
- [153] D. Greszta, D. Mardare, K. Matyjaszewski, *Macromolecules*, **1994**, *27*, 638-644.
- [154] K. Matyjaszewski, *J. M. S.-Pure Appl. Chem.*, **1997**, *A34*, 1785-1801.
- [155] M. Szwarc, *Nature*, **1956**, *178*, 1168-1169.
- [156] K. Davis, K. Matyjaszewski, *Adv. Polym. Sci.*, **2002**, *159*, 1-169.
- [157] J.-F. Lutz, K. Matyjaszewski, *J. Polym. Sci. A : Polym. Chem.*, **2005**, *43*, 897-910.
- [158] K. Matyjaszewski, W. Tang, *Macromolecules*, **2005**, *38*, 2015-2018.
- [159] K. Tokuchi, T. Ando, M. Kamiaito, M. Sawamoto, *J. Polym. Sci. A: Polym. Chem.*, **2000**, *38*, 4735-4748.
- [160] H. Fischer, *J. Polym. Sci. A: Polym. Chem.*, **1999**, *37*, 1885-1901.
- [161] J. L. Wang, T. Grimaud, K. Matyjaszewski, *Macromolecules*, **1997**, *30*, 6507-6512.
- [162] D. M. Haddleton, M. C. Crossman, B. H. Dana, D. J. Duncalf, A. M. Heming, D. Kukulj, A. J. Shooter, *Macromolecules*, **1999**, *32*, 2110-2119.
- [163] K. A. Davis, H. J. Paik, K. Matyjaszewski, *Macromolecules*, **1999**, *32*, 1767-1776.
- [164] V. Percec, B. Barboiu, H. J. Kim, *J. Am. Chem. Soc.*, **1998**, *120*, 305-316.
- [165] S. Pascual, B. Coutin, M. Tardi, A. Polton, J. P. Vairon, *Macromolecules*, **1999**, *32*, 1432-1437.
- [166] H. Fischer, *Macromolecules*, **1997**, *30*, 5666-5672.
- [167] K. Ohno, Y. Tsujii, T. Miyamoto, T. Fukuda, *Macromolecules*, **1998**, *31*, 1064-1069.
- [168] J. F. Lutz, P. Lacroix-Desmazes, B. Boutevin, *Macromol. Rapid Commun.*, **2001**, *22*, 189-193.
- [169] H. Zhang, B. Klumperman, W. Ming, H. Fischer, R. van der Linde, *Macromolecules*, **2001**, *34*, 6169-6173.
- [170] O. Prucker, J. Rühle, *Macromolecules*, **1998**, *31*, 602-613.

- [171] S. Minko, A. Sidorenko, M. Stamm, G. Gafijchuk, V. Senkovsky, S. Voronov, *Macromolecules*, **1999**, *32*, 4532-4538.
- [172] M. Ejaz, K. Ohno, Y. Tsujii, T. Fukuda, *Macromolecules*, **2000**, *33*, 2870-2874.
- [173] D. M. Jones, W. T. S. Huck, *Adv. Mater.*, **2001**, *13*, 1256-1259.
- [174] D. Xiao, M. J. Wirth, *Macromolecules*, **2002**, *35*, 2919-2925.
- [175] K. Matyjaszewski, P. J. Miller, N. Shukla, B. Immaraporn, A. Gelman, B. B. Luokala, T. M. Siclovan, G. Kickelbick, T. Vallant, H. Hoffmann, T. Pakula, *Macromolecules*, **1999**, *32*, 8716-8724.
- [176] D. M. Jones, A. A. Brown, W. T. S. Huck, *Langmuir*, **2002**, *18*, 1265-1269.
- [177] H. Ma, M. Wells, T. P. Beebe, A. Chilkoti, *Adv. Funct. Mater.*, **2006**, *16*, 640-648.
- [178] J.-B. Kim, W. Huang, M. D. Miller, G. L. Baker, M. L. Bruening, *J. Polym. Sci. A: Polym. Chem.*, **2003**, *41*, 386-394.
- [179] S. Belegriou, S. Menon, D. Dobrunz, W. Meier, *Soft Matter*, **2011**, *7*, 2202-2210.
- [180] S. M. Christensen, D. Stamou, *Soft Matter*, **2007**, *3*, 828-836.
- [181] R. Michel, I. Reviakine, D. Sutherland, C. Fokas, G. Csucs, G. Danuser, M. Textor, *Langmuir*, **2002**, *18*, 8580-8586.
- [182] J. P. Renault, A. Bernard, A. Bietsch, B. Michel, H. R. Bosschar, E. Delamarque, M. Kreiter, B. Hecht, U. P. Wild, *J. Phys. Chem. B*, **2003**, *107*, 703-711.
- [183] B. Städler, D. Falconnet, I. Pfeiffer, F. Höök, J. Vörös, *Langmuir*, **2004**, *20*, 11348-11354.
- [184] K. Salaita, Y. H. Wang, J. Fragala, R. A. Vega, C. Liu, C. A. Mirkin, *Angew. Chem. Int. Ed.*, **2006**, *45*, 7220-7223.
- [185] A. A. Brian, H. M. McConnell, *Proc. Natl. Acad. Sci. U. S. A.*, **1984**, *81*, 6159-6163.
- [186] E.-M. Erb, K. Tangemann, B. Bohrmann, B. Müller, J. Engel, *Biochemistry*, **1997**, *36*, 7395-7402.
- [187] A. Kloboucek, A. Behrisch, J. Faix, E. Sackmann, *Biophys. J.*, **1999**, *77*, 2311-2328.
- [188] S. Y. Qi, J. T. Groves, A. K. Chakraborty, *Proc. Natl. Acad. Sci. U. S. A.*, **2001**, *98*, 6548-6553.
- [189] L. K. Tamm, H. M. McConnell, *Biophys. J.*, **1985**, *47*, 105-113.
- [190] E. Sackmann, *Science*, **1996**, *271*, 43-48.
- [191] M. Tanaka, E. Sackmann, *Phys. Stat. Sol. (a)*, **2006**, *203*, 3452-3462.
- [192] E. K. Sinner, W. Knoll, *Curr. Opin. Chem. Biol.*, **2001**, *5*, 705-711.
- [193] M. Tanaka, E. Sackmann, *Nature*, **2005**, *437*, 656-663.
- [194] C. Rossi, J. Chopineau, *Eur. Biophys. J.*, **2007**, *36*, 955-965.

- [195] W. Knoll, C. W. Frank, C. Heibel, R. Naumann, A. Offenhausser, J. Ruhe, E. K. Schmidt, W. W. Shen, A. Sinner, *Rev. Mol. Biotechnol.*, **2000**, *74*, 137-158.
- [196] N. Bunjes, E. K. Schmidt, A. Jonczyk, F. Rippmann, D. Beyer, H. Ringsdorf, P. Graeber, W. Knoll, R. Naumann, *Langmuir*, **1997**, *13*, 6188-6194.
- [197] A. Foertig, R. Jordan, K. Graf, G. Schiavon, O. Prucker, M. Tanaka, *Macromol. Symp.*, **2004**, *210*, 329-338.
- [198] S. M. Schiller, R. Naumann, K. Lovejoy, H. Kunz, W. Knoll, *Angew. Chem. Int. Ed.*, **2003**, *42*, 208-211.
- [199] P. Mansky, Y. Liu, E. Huang, T. P. Russell, C. Hawker, *Science*, **1997**, *275*, 1458-1460.
- [200] K. Norrman, A. Ghanbari-Siahkali, N. B. Larsen, *Annu. Rep. Prog. Chem., Sect. C*, **2005**, *101*, 174-201.
- [201] G. Decher, *Science*, **1997**, *277*, 1232-1237.
- [202] M. L. Wagner, L. K. Tamm, *Biophys. J.*, **2000**, *79*, 1400-1414.
- [203] K. B. Blodgett, *J. Am. Chem. Soc.*, **1935**, *57*, 1007-1022.
- [204] I. Langmuir, V. J. Schaefer, *J. Am. Chem. Soc.*, **1938**, *60*, 2803-2810.
- [205] H. Lang, C. Duschl, H. Vogel, *Langmuir*, **1994**, *10*, 197-210.
- [206] V. Von Tscharner, H. M. McConnell, *Biophys. J.*, **1981**, *36*, 409-419.
- [207] M. P. Goertz, L. E. Marks, G. A. Montaña, *J. Am. Chem. Soc.*, **2012**, *6*, 1532-1540.
- [208] B. Zhao, W. J. Brittain, *Prog. Polym. Sci.*, **2000**, *25*, 677-710.
- [209] A. Jagoda, J. Kowal, M. Delcea, C. G. Palivan, W. Meier; bookchapter in *Biomaterials Surface Science*, Wiley-VCH Verlag GmbH & Co. KGaA, Weinheim, Germany, **2013**.
- [210] T. Rosenkranz, A. Katranidis, D. Atta, I. Gregor, J. Enderlein, M. Grzelakowski, P. Rigler, W. Meier, J. Fitter, *ChemBioChem*, **2009**, *10*, 702-709.
- [211] K. Langowska, C. G. Palivan, W. Meier, *Chem. Commun.*, **2013**, *49*, 128-130.
- [212] K. Langowska, J. Kowal, C. G. Palivan, W. Meier, *J. Mater. Chem. B*, **2014**, *2*, 4684-4693.
- [213] O. Casse, O. Colombani, K. Kita-Tocarczyk, A. H. E. Müller, W. Meier, A. Taubert, *Faraday Discuss.*, **2008**, *139*, 179-197.
- [214] A. Jagoda, M. Zinn, E. Bieler, W. Meier, K. Kita-Tokarczyk, *J. Mater. Chem. B*, **2013**, *1*, 368-378.
- [215] C. L. Draghici, J. Kowal, A. Darjan, W. Meier, C. G. Palivan, *Langmuir*, **2014**, *30*, 11660-11669.
- [216] X. Zhang, W. Fu, C. Palivan, W. Meier, *Scientific reports* *3*, **2013**, 2196, 1-7.
- [217] J. L. Kowal, J. K. Kowal, D. Wu, H. Stahlberg, C. G. Palivan, W. Meier, *Biomaterials*, **2014**, *35*, 7286-7294.

[218] E. Rakhmatullina, A. Manton, T. Burgi, V. Malinova, W. Meier, *J. Polym. Sci. Part A: Polym. Chem.*, **2008**, *47*, 1-13.

2. Scope of the thesis

2.1. Aim and motivation

The research work in this thesis aimed at developing novel biomimetic nanostructures based on amphiphilic triblock copolymers membranes in solution and on solid supports. For both systems, synthesis as well as physical and chemical characterization were conducted.

In solution, these self-assembled structures were investigated as potential intracellular drug delivery systems. At first, we studied the influence of the chain length and the hydrophilic to hydrophobic ratio on the macromolecular self-assembly. Then, the ability of these self-assemblies to encapsulate and release small molecules was investigated. For the release process, a strategy was developed for the disintegration of nanostructures in the way that the degradation products would be either water-soluble or could potentially be cleared from the body or cells. Also, the block copolymers were designed in order to be further used as polymeric bilayers on solid supports.

On solid substrates, systems based on amphiphilic triblock copolymers were developed that mimic the structure of cell membranes and that allow for the insertion of membrane proteins. Of particular interest was the effect of the membrane density on the membrane's ability to host functional pore-forming proteins. First, we investigated the best synthesis strategy to build a suitable matrix that allowed channel protein reconstitution inside an artificial membrane. For this purpose, the block copolymers mentioned above were used for consecutive monolayer transfers on solid supports. In parallel, polymer brushes were synthesized directly from the surface. For this second system, the effect of grafting density on the self-assembly behavior of the brushes and on protein reconstitution were studied. Upon insertion of compatible channel proteins, these systems could find their potential applications as biosensor devices.

2.2. Strategies and approaches

The self-assembled structures in solution and the solid supported polymer membranes are based on methacrylate amphiphilic triblock copolymers, made of poly (2-hydroxyethyl methacrylate)-*block*-poly (butyl methacrylate)-*block*-poly (2-hydroxyethyl methacrylate) (PHEMA-*b*-PBMA-*b*-PHEMA), that exhibit a hydrophilic-hydrophobic-hydrophilic structure. Their self-assembly was studied in solution and on surfaces. PHEMA and PBMA are interesting choices as polymers for biomedical applications because of their biocompatibility and biodegradability.^[1, 2] Furthermore, the –OH groups from PHEMA allow further functionalization for specific use. For the synthesis of this triblock copolymer in solution and on solid supports, atom transfer radical polymerization (ATRP) was used. ATRP is a robust technique since

it can fine-tune well-designed polymers with narrow polydispersity index.^[3, 4] Polydispersity is actually a key parameter both for the self-assembly in solution and for the homogeneity of polymer brushes on surfaces. PBMA was also chosen for its mobility, as it is one of the most flexible hydrophobic polymer that can be synthesized by ATRP, with a glass transition temperature of 20°C-27°C.^[5, 6]

As mentioned above, PHEMA-*b*-PBMA-*b*-PHEMA self-assembled in solution to form nanostructures that can be further used as potential intracellular drug delivery systems. To study the effect of the chain structure on the self-assembly and to favor the formation of nanoobjects, hydrophilic to hydrophobic ratio as well as the polymers chain length were varied. Here, the triblock copolymer was designed as a reduction-sensitive amphiphilic block copolymer. The characteristic feature of these polymeric structures is their cleavable disulfide bond in the center of the hydrophobic block, obtaining the polymer PHEMA-*b*-PBMA-S-S-*b*-PBMA-*b*-PHEMA. Therefore, the triblock copolymer can be cleaved into amphiphilic diblock copolymers. As the degradation products of the nanoobjects are amphiphilic, they should therefore allow for facile clearing from biological systems. Moreover, the self-assembly can be cleaved by using biological reducing agents such as glutathione. As concentration gradients of this reducing agent are commonly found in biological systems, the nanostructures could be used as redox-sensitive nanocarriers for the intracellular delivery of drugs.

Also, planar membranes on solid supports were elaborated in order to mimic the cell membrane. Actually, their hydrophilic-hydrophobic-hydrophilic configuration exhibits a similar structure as lipid bilayers. PHEMA-*b*-PBMA-S-S-*b*-PBMA-*b*-PHEMA used above for the formation of nanoobjects was investigated as a membrane mimic by consecutive Langmuir transfer techniques, Langmuir-Blodgett (LB) and Langmuir-Schaefer (LS), on gold supports. Then, the possibility of channel protein insertion into this obtained artificial bilayer membrane was studied using both attenuated total reflectance Fourier transform infrared spectroscopy (ATR-FTIR) and electrochemical impedance spectroscopy (EIS).

In addition, PHEMA-*b*-PBMA-*b*-PHEMA was synthesized directly from gold substrates using surface-initiated ATRP to obtain homogeneous membranes with minor defects. As packing density is a key parameter for protein insertion, the “grafting-from” approach was selected instead of the “grafting-to” and the vesicle spreading because of the possibility to control over the polymer grafting density. By varying the grafting density, a potential matrix for the insertion of channel protein can be found. The control over the packing density can be monitored with surface-sensitive technique such as neutron reflectivity. However, a spacer between the solid substrate and the polymeric membrane is needed to avoid protein denaturation by contact with the surface. For that, the ATRP initiator molecule containing a disulfide bond will be covalently attached to the gold surface, forming a self-assembled monolayer (SAM). This initiator SAM acts as a spacer between the membrane and the metallic substrate. Along with the covalent attachment to the initiator molecule, gold is an interesting choice as a solid support for its dielectric properties, useful for surface-sensitive characterization methods, such as surface plasmon

resonance (SPR), neutron reflectivity or polarization modulated infrared reflection absorption spectroscopy (PM-IRRAS). Moreover, gold dielectric properties may also find their use for the insertion of channel proteins using electrochemical impedance spectroscopy (EIS).^[7, 8] Furthermore, recent work showed solvent response of amphiphilic triblock copolymer PHEMA-*b*-PBMA-*b*-PHEMA through their reversible rehydration.^[9] Therefore, because of this solvent response, upon insertion of channel proteins, this membrane can be potentially used as air-stable and reusable biosensor devices.

2.3. References

- [1] B. D. Ratner, T. Horbett, A. S. Hoffmann, S. D. Hauschka, *Journal of Biomedical Materials Research*, **1975**, 9, 407-422.
- [2] S. M. Derkaoui, A. Labbé, A. Purnama, V. Gueguen, C. Barbaud, T. Avramoglu, D. Letourneur, *Acta Biomaterialia*, **2010**, 6, 3506-3513.
- [3] W. A. Braunecker, K. Matyjaszewski, *Prog. Polym. Sci.*, **2007**, 32, 93-146.
- [4] K. Matyjaszewski, *Macromolecules*, **2012**, 45, 4015-4039.
- [5] D. K. Aktaş, *Phase Transitions*, **2006**, 79, 863-873.
- [6] G. Fytas, A. Patkowski, G. Meier, T. Dorfmueller, *Journal of Chemical Physics*, **1984**, 80, 2214-2220.
- [7] X. Zhang, W. Fu, C. Palivan, W. Meier, *Scientific reports* 3, **2013**, 2196, 1-7.
- [8] J. L. Kowal, J. K. Kowal, D. Wu, H. Stahlberg, C. G. Palivan, W. Meier, *Biomaterials*, **2014**, 35, 7286-7294.
- [9] E. Rakhmatullina, A. Manton, T. Bürgi, V. Malinova, W. Meier, *J. Polym. Sci. Part A: Polym. Chem.*, **2008**, 47, 1-13.

3. Self-organization behavior of methacrylate-based reduction-sensitive amphiphilic triblock copolymers in solution

Parts of this chapter were published in: S. Toughraï, V. Malinova, R. Masciadri, S. Menon, P. Tanner, C. G. Palivan, N. Bruns, W. Meier, “Reduction-Sensitive Amphiphilic Triblock Copolymers Self-Assemble into Stimuli-Responsive Micelles for Drug Delivery”, *Macromolecular Bioscience*, **2014**, DOI: 10.1002/mabi.201400400.

3.1. Introduction

Stimuli-responsive amphiphilic block copolymers that self-assemble into well-defined nanostructures have a great potential for many applications, such as nanoreactors or controlled drug delivery systems.^[1-3] The self-assembly of amphiphilic block copolymers with designed architectures, including diblock,^[4-7] triblock,^[8-10] but also dendritic^[11-13] and graft^[14] copolymers, has been shown to result in the formation of various supramolecular structures, such as micelles and vesicles.^[15-17] These nanostructures are regarded as good candidates for the encapsulation and controlled intracellular delivery of drugs and other biological compounds.^[18] For many of them, the underlying strategy is the use of an external stimulus, like temperature,^[2, 19] pH^[2] or light,^[20] to induce destabilization of micelles or vesicles, hence triggering the release of a payload.^[21, 22] The structures can be destabilized, *e.g.*, by modifying the hydrophilic block,^[22-24] by selectively degrading one block,^[25-27] or by cleaving a linker between blocks.^[20, 28, 29] Redox-responsive drug-delivery nanovehicles take advantage of naturally occurring reducing agents, such as glutathione.^[30, 31] The concentration of glutathione in cytosol, mitochondria and cellular nuclei is around 2-10 mM; whereas the concentration in extracellular fluids is 500-1000 times lower.^[32-34] This concentration gradient can be harnessed to trigger the disruption of carriers and the release of their cargo within cells.^[33-35] A common reduction-sensitive motif is the disulfide bond. Cleavage of S-S bonds in redox-responsive polymer nanovehicles can be achieved with concentrations of glutathione similar to those in intracellular environment.^[36] Reduction of S-S bonds of polymers has also been reported with chemical reducing agents such as TCEP, cysteine or DTT, *e.g.* for the release of doxorubicin.^[36-38] Moreover, a combination of reducing agent and high intensity focused ultrasound allowed fine-tuning of the release kinetics of payload from polymeric micelles.^[39] Various redox-sensitive nanostructures such as reversible shell-crosslinked or core-crosslinked micelles, as well as micelles with a reductively degradable core have been demonstrated to release therapeutic payloads in response to intracellular level of glutathione.^[34] Most of the reduction-responsive systems are made of block copolymers that feature a hydrophilic block A linked by a disulfide-containing linker to a hydrophobic block B, *i.e.* with a structure A-S-S-B.^[28] Polymers that were used in such redox-responsive block copolymer systems were often poly(ethylene glycol) (PEG) in combination with biodegradable polymers such as polyesters (poly(lactic

acid), poly (γ -methyl- ϵ -caprolactone))^[37] or polypeptides.^[1] The cleavage of the S-S bond in this kind of polymers yields hydrophilic and hydrophobic homopolymers. One dilemma with such systems is that the hydrophobic residues can accumulate in the body, especially if the biodegradation of the hydrophobic block is slow.^[34] This can make the application of such systems in drug delivery problematic. Reduction-sensitive polymers with a different molecular architecture can circumvent this problem. Sun *et al.* reported amphiphilic polyamide amine-*graft*-polyethylene glycol copolymers with S-S bonds in the hydrophobic main chain.^[40] Poly (2-hydroxyethyl methacrylate) hydrogels with a disulfide-containing crosslinker were synthesized by Ejaz *et al.* and yield hydrophilic polymers upon reduction.^[41]

Here we present reduction-sensitive nanostructures for intracellular drug delivery that are based on amphiphilic triblock copolymers with a disulfide bond in the middle of the hydrophobic block, *i.e.* with an A-B-S-S-B-A (hydrophilic-hydrophobic-S-S-hydrophobic-hydrophilic) architecture. This structure results in amphiphilic A-B-SH diblock copolymers upon cleavage of the S-S bond. The degradation products are either water-soluble or self-assemble into new nanoobjects and could therefore potentially be cleared from the body or cells. The nanovehicles presented in this study are attractive candidates for intracellular drug delivery systems that could circumvent the problem of accumulation of hydrophobic polymers. We studied the capability of these systems to encapsulate and release payloads, and investigated the dynamic behavior of the structures obtained after its degradation with reducing agents. A-B-S-S-B-A block copolymers with poly (2-hydroxyethyl methacrylate) (PHEMA) as the hydrophilic block and poly (butyl methacrylate) (PBMA) as the hydrophobic part were synthesized by sequential atom transfer radical polymerization (ATRP) from a bifunctional bromoisobutyrate initiator containing an internal disulfide.^[42] ATRP was used since it is a robust technique towards functional groups and a versatile living/controlled polymerization that affords well-defined copolymers.^[43, 44] PHEMA and PBMA are interesting choices for biomedical applications because both polymers are biocompatible.^[45, 46] In this chapter, two triblock copolymer systems were synthesized and characterized. Both systems are different by their chain length and their hydrophilic to hydrophobic ratio in order to investigate the differences in their self-assembly in solution. Systems that can lead to micelles or vesicles in solution will be further considered for release studies.

3.2. Results and discussion

3.2.1. Formation of micelles

3.2.1.1. Synthesis of triblock copolymer

The bifunctional ATRP initiator 11,11'-dithiobis [1-(2-bromo-2-methylpropionyloxy)undecane] was synthesized. It bears a cleavable disulfide bond in the middle of the molecule and bromine groups at each end. It was used to initiate the polymerization of BMA by ATRP with CuBr/PMDETA as catalyst, yielding a Br-(PBMA_m-S-S-PBMA_m)-Br macroinitiator. The latter was used to initiate the polymerization of HEMA, yielding a triblock copolymer PHEMA_n-b-(PBMA_m-S-S-PBMA_m)-b-PHEMA_n (for simplicity termed ABA1 in this text) (Figure 3-1).

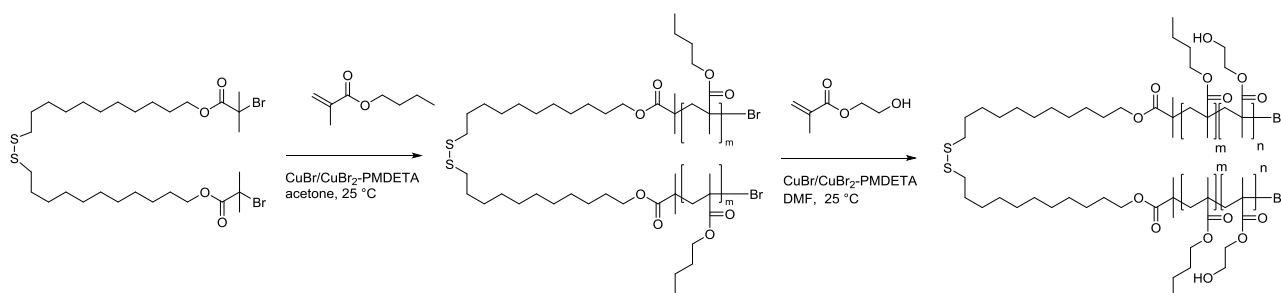


Figure 3-1: Synthesis of PHEMA_n-b-(PBMA_m-S-S-PBMA_m)-b-PHEMA_n triblock copolymer ABA1.

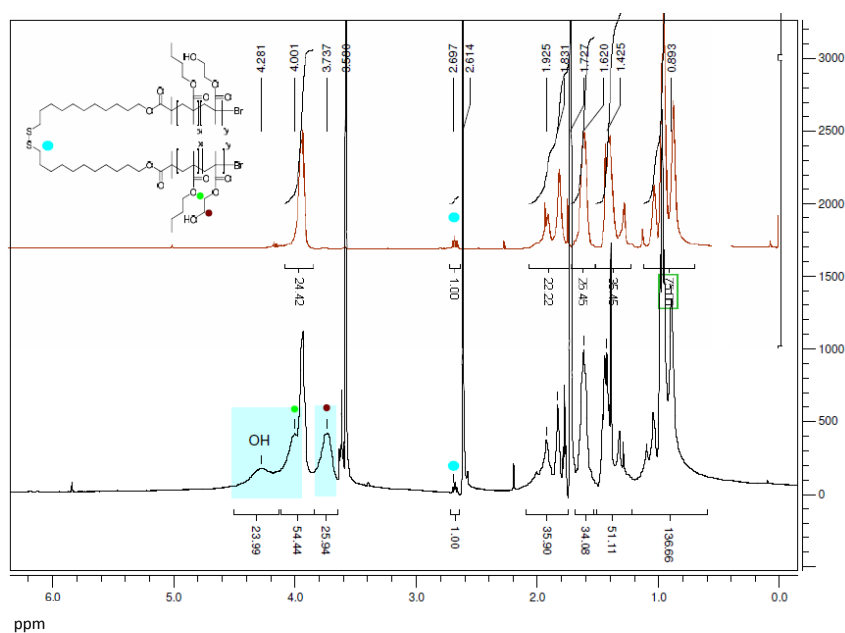


Figure 3-2: ¹H NMR spectra of Br-(PBMA₂₅-S-S-PBMA₂₅)-Br (B1) and PHEMA₂₅-b-(PBMA₂₅-S-S-PBMA₂₅)-b-PHEMA₂₅ (ABA1).

The degree of polymerization and the molecular weight of both macroinitiator and triblock copolymer were determined by ^1H NMR and GPC (Figures 3-2 and 3-3) and are reported in Table 3-1. The GPC curves of the copolymer revealed a clear shift toward higher molecular weight when compared to the Br-(PBMA_m-S-S-PBMA_m)-Br macroinitiator. Moreover, the triblock copolymer traces were unimodal.

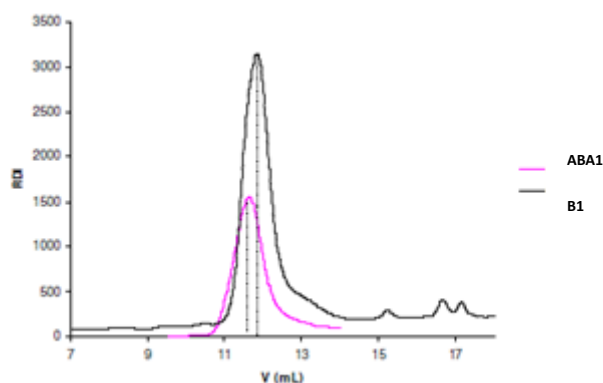


Figure 3-3: GPC traces of Br-(PBMA₂₅-S-S-PBMA₂₅)-Br (B1) and PHEMA₂₅-b-(PBMA₂₅-S-S-PBMA₂₅)-b-PHEMA₂₅ (ABA1).

Table 3-1: Characteristics of macroinitiator B1 and block copolymer ABA1.

Polymer	Structure	DP ^a (PBMA)	DP ^a (PHEMA)	M _n (NMR) (g/mol)	M _n (GPC) (g/mol)	PDI ^b	f ^c
B1	Br-(PBMA ₂₅ -S-S-PBMA ₂₅)-Br	50	--	7815	7690	1.3	--
ABA1	PHEMA ₂₅ -b-(PBMA ₂₅ -S-S-PBMA ₂₅)-b-PHEMA ₂₅	50	50	14320	11460	1.6	0.83

^a Degree of polymerization (DP) values calculated from ^1H NMR. ^b Polydispersity index (PDI) obtained by GPC, using poly (methyl methacrylate) standards. ^c Hydrophilic to hydrophobic ratio as M_n(PHEMA)/M_n(PBMA).

3.2.1.2. Formation of the self-assembled structures

The self-assembly was performed with ABA1 polymers under conditions described in the experimental part (see section 7.2.2. in Chapter 7). ABA1 formed micelles, as confirmed by dynamic and static light scattering (DLS and SLS) and transmission electron microscopy (TEM) (Figures 3-4 and 3-5).

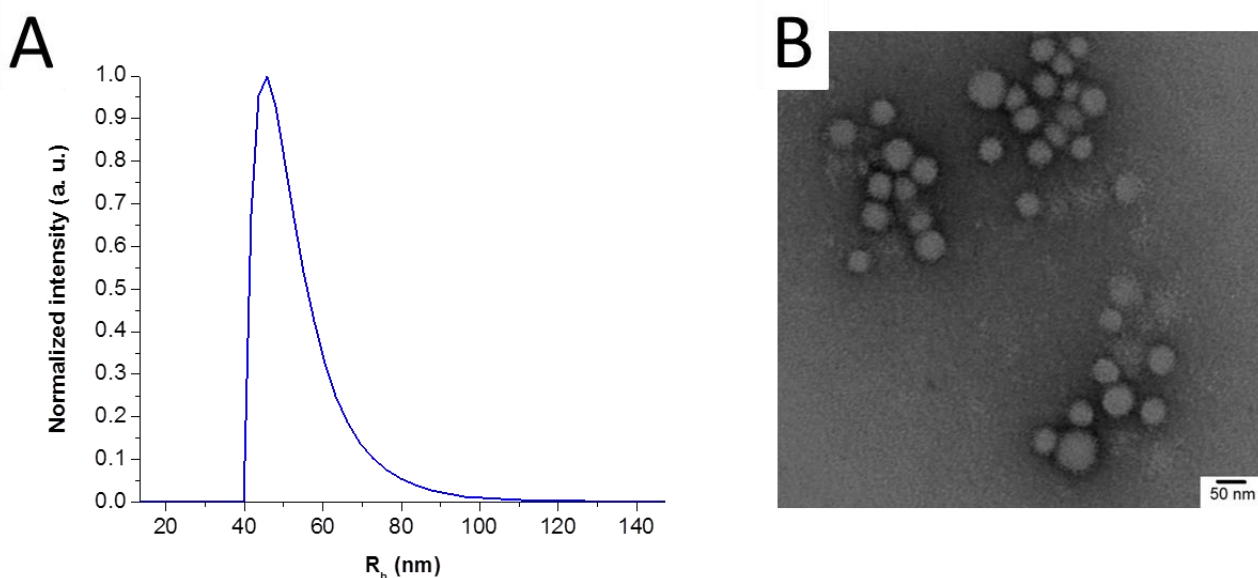


Figure 3-4: A) Number-averaged size distribution obtained by dynamic light scattering (DLS) at 90° of a self-assembled ABA1 solution in water; B) TEM micrograph of micelles formed by self-assembly of ABA1 in water. Concentration 0.1 mg mL^{-1} .

The DLS-derived size distribution histogram of the ABA1 solution shows one population with a hydrodynamic radius (R_h) of $44 \pm 3 \text{ nm}$, which are most probably micelles. SLS data (using cumulant analysis and Zimm plots, see Figure 3-5) gave a radius of gyration (R_g) of 108 nm, $R_h = 145 \text{ nm}$ and a ratio R_g/R_h of 0.74. This ratio is close to 0.78, which is the typical value for hard-sphere micelles.^[47] However, SLS was measured with a polymer concentration range from 0.1 to 1.0 mg mL^{-1} and the presence of aggregates along with the micelles was observed in concentrations above 0.5 mg mL^{-1} . This may explain the differences in the hydrodynamic radii between DLS and SLS. TEM micrographs reveal the presence of special structures of diameters ranging from 40 to 60 nm, in good agreement with the dynamic light scattering data. The combination of all this data implies that ABA1 block copolymers self-assembled into micelles.

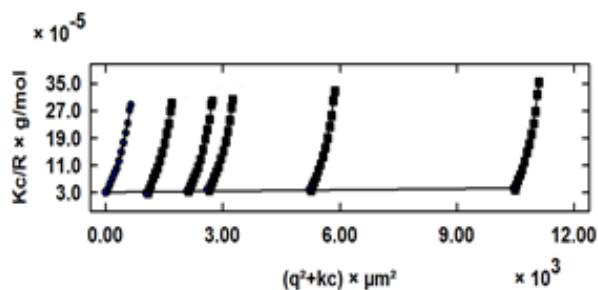


Figure 3-5: SLS measurements of ABA1. Measurements were performed from 30° to 150° . Zimm plot model, q :2nd order and c :1st order. Concentration range: 0.1 to 1.0 mg mL^{-1} .

In order to estimate the long-term stability of the self-assemblies, an aliquot of a micellar solution was stored at room temperature for two years and measured by DLS and TEM thereafter. TEM micrographs revealed similar particle sizes and shapes as the freshly prepared solutions, and DLS shows similar

hydrodynamic radius ($R_h = 40 \pm 2$ nm) (see *Figure 3-6*). Therefore, the micelles remained the same and were stable.

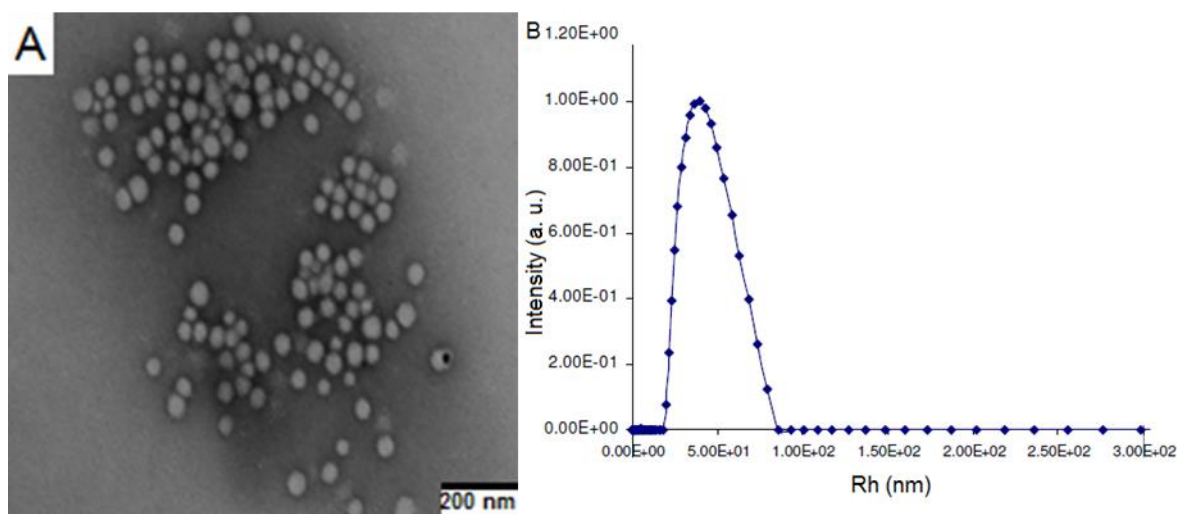


Figure 3-6: A) TEM micrograph showing ABA1 micelles after 2 years of storage at room temperature; B) Number-averaged size distribution obtained by dynamic light scattering (DLS) at 90° of ABA1 after 2 years at room temperature. Concentration of polymer = 0.1 mg mL⁻¹.

3.2.1.3. Degradation of redox-sensitive block copolymers in organic solvents

Prior studying the degradation process of the self-assemblies in solution, a preliminary experiment was conducted to investigate the disulfide bond cleavage upon reduction in an organic environment. GPC data show that the addition of tributylphosphine to ABA1 resulted in a shift towards smaller M_w after 2h, 5h, and 24h, proving the cleavage of the polymer in organic solvent (*Figure 3-7*).

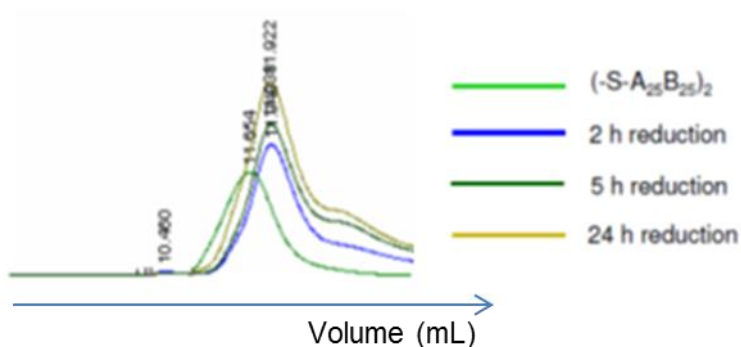


Figure 3-7: GPC traces of ABA1 during reduction with tributylphosphine (after 2h, 5h and 24h reduction).

3.2.1.4. Degradation of the self-assembled structures upon reduction of the disulfide bond

For a better understanding of the release process of small molecules from such polymeric micelles, degradation studies in aqueous solutions were conducted. To this end, disulfide bonds in the self-assembled structures were cleaved with two different reducing agents, TCEP and glutathione. TCEP was chosen as a chemical reducing agent because it performs selective, fast and complete reduction of disulfide bonds^[48] and it is resistant to air oxidation. Glutathione is also selective, fast and efficient in reducing S-S bonds. Importantly, glutathione is present inside of cells^[30-34] and is therefore a suitable agent to investigate S-S reduction under biological relevant conditions. DLS and TEM were performed in order to observe the changes in size over time (*Figures 3-8 and 3-9*). In both reduction scenarios (*e.g.* TCEP and glutathione), an increase of the particle sizes of ABA1 micelles was observed by DLS within the first 4 hours (*Figures 3-8 and 3-10*). Large particles were formed with hydrodynamic radii between 150 and 450 nm during the first hour and above 500 nm after 2 hours. Most likely, the observed increase in particle size is due to the formation of aggregates from totally or partially disintegrated micelles after addition of the reducing agents. TEM images support this hypothesis. The micrograph in *Figure 3-9A* was recorded after 1 hour of reduction with glutathione and shows not only aggregates, but also the formation of particles with diameters that range from 100 to 200 nm. After 3 hours of reduction, particles with diameters from 50 to 120 nm were formed, with the presence of agglomerates (*Figure 3-9B*). Most probably, upon reduction of the disulfide bond, the resultant amphiphilic diblock copolymer PHEMA_m-PBMA_n-SH reassembled to larger particles. The agglomeration of those particles may explain the increase in particles size observed by DLS. DLS measurements that were conducted after 24 h of reduction revealed apparent R_h between 1 to 2 μ m, independent of the reducing agent used (see *Figures 3-8 and 3-10*). As macroscopic aggregates were observed by eye, these findings indicate the complete disruption and aggregation of the previous formed particles. The resulting aggregates were too large to be detectable by light scattering methods.

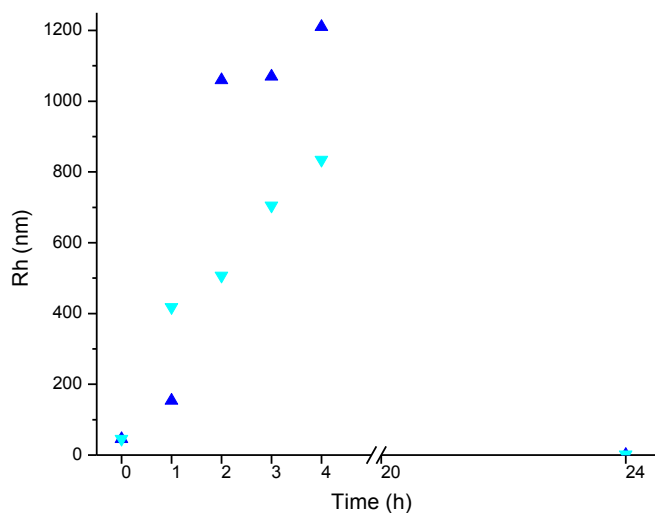


Figure 3-8: Evolution of R_h vs. time for ABA1 upon reduction with TCEP (▲) and glutathione (▼). The particle size increased within the first 4 hours, proving that the cleaved polymers formed aggregates and larger particles. After 24h, apparent R_h is between 1 and 2 nm, indicating the complete disruption of the micelles.

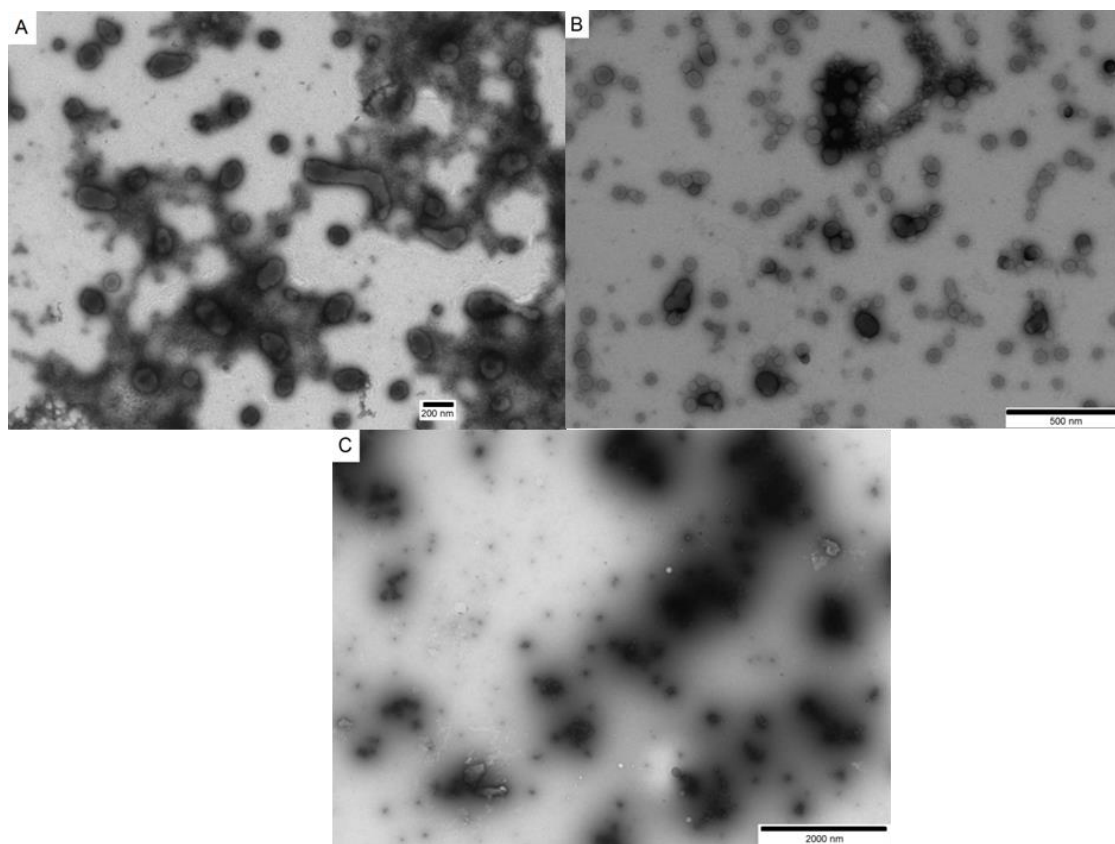


Figure 3-9: Morphology change observed by TEM micrographs of ABA1 micelles: A) After 1 h reduction. B) After 3 h reduction. C) After 24 h reduction. Reducing agent: 17.5 mM glutathione.

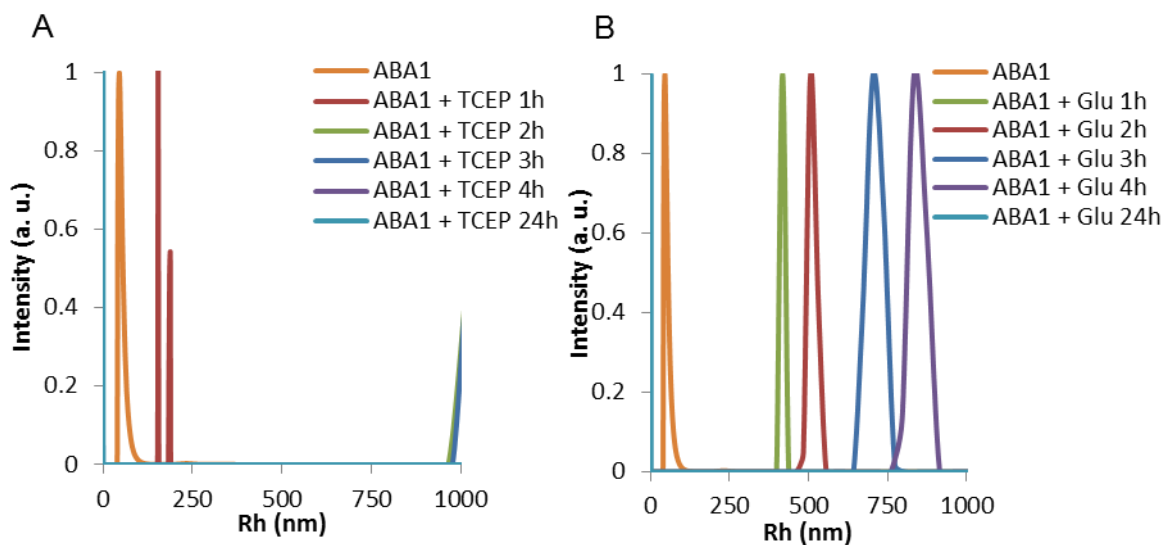


Figure 3-10: Evolution of number-averaged size distributions obtained by DLS at 90° of ABA1 during reduction with TCEP (A) and glutathione (B) (after 1h, 2h, 3h, 4h, and 24 h). As DLS does not give reliable results from $R_h > 1000$ nm because of the formation of aggregates, the size distributions histograms are only presented from 0 to 1000 nm.

The degradation of the ABA polymers upon the reduction of the disulfide bond was also investigated by the ThioGlo assay, which is commonly used to determine the presence of SH groups.^[49] In these experiments, TCEP was used as a reducing agent because it does not interfere with the conjugation of free thiols with the maleimide moiety of the ThioGlo-5 reagent.^[48] An increase in the fluorescence intensity over time was observed for the micelles mixed with the TCEP solution, which can be explained by the cleavage of the disulfide bond, and the reaction of the resulting free thiol groups with the ThioGlo reagent (Figure 3-11).

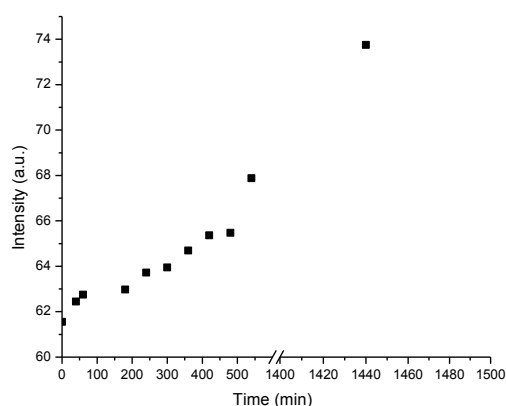


Figure 3-11: Formation of free thiol groups upon reduction of ABA1 micelles with TCEP as determined by the ThioGlo assay. Fluorescence (maximum emission intensity at $\lambda = 525$ nm) vs. time of reduction.

3.2.1.5. Encapsulation and release of low molecular weight molecules

In order to test whether the polymeric micelles can be used as redox-responsive nanovehicles, the encapsulation and the release of small hydrophobic molecules were studied. Micelles were loaded with hydrophobic dyes by adding Nile Red and BodiPy 630/650, respectively, to polymer solutions during the self-assembly process. TEM micrographs of micelles that were prepared in the presence of BodiPy show that the hydrophobic cargo did not change the morphology of the self-assemblies (*Figure 3-12A*). In order to determine the concentration of encapsulated BodiPy in the micelles, UV-vis spectra of BodiPy-loaded micelles were recorded. The spectrum of encapsulated BodiPy in micelles shows BodiPy's maximum absorbance at 630 nm, indicating the presence of the dye (see *Figure 3-12B*). The concentration of BodiPy in the polymeric solution at the beginning of the self-assembly process was 72 μM . Inside the micelles the concentration was 11 μM (see *Figure 3-13* for the calibration curve). Therefore, an encapsulation efficiency of 15 % was achieved. Both observations from TEM and UV-vis prove that the self-assemblies were able to encapsulate hydrophobic guests. The fluorescence of Nile Red strongly depends on the polarity of the dye's environment. In hydrophobic surroundings the dye fluoresces, while in water it does not fluoresce. A calibration curve that reliably quantifies the concentration of the dye in the hydrophobic polymer phase of the micelles could not be obtained and therefore the encapsulation efficiency of Nile Red could not be determined.

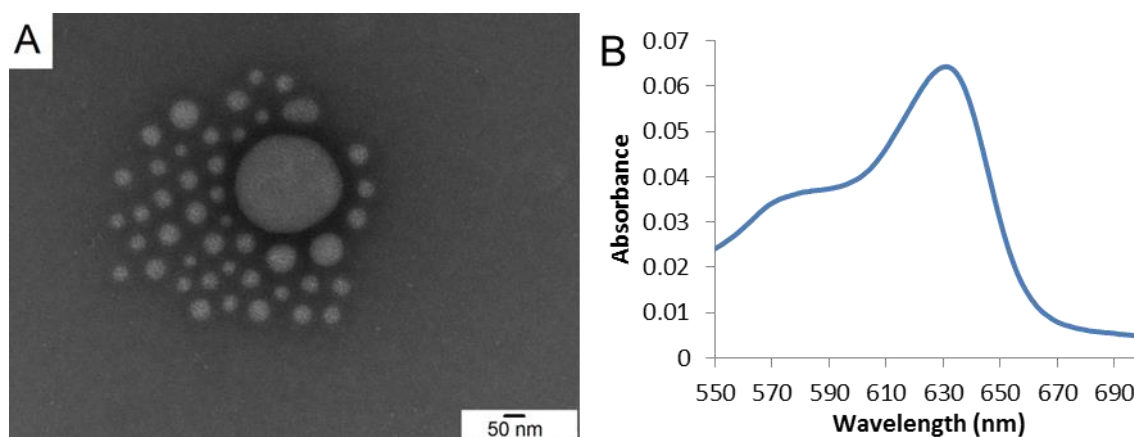


Figure 3-12: A) TEM micrograph of ABA1 micelles that encapsulate BodiPy 630/650. B) UV-vis spectrum of encapsulated BodiPy in micelles, showing the characteristic absorbance band of BodiPy with a maximum at 630 nm.

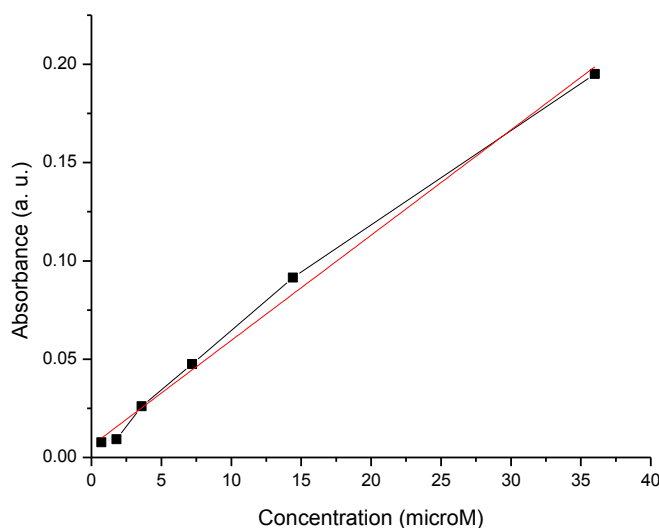


Figure 3-13: Calibration curve of dilution series of BodiPy 630/650. Absorbance (maximum absorbance at $\lambda = 630$ nm) vs. BodiPy concentration. The red solid line corresponds to the linear fit.

The release of Nile Red upon reduction of micelles was followed by fluorescence spectroscopy. Glutathione caused a strong decrease of the fluorescence intensity within the first hour, due to release of dye from the hydrophobic core of micelles into water (*Figures 3-14A and 3-16A*). The fluorescence continued to decrease slightly for 9 hours, indicating a continued release of dye. Not surprisingly, reduction of empty micelles did not result in fluorescence. Nile Red-loaded micelles that were incubated in the absence of a reducing agent retained their fluorescence (*Figure 3-16A*). Therefore, the observed release of dye in the presence of reducing agents was caused by the reduction of the polymers and not by a diffusion of dye from the micelles. Reduction with TCEP gave similar results (*Figure 3-14B*). Within the first 45 minutes the fluorescence intensity of loaded micelles decreased to approximately one third of its initial value. The loss of fluorescence continued at longer reduction times, and the fluorescence intensity reached zero within 24 hours. This indicates that the whole amount of encapsulated Nile Red was released. The combination of these results along with the DLS and TEM data allows drawing the following conclusion: the self-assembled polymer micelles lose their stability within the first hour of reduction by aggregating and starting to form particles. This leads to a pronounced release of their payload. The formed particles probably retain or encapsulate residual dye, which is then slowly released while the amphiphilic A-B-SH block copolymers further aggregate.

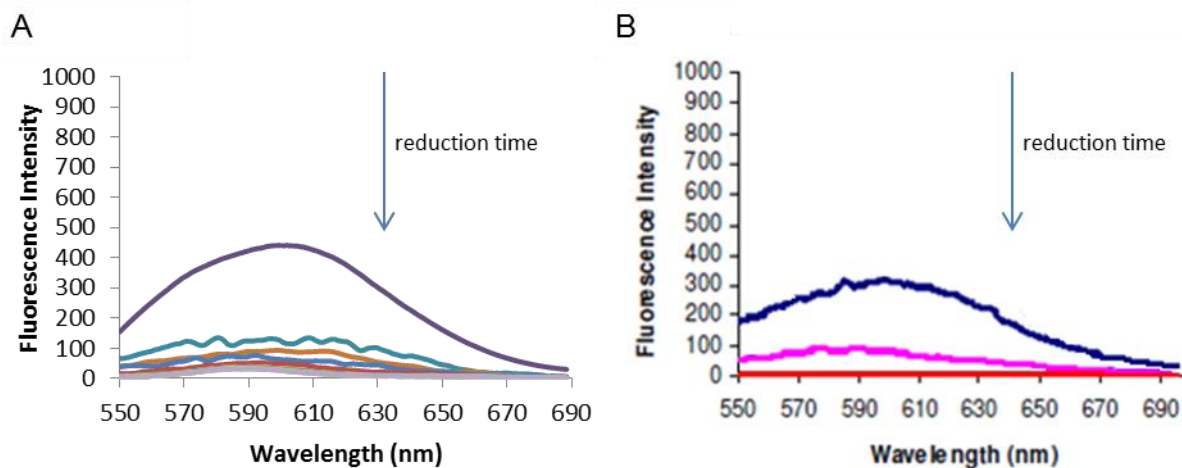


Figure 3-14: Fluorescence spectra of Nile Red-loaded micelles upon reduction with glutathione recorded every 5 minutes during the first hour, then every 2 hours over a time of 8 hours (A), and with TCEP after 45 minutes and 24 hours (B), showing a decrease in fluorescence over time.

Fluorescence correlation spectroscopy (FCS) was used to gain further insight into the glutathione-triggered release of payloads from ABA1 micelles because it is a very sensitive method, detecting at a single molecule level. Moreover, FCS allows determining the size of polymeric nanostructures present in solution. These experiments were carried out with BodiPy 630/650 instead of Nile Red, because the latter dye immediately forms aggregates in aqueous solution and can therefore not be quantified by FCS. The normalized autocorrelation curves of dye-loaded micelles and of free dye are presented in Figure 3-15. The encapsulation of BodiPy in micelles shifted the curve to significant higher diffusion times. These curves allow calculating diffusion times of the fluorophore and as a consequence the hydrodynamic radius of the diffusing species according to the Stokes-Einstein equation.^[50] The autocorrelation data of free BodiPy was fitted with a single component function and resulted in a diffusion time of $42 \pm 1 \mu\text{s}$ and a R_h around 0.4 nm. This size is close to the theoretical value of 0.6 nm, based on the molecular weight of the dye. The autocorrelation curve of the dye-containing micelle solution had to be fitted taking two populations into account. The first population, which contributed to 40% of the signal, had a diffusion time of $3.2 \pm 1 \text{ ms}$. This translates into a hydrodynamic radius of $33 \pm 10 \text{ nm}$ which indicates that BodiPy was encapsulated in the micelles. The FCS-derived size of the micelles is in agreement with the radius and diameter of micelles calculated from DLS and TEM data (Figure 3-4). The second population had a larger diffusion time of $22 \pm 4 \text{ ms}$ (population size 60%) and, consequently, a larger hydrodynamic radius of around 200-230 nm. Most likely this population consisted in dye-containing aggregates, as the presence of micellar aggregates was observed for polymer concentrations $> 0.5 \text{ mg mL}^{-1}$ (used here for FCS measurements).

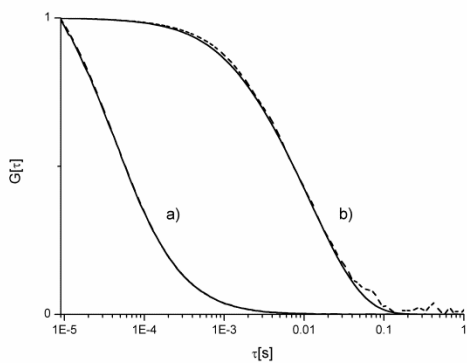


Figure 3-15: Normalized FCS auto-correlation curves (experimental data: dotted lines, fitted data: continuous lines) obtained for (a) a solution of free BodiPy in water based on a single component autocorrelation function and (b) a solution of encapsulated micelles with BodiPy 630/650 in water based on a two-component autocorrelation function.

In order to follow the release of BodiPy from the micelles, the micelles were treated with the reducing agent glutathione using the same procedure as with fluorescence measurements. FCS measurements were performed in regular time intervals (*Figure 3-16B*). Nearly 80 % of the dye in micelles and aggregates vanished with the first 13 min of reduction and dye-filled micelles and dye-containing aggregates vanished. The fraction of free dye slowly increased upon longer reduction time. Most of the dye was released within 30 min after the start of the experiment.

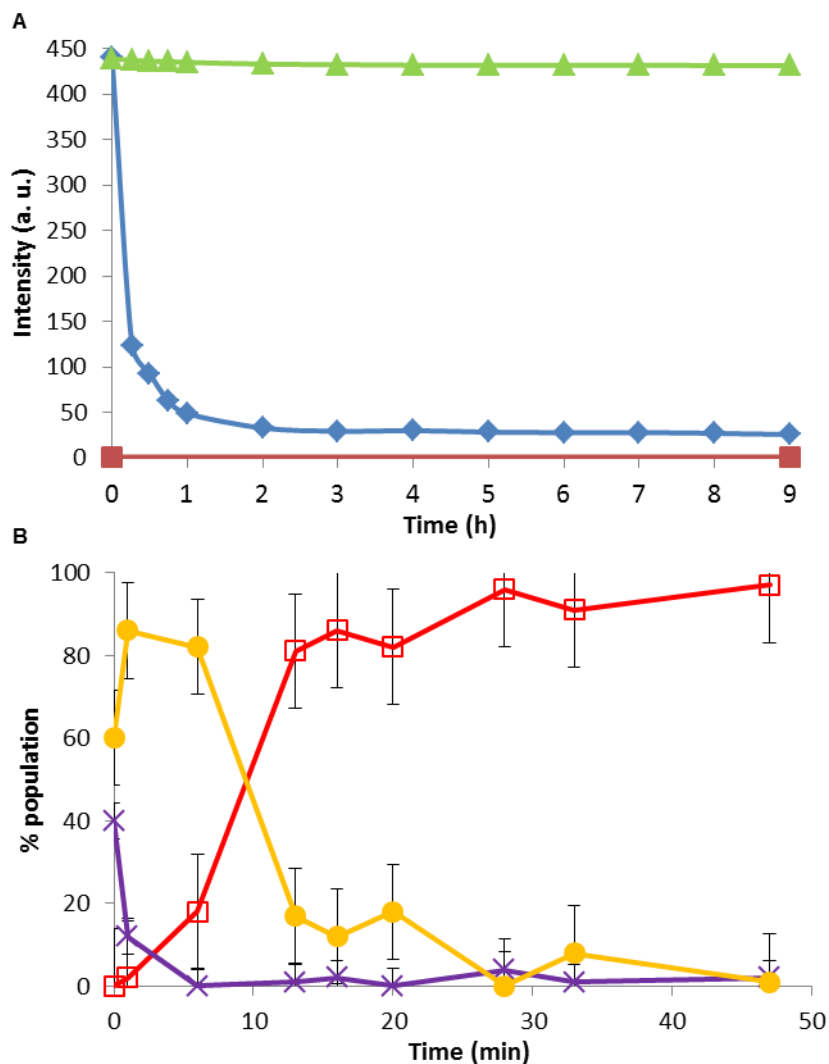


Figure 3-16: Reduction-triggered release of hydrophobic payloads from ABA1 micelles. A) Plot of fluorescence vs. reduction time with glutathione for Nile Red-loaded micelles (♦) and empty micelles as control experiment (■); Nile-Red-loaded-micelles in the absence of reducing agent (▲) (maximum emission intensity at $\lambda = 600$ nm). B) FCS-detectable species during reduction of BodiPy 630/650-loaded self-assembled polymer structures with glutathione: free dye (□), micelles (X) and aggregates (●). The release was fitted with three-component auto-correlation function (free dye, micelles, and aggregates).

3.2.2. Formation of nanoparticles

3.2.2.1. Synthesis of triblock copolymer

The synthesis and the characterization of the triblock copolymer ABA2 were conducted the same way as previously for the ABA1 polymer. The polymerization of BMA and HEMA in ABA2 as well as the degree of polymerization and the molecular weight were evidenced similarly to ABA1 (see Figures 3-17 and 3-18 and Table 3-2).

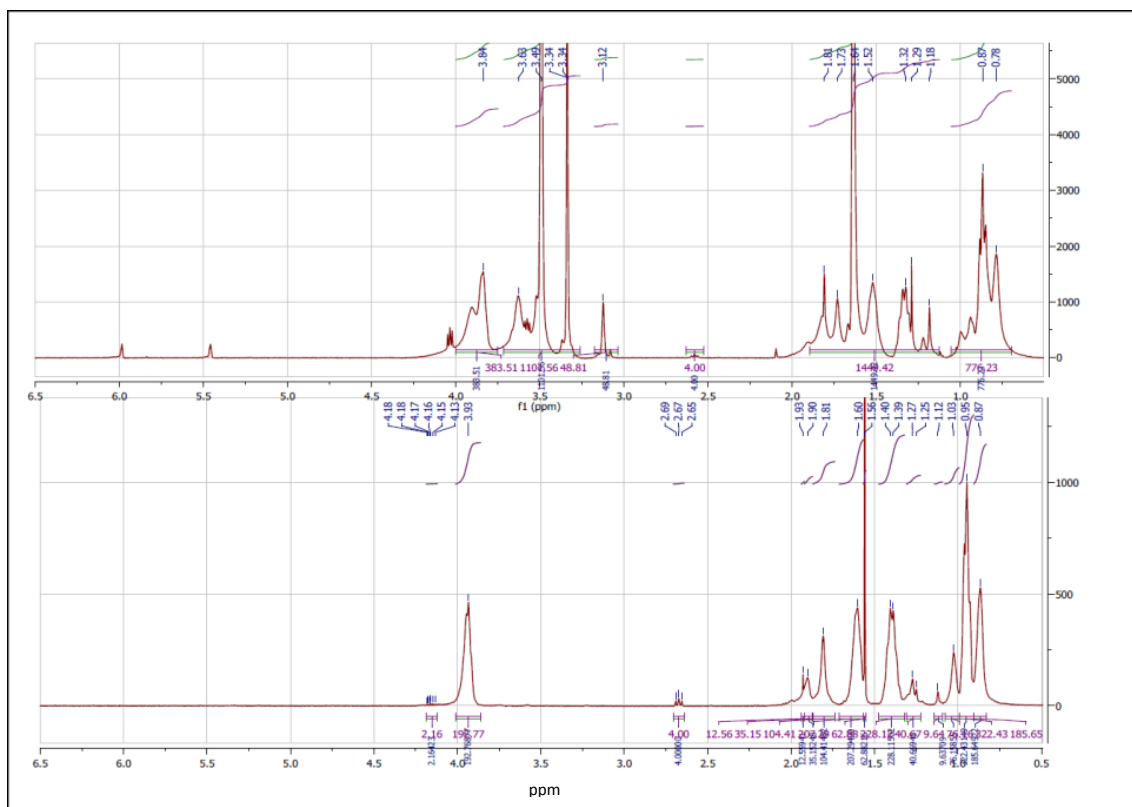


Figure 3-17: ^1H NMR spectra of $\text{Br}-(\text{PBMA}_{20}\text{-S-S-PBMA}_{20})\text{-Br}$ (B2) and $(\text{PHEMA}_{13}\text{-}b\text{-}(\text{PBMA}_{20}\text{-S-S-PBMA}_{20})\text{-}b\text{-PHEMA}_{13})$ (ABA2).

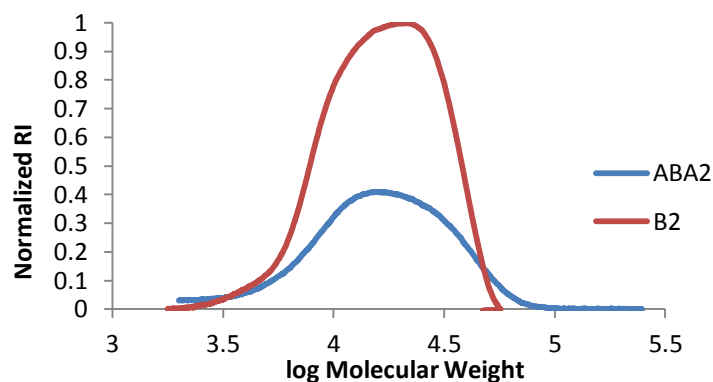


Figure 3-18: GPC traces of $\text{Br}-(\text{PBMA}_{20}\text{-S-S-PBMA}_{20})\text{-Br}$ (B2) and $(\text{PHEMA}_{13}\text{-}b\text{-}(\text{PBMA}_{20}\text{-S-S-PBMA}_{20})\text{-}b\text{-PHEMA}_{13})$ (ABA2).

Table 3-2: Characteristics of macroinitiator B2 and block copolymer ABA2.

Polymer	Structure	DP ^a (PBMA)	DP ^a (PHEMA)	M _n (NMR) (g/mol)	M _n (GPC) (g/mol)	PDI ^b	f ^c
B2	$\text{Br}-(\text{PBMA}_{20}\text{-S-S-PBMA}_{20})\text{-Br}$	40	--	7530	7680	1.5	--
ABA2	$\text{PHEMA}_{13}\text{-}b\text{-}(\text{PBMA}_{20}\text{-S-S-PBMA}_{20})\text{-}b\text{-PHEMA}_{13}$	40	26	11070	12275	1.6	0.47

^a Degree of polymerization (DP) values calculated from ^1H NMR. ^b Polydispersity index (PDI) obtained by GPC, using poly (methyl methacrylate) standards. ^c Hydrophilic to hydrophobic ratio as $M_n(\text{PHEMA})/M_n(\text{PBMA})$.

3.2.2.2. Formation of the self-assembled structures

Self-assembly of ABA2 polymer was performed under identical conditions as with ABA1.

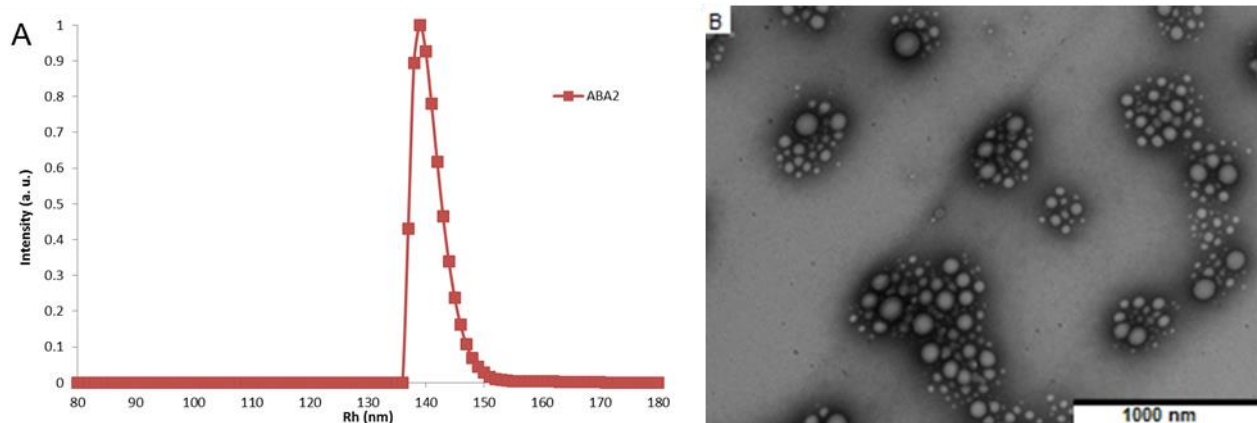


Figure 3-19: A) Number-averaged size distribution obtained by dynamic light scattering (DLS) at 90° of ABA2; B) TEM micrograph showing formation of ABA2 nanoparticles in water. Concentration 0.1 mg mL^{-1} .

The size distribution histogram of ABA2 solution shows one population with $R_h = 129 \pm 12 \text{ nm}$ (Figure 3-19A). SLS data (using cumulant analysis and Zimm plots, see Figure 3-20) gave $R_g = 136 \text{ nm}$ and $R_h = 139 \text{ nm}$, and a ratio of 0.98 between R_g and R_h . This value is comparable to the theoretical value given for hollow spheres ($R_g/R_h = 1.0$),^[51] and may indicate the formation of polymer vesicles. TEM micrographs reveal the presence of spherical structures of diameters ranging from 100 to 200 nm, and only a few smaller ones (diameter $< 100 \text{ nm}$) (Figure 3-19B).

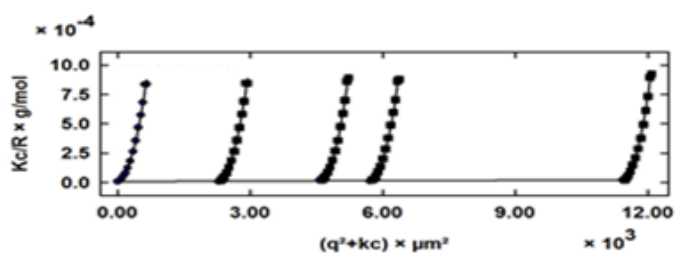


Figure 3-20: SLS measurements of ABA2. Measurements were performed from 30° to 150° . Zimm plot model, q :2nd order and c :1st order. ABA2: concentration range: 0.1 to 0.5 mg mL^{-1} .

In order to confirm the presence of polymeric vesicles, *i.e.* hollow spheres, cryo-TEM experiments were performed. The micrographs reveal the presence of spherical structures with diameters range from 100 to 300 nm (see Figure 3-21). However, even if previous light scattering data indicate the formation of vesicles, the absence of the characteristic membrane usually present in polymersomes proved that the polymers self-assembled into polymeric nanoparticles, *i.e.* into filled spheres.

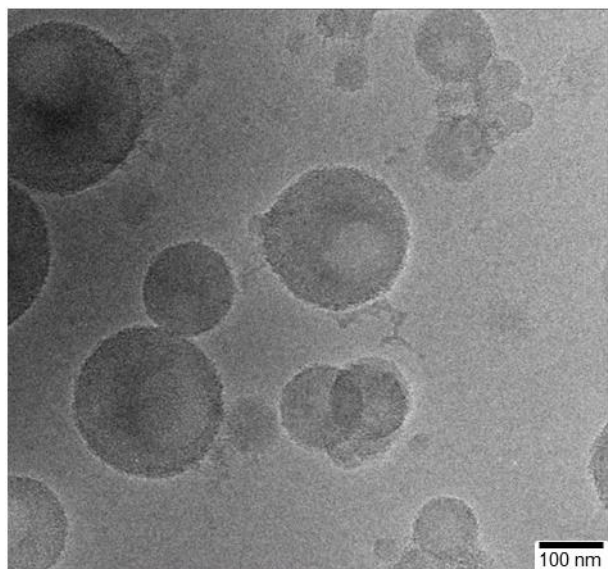


Figure 3-21: Visualization of hard spheres nanoparticles by cryo-TEM. Concentration 1.0 mg mL^{-1} .

The storage stability of the self-assemblies was estimated by measuring with DLS and TEM an aliquot of a polymer solution stored at room temperature for two years. Similar particle sizes and shapes as the freshly prepared solutions were shown by TEM micrographs (Figure 3-22A) and similar hydrodynamic radius ($R_h = 128 \pm 11 \text{ nm}$) was measured by DLS (see Figure 3-22B). Therefore, the nanoparticles remained the same and were stable.

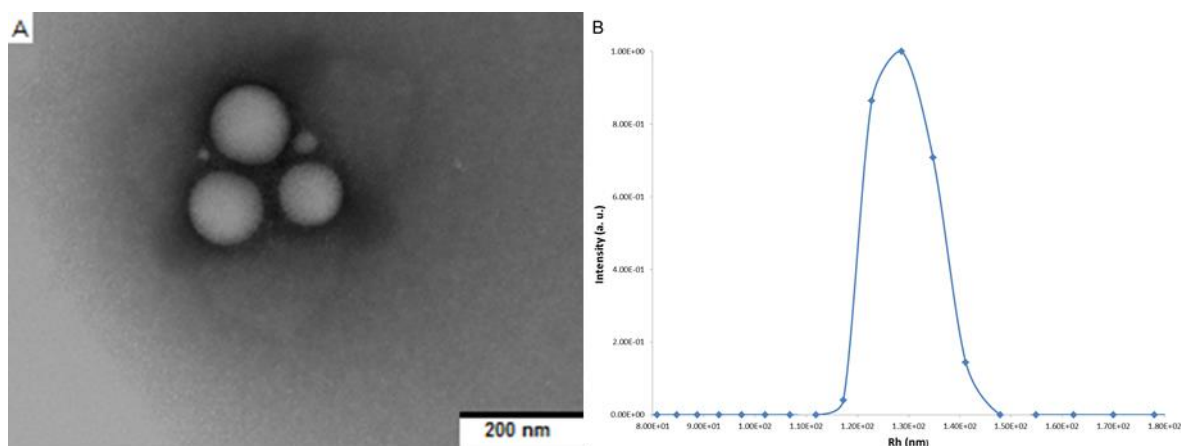


Figure 3-22: A) TEM micrograph showing ABA2 nanoparticles after 2 years of storage at room temperature; B) Number-averaged size distribution obtained by dynamic light scattering (DLS) at 90° of ABA2 after 2 years at room temperature. Concentration of polymer = 0.1 mg mL^{-1} .

3.2.2.3. Degradation of the self-assembled structures upon reduction of the disulfide bond

Degradation studies were conducted for a better understanding of the behavior of the self-assemblies after splitting their disulfide bond. To this end, the cleavage of the disulfide bond was performed under the same conditions as for ABA1, using the same reducing agents, *e.g.* TCEP and glutathione. The changes over time in shape and size were monitored by DLS and TEM. In both reduction scenarios, DLS data reveal an increase of the particles size of ABA2 nanoparticles during the first 4 hours (see *Figures 3-23 and 3-24*). The formation of larger nanoparticles was observed, with hydrodynamic radii between 200 and 300 nm during the first 2 hours and above 600 nm after 3 hours. This observed increase in particle size is most probably due to the formation of aggregates from disintegrated nanoparticles after addition of the reducing agent. Also, the changes in size and shape during reduction were observed by TEM micrographs (*Figure 3-25*), with the formation of aggregates and broken nanoparticles (see *Figure 3-25A*). This is in a good agreement with DLS data. Most likely, this particle increase is due to the reformation of aggregates from the totally or partially disintegrated nanoparticles after addition of both reducing agents. However, 24 hours after reduction, micelles and micellar aggregates with a size of 50 nm in diameter were formed (*Figure 3-25B*). Most probably, upon reduction of the disulfide bond beyond 4 hours, the resultant amphiphilic diblock copolymers PHEMA_m-PBMA_n-SH reaggregated to micelles. Also, according to DLS, a decrease in the particles size occurred after 24 hours of reduction, with a R_h close to zero (see *Figures 3-23, 3-24A and 3-24B*), supposing the complete disruption of particles. However, micelles were observed in TEM micrographs (*Figure 3-25B*). This result can be explained by dissolution of the aggregates into individual polymer chains at a polymer concentration below the CMC that cannot be detected by DLS. Moreover, CMC could not be detected by surface tension, proving that individual polymer chains along with few micellar structures were formed after 24 hours.

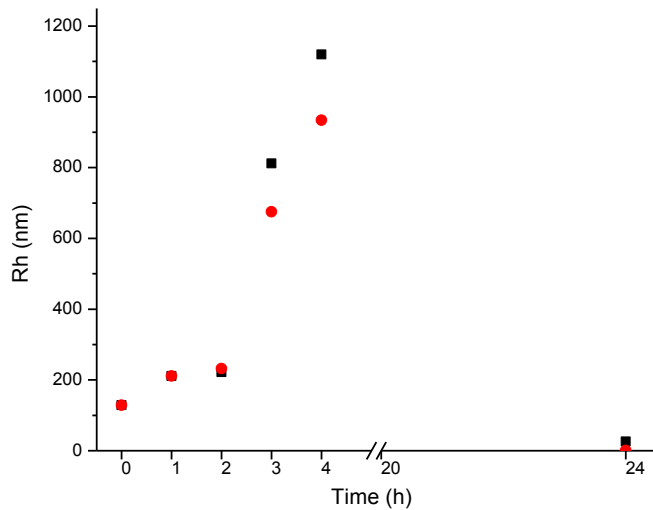


Figure 3-23: Evolution of R_h vs. time for ABA2 during reduction with TCEP (■) and glutathione (●). The particles size increased within the first 4 hours, proving that the cleaved polymers formed aggregates. After 24h, R_h is close to zero, indicating that the aggregates dissolved or formed micelles.

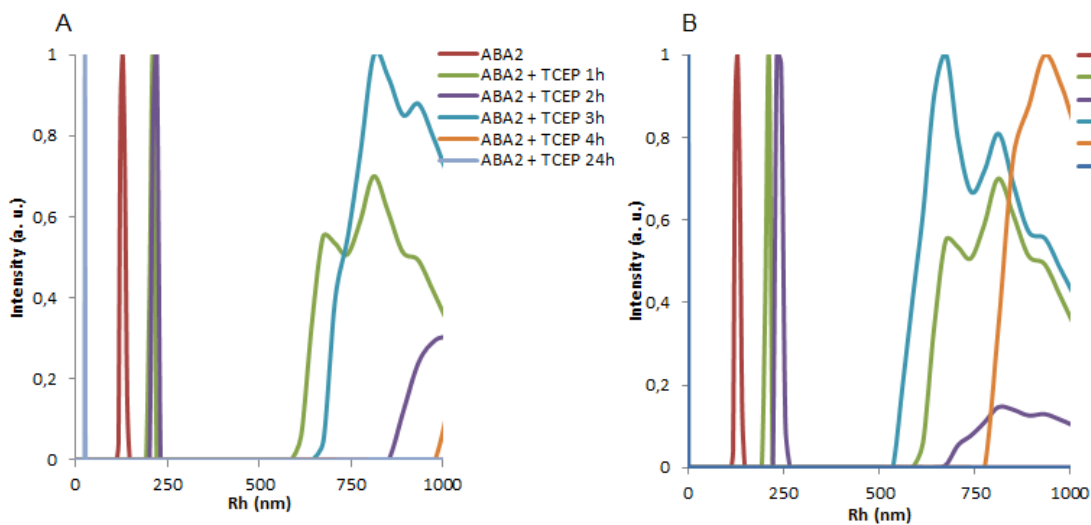


Figure 3-24: Evolution of number-averaged size distributions obtained by DLS at 90° of ABA2 during reduction with TCEP (A) and glutathione (B) (after 1h, 2h, 3h, 4h, and 24 h). As DLS does not give reliable results from $R_h > 1000$ nm because of the formation of aggregates, the size distributions histograms are only presented from 0 to 1000 nm.

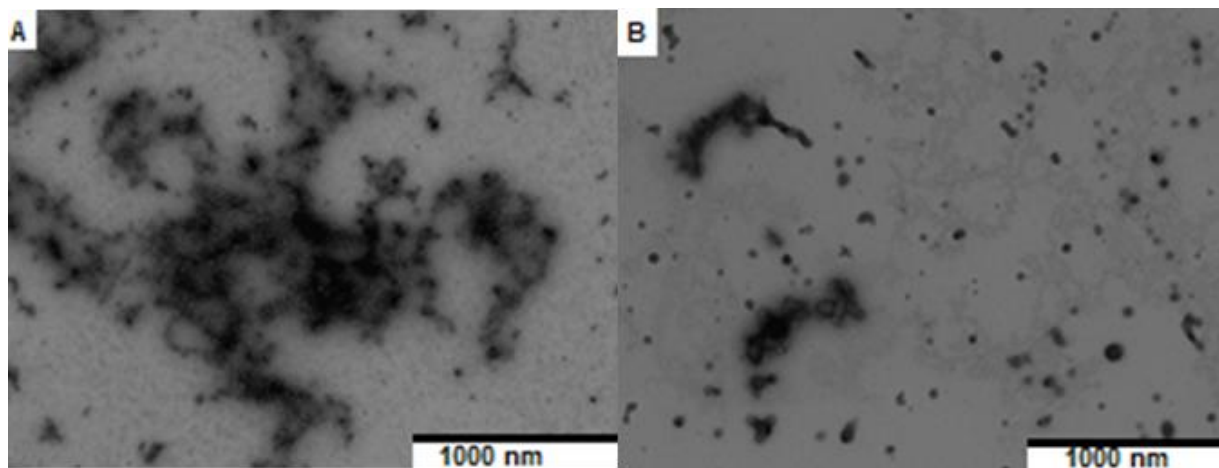


Figure 3-25: Morphology change observed by TEM micrographs of ABA2 nanoparticles: A) after 1 h reduction, aggregates B), after 24h reduction, micelles and micellar aggregates. Reducing agent: 17.5 mM glutathione.

Similarly to ABA1 micelles, the degradation of the ABA polymers upon the reduction of the disulfide bond was also investigated by the ThioGlo assay. A significant increase in the fluorescence intensity over time was observed for the nanoparticles mixed with the TCEP solution, which is the result of the cleavage of the disulfide bond, and the reaction of the resulting free thiol groups with the ThioGlo reagent (Figure 3-26).

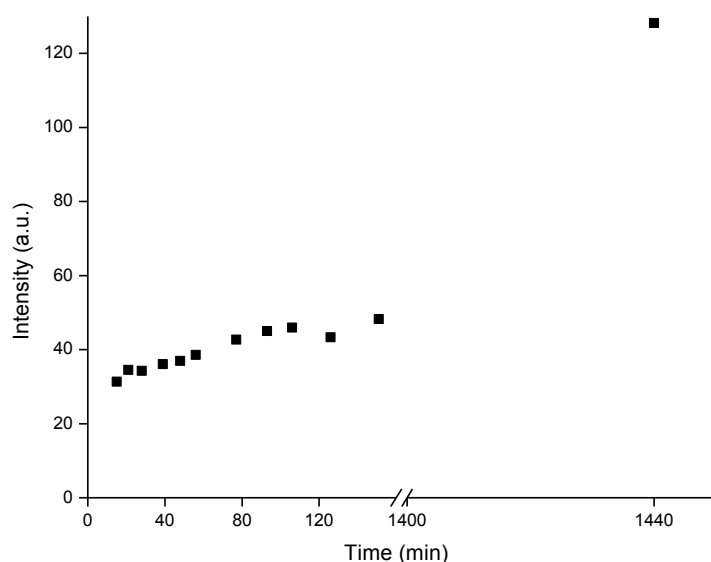


Figure 3-26: Formation of free thiols groups upon reduction of ABA2 nanoparticles with TCEP as determined by the ThioGlo assay. Fluorescence (maximum emission intensity at $\lambda = 515$ nm) vs. time of reduction with TCEP.

3.3. Conclusions and outlook

Novel amphiphilic triblock copolymers with a disulfide bond as a redox-sensitive functional group within the main chain of the hydrophobic block were synthesized. These polymers self-assembled into micelles and nanoparticles. The disulfide bond of these polymers can be broken by a reduction with a chemical (TCEP) or a biological (glutathione) reducing agent, resulting in two amphiphilic block copolymers that either form larger particles and latter aggregate, or aggregate and then form particles. Destabilization of the micelles via reduction of disulfide bond triggered the successful release of payloads from the system. The release of hydrophobic model substances from the micelles show that these self-assembled nanostructures could serve as efficient reduction-sensitive systems for intracellular drug delivery. Further investigations, such as modification of the micelles with targeting ligands and in vitro drug delivery assays would elucidate the full potential of these polymer-based nanostructures. However, prior to in vitro studies, cell viability tests on those polymeric systems should be investigated. Also, residual THF from the self-assembly with the co-solvent method should be removed in order to circumvent a cause of possible toxicity of the nanoobjects. Alternatively, the micelles could be used for the encapsulation of supra paramagnetic iron oxide nanoparticles (SPION) inside the hydrophobic core of the micelles for targeted and controlled therapy.^[52] Similarly, the functionalization of our polymeric nanoparticles could lead to a novel system based on targeted ligand for cancer chemotherapy.^[53] Moreover, in a more chemical aspect, further investigations in the synthesis and characterization of the triblock copolymers could be also conducted by varying the chain lengths or the hydrophilic to hydrophobic ratios for a same chain length in order to study their self-assembly behaviors in aqueous solution or to establish a phase diagram of this system.

3.4. References

- [1] M.-H. Li, P. Keller, *Soft Matter*, **2009**, *5*, 927-937.
- [2] F. Meng, Z. Zhong, J. Feijen, *Biomacromolecules*, **2009**, *10*, 197-209.
- [3] K. Renggli, P. Baumann, K. Langowska, O. Onaca, N. Bruns, W. Meier, *Advanced Functional Materials*, **2011**, *21*, 1241-1259.
- [4] H. Bermudez, A. K. Brannan, D. A. Hammer, F. S. Bates, D. E. Discher, *Macromolecules*, **2002**, *35*, 8203-8208.
- [5] B. M. Discher, Y.-Y. Won, D. S. Ege, J. C. M. Lee, F. S. Bates, D. E. Discher, D. A. Hammer, *Science*, **1999**, *284*, 1143-1146.
- [6] H. Kukula, H. Schlaad, M. Antonietti, S. Förster, *J. Am. Chem. Soc.*, **2002**, *124*, 1658-1663.
- [7] L. Zhang, A. Eisenberg, *Science*, **1995**, *268*, 1728-1731.
- [8] C. Nardin, T. Hirt, J. Leukel, W. Meier, *Langmuir*, **2000**, *16*, 1035-1041.
- [9] A. Wittemann, T. Azzam, A. Eisenberg, *Langmuir*, **2007**, *23*, 2224-2230.
- [10] W. Zhao, D. Chen, Y. Hu, G. M. Grason, T. P. Russell, *ACS Nano*, **2011**, *5*, 486-492.
- [11] J. del Barrio, L. Oriol, C. Sanchez, J. L. Serrano, A. Di Cicco, P. Keller, M.-H. Li, *J. Am. Chem. Soc.*, **2010**, *132*, 3762-3769.
- [12] Z. Shi, Y. Zhou, D. Yan, *Macromol. Rapid Commun.*, **2008**, *29*, 412-418.
- [13] J. C. M. van Hest, D. A. P. Delnoye, M. W. P. L. Baars, M. H. P. van Genderen, E. W. Meijer, *Science*, **1995**, *268*, 1592-1595.
- [14] H. J. Lee, S. R. Yang, E. J. An, J.-D. Kim, *Macromolecules*, **2006**, *39*, 4938-4940.
- [15] A. Choucair, A. Eisenberg, *Eur. Phys. J. E*, **2003**, *10*, 37-44.
- [16] R. C. Hayward, D. J. Pochan, *Macromolecules*, **2010**, *43*, 3577-3584.
- [17] S. J. Holder, N. A. J. M. Sommerdijk, *Polym. Chem.*, **2011**, *2*, 1018-1028.
- [18] O. Onaca, R. Enea, D. W. Hughes, W. Meier, *Macromol. Biosci.*, **2009**, *9*, 129-139.
- [19] J. E. Chung, M. Yokoyama, M. Yamato, T. Aoyagi, Y. Sakurai, T. Okano, *Journal of Controlled Release*, **1999**, *62*, 115-127.
- [20] E. Cabane, V. Malinova, S. Menon, C. G. Palivan, W. Meier, *Soft Matter*, **2011**, *7*, 9167-9176.
- [21] S. Qin, Y. Geng, D. E. Discher, S. Yang, *Adv. Mater.*, **2006**, *18*, 2905-2909.
- [22] F. Ahmed, D. E. Discher, *J. Controlled Release*, **2004**, *96*, 37-53.
- [23] J. Du, Y. Tang, A. L. Lewis, S. P. Armes, *J. Am. Chem. Soc.*, **2005**, *127*, 17982-17983.
- [24] A. Napoli, M. Valentini, N. Tirelli, M. Muller, J. A. Hubbell, *Nat. Mater.*, **2004**, *3*, 183-189.
- [25] F. Ahmed, R. I. Pakunlu, A. Brannan, F. Bates, T. Minko, D. E. Discher, *J. Controlled Release*, **2006**, *116*, 150-158.

- [26] P. P. Ghoroghchian, G. Li, D. H. Levine, K. P. Davis, F. S. Bates, D. A. Hammer, M. J. Therien, *Macromolecules*, **2006**, *39*, 1673-1675.
- [27] F. Meng, C. Hiemstra, G. H. M. Engbers, J. Feijen, *Macromolecules*, **2003**, *36*, 3004-3006.
- [28] S. Cerritelli, D. Velluto, J. A. Hubbell, *Biomacromolecules*, **2007**, *8*, 1966-1972.
- [29] S. Lin, F. Du, Y. Wang, S. Ji, D. Liang, L. Yu, Z. Li, *Biomacromolecules*, **2007**, *9*, 109-115.
- [30] R. Cheng, F. Meng, C. Deng, Z. Zhong, in *Smart Materials for Drug Delivery: Volume 1*, Vol. 1, The Royal Society of Chemistry, **2013**, p. 208.
- [31] V. P. Torchilin, *Nat. Rev. Drug Discovery*, **2014**, *13*, 813-827.
- [32] R. Cheng, F. Feng, F. Meng, C. Deng, J. Feijen, Z. Zhong, *Journal of Controlled Release*, **2011**, *152*, 2-12.
- [33] D. J. Phillips, M. I. Gibson, *Antioxidants and Redox Signaling*, **2014**, *21*, 786-803.
- [34] H. Sun, F. Meng, R. Cheng, C. Deng, Z. Zhong, *Antioxidants and Redox Signaling*, **2014**, *21*, 755-767.
- [35] M. Huo, J. Yuan, L. Tao, Y. Wei, *Polym. Chem.*, **2014**, *5*, 1519-1528.
- [36] J. O. Kim, G. Sahay, A.V. Kabanov, T.K. Bronich, *Biomacromolecules*, **2010**, *11*, 919-926.
- [37] H. L. Sun, B. N. Guo, R. Cheng, F. H. Meng, H. Y. Liu, Z. Y. Zhong, *Biomaterials*, **2009**, *30*, 6358-6366.
- [38] T-B. Ren, W-J. Xia, H-Q. Dong, Y-Y. Li, *Polymer*, **2011**, *52*, 3580-3586.
- [39] Y. Li, R. Tong, H. Xia, H. Zhang, J. Xuan, *Chem. Commun.*, **2010**, *46*, 7739-7741.
- [40] Y. Sun, X. Yan, T. Yuan, J. Liang, Y. Fan, Z. Gu, X. Zhang, *Biomaterials*, **2010**, *31*, 7124-7131.
- [41] M. Ejaz, H. Yu, Y. Yana, D. A. Blake, R. S. Ayyala, S. M. Grayson, *Polymer*, **2011**, *52*, 5262-5270.
- [42] S. Belegriou, V. Malinova, R. Masciadri, W. Meier, *Synth. Comm.*, **2010**, *40*, 3000-3007.
- [43] W. A. Braunecker, K. Matyjaszewski, *Prog. Polym. Sci.*, **2007**, *32*, 93-146.
- [44] K. Matyjaszewski, *Macromolecules*, **2012**, *45*, 4015-4039.
- [45] B. D. Ratner, T. Horbett, A. S. Hoffmann, S. D. Hauschka, *Journal of Biomedical Materials Research*, **1975**, *9*, 407-422.
- [46] S. M. Derkaoui, A. Labbé, A. Purnama, V. Gueguen, C. Barbaud, T. Avramoglu, D. Letourneur, *Acta Biomaterialia*, **2010**, *6*, 3506-3513.
- [47] W. Burchard, *Combined static and dynamic light scattering*, in *Light Scattering-Principles and Development*, ed. W. Brown, Clarendon Press, Oxford, U.K., **1996**, 439-476.
- [48] Y. Li, B. S. Lokitz, S. P. Armes, C. L. McCormick, *Macromolecules*, **2006**, *39*, 2726-2728.
- [49] B. B. Hasinoff, X. Wu, O. V. Krokhin, W. Ens, K. G. Standing, J. L. Nitiss, T. Sivaram, A. Giorgianni, S. Yang, Y. Jiang, J. C. Yalowitch, *Molecular Pharmacology*, **2005**, *67*, 937-947.
- [50] A. Tcherniak, C. Reznik, S. Link, C. F. Landes, *Anal. Chem.*, **2009**, *81*, 746-754.
- [51] J. Hotz, W. Meier, *Langmuir*, **1998**, *14*, 1031-1036.

[52] C. Bonnaud, D. Vanhecke, D. Demurtas, B. Rothen-Rutishauser, A. Fink, *IEEE Transactions on magnetics*, **2013**, *49*, 166-171.

[53] Y. A. Zhong, F. H. Meng, C. Deng, Z. Y. Zhong, *Biomacromolecules*, **2014**, *15*, 1955-1969.

4. Solid-supported amphiphilic block copolymer membranes using Langmuir techniques

4.1. Introduction

Cell membranes are highly specialized and inherently complex multi-component assemblies, in which multiple chemical and structural processes occur simultaneously, such as in cellular differentiation, growth, and interactions with the environment.^[1, 2] They are essentially characterized by a “bilayer structure” that exhibits a finely tuned hydrophilic/hydrophobic balance.^[3] It is thus essential to study the membrane barrier properties as well as the changes that occur when membrane proteins incorporated into the lipid membrane are activated or blocked.^[4] In this context, artificial membranes meet increasing interest as model systems that mimic biomembranes and organelles or even whole cells.^[1, 2] Placing of model membranes on solid supports has become a very popular approach,^[5, 6] both for studying basic membrane processes and for possible biotechnological applications such as biosensing.^[7-10] Various systems have been suggested including solid-supported lipid bilayers,^[11, 12] polymer-cushioned lipid bilayers,^[13, 14] hybrid bilayers,^[15, 16] tethered lipid bilayers,^[17] suspended lipid bilayers,^[18, 19] or supported vesicular layers.^[20] A variety of methods to immobilize lipid bilayers on diverse solid substrates (glass, silicon, gold, platinum, etc) have been suggested.^[21] However, severe drawbacks such as lack of stability and “adaptability” limit technical applications of the lipid-based models.^[2, 3] Hence it is necessary to develop simplified biomimetic model membranes based on block copolymers attached to a surface. This offers inherent stability of the system due to the underlying supporting surface and allows the application of surface sensitive analytical techniques for monitoring of membrane-protein binding.^[22] Frequently, the synthetic block copolymer membranes are thicker,^[23] more stable,^[24] highly flexible and compressible, and the versatility of polymer chemistry allows adapting of relevant properties for a wide range of applications.^[22]

The aim of this work consists in mimicking biological cell membranes by developing novel bilayer films from artificial amphiphilic block copolymers. Easy routes for the creation of planar membranes made of poly (butadiene)-*b*-poly (ethylene oxide) (PB-PEO) by spreading micelles or vesicles have been previously described.^[25-27] Goertz *et al.* reported the adsorption of PB-PEO micelles on solid substrates, forming either bilayers or monolayers.^[25] Dorn *et al.* demonstrated the effectiveness of PB-PEO vesicles spreading on glass and on ultrasmooth gold surfaces.^[26] Also, spreading of polyelectrolyte vesicles made of poly (2,2-dimethylaminoethyl methacrylate)-*block*-poly (butyl methacrylate)-*block*-poly (2,2-dimethylaminoethyl methacrylate) (PDMAEMA-*b*-PBMA-*b*-PDMAEMA) on negatively charged silicon oxide and on mica substrates induced the formation of solid-supported block copolymer membranes.^[27] So far, the most recent achievements in the field of biomimetic membranes have been solid-supported amphiphilic polymeric bilayers covalently attached to a gold support.^[28] The inner leaflet of this bilayer

consists of sulfur-functionalized poly (butadiene)-*block*-poly (ethylene oxide) block copolymers (PB-PEO-LA) transferred with the Langmuir-Blodgett (LB) technique and the outer leaflet consists of hydroxyl-functionalized poly (butadiene)-*block*-poly (ethylene oxide) (PB-PEO-OH) polymers deposited with the Langmuir-Schaefer (LS) method. This system showed the characteristic hydrophilic-hydrophobic-hydrophilic structure similar to biological membranes. Moreover, the channel protein alpha-hemolysin (α -HL) was successfully incorporated into this polymeric system with the help of electrical current,^[29] having here the reconstitution of a real biomimetic membrane from amphiphilic block copolymers. Very recently, by using a similar approach, the successful reconstitution of potassium channel protein MloK1 into a polymeric bilayer based on poly (dimethylsiloxane)-*block*-poly (2-methyl-2-oxazoline) (PDMS-*b*-PMOXA) was reported.^[30]

Here, an approach is presented that uses methacrylate-based amphiphilic triblock copolymers as solid-supported biomimetic membranes. PHEMA₂₅-*b*-(PBMA₂₅-S-S-PBMA₂₅)-*b*-PHEMA₂₅ polymer (ABA1, see *Chapter 3*) was employed as potential membrane mimics, composed of amphiphilic triblock copolymers with an internal disulfide bond in the middle of the hydrophobic block. The molecular weight, the chain length as well as the flexibility of this block copolymer suggests the transfer of thin bilayers < 10 nm on solid supports, suitable for potential protein reconstitution. For protein insertion experiments, the tested proteins are Outer Membrane Protein F (OmpF), Aquaporin Z (AqpZ) and alpha-hemolysin (α -HL). OmpF is an E. Coli derived channel protein that allows passive diffusion of molecules smaller than 600 Da. OmpF is a firmly built trimeric channel, stability given by its trimeric form. The monomer consists of 16 antiparallel β -sheets connected by eight loops situated on the outer part of the cell, respectively on the periplasmic site.^[31] The water channel AqpZ, also derived from E. Coli, remains associated as a homotetramer, and assembles into highly ordered two-dimensional tetragonal crystals with unit cell dimensions $a = b = 95 \text{ \AA}$.^[32] The structure of water-soluble protein α -HL from the human pathogen *Staphylococcus aureus* has been determined as a mushroom-shaped heptameric transmembrane pore channel, with 10 nm in length that runs along the sevenfold axis ranged from 1.4 to 4.6 nm in diameter. The lytic, transmembrane domain comprises the lower half of a 14-strand antiparallel β barrel, to which each protomer contributes two β strands, each 6.5 nm long. The interior of the β barrel is primarily hydrophilic, and the exterior has a hydrophobic belt 28 \AA wide.^[33] Additionally, PHEMA and PBMA are attractive choices for this system because of their flexibility and biocompatibility. Here we present a combination of sequential LB and LS monolayer transfer techniques to deposit individual polymeric monolayers on solid supports. Transfers on silicon wafers were carried out for structure characterization by ellipsometry, contact angle measurements, ATR-FTIR, and atomic force microscopy to gain insights into the morphology, homogeneity, and thickness of the layers. Bilayers deposited on germanium surface and on ultrasmooth template stripped gold (TSG) were used further for protein incorporation experiments.

4.2. Results and discussion

4.2.1. Monolayers at the air-water interface

The triblock copolymer used for the assembly of solid-supported membranes by Langmuir monolayer transfers was PHEMA₂₅-*b*-(PBMA₂₅-S-S-PBMA₂₅)-*b*-PHEMA₂₅ (ABA1). It was first characterized at the air-water interface by surface pressure-area isotherms (π -A).

Representative isotherms of the polymer film recorded at 20 °C on ultrapure water are presented in *Figure 4-1*. Unlike low molecular weight amphiphiles, polymers usually do not display clear, well-defined phase transitions.^[34]

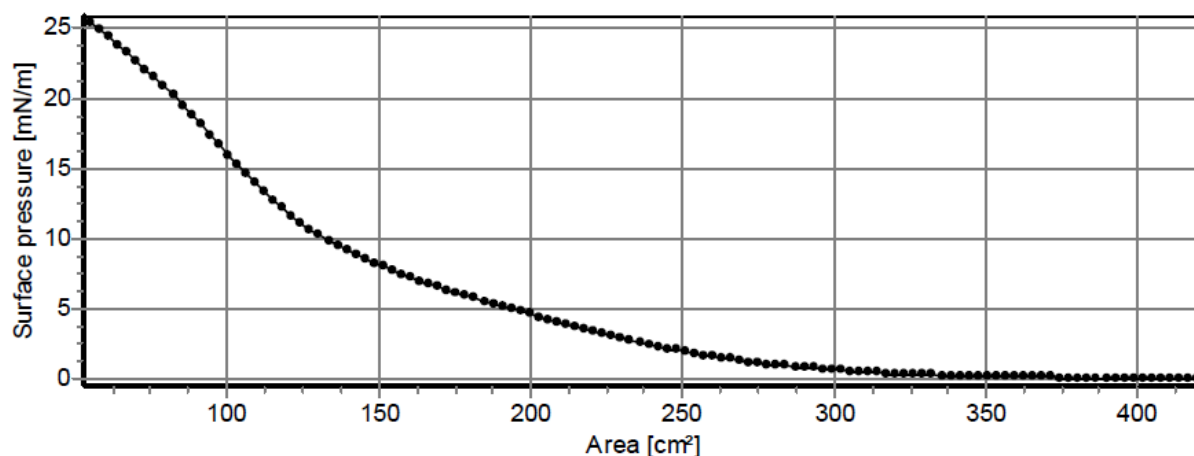


*Figure 4-1: Surface pressure (π) versus area for the PHEMA₂₅-*b*-(PBMA₂₅-S-S-PBMA₂₅)-*b*-PHEMA₂₅ (ABA1) polymer. The isotherm was recorded at 20°C.*

At low surface pressures and areas > 375 cm², no difference in the π -A isotherms of the hydrophilic and the hydrophobic part of the polymer was recognizable, suggesting that the polymer films are in a gas-like, expanded state (“pancake” conformation). In this relaxed state, the hydrophobic PBMA blocks were supposed to be lying flat at the air-water interface, and anchored at the interface to the PHEMA blocks.

Upon compression, a constant increase in surface pressure of the polymer was observed, with a higher increase at areas < 125 cm², indicating that the films undergo a transition from a gas-like to a more condensed phase, until 25 mN m⁻¹. Above this value, a collapse of the polymer film could start. As reported previously, PHEMA monolayers reached a plateau upon high compression for a surface pressure at 10 mN m⁻¹^[35] and PBMA monolayers at 20 mN m⁻¹.^[36] The PBMA blocks may have an effect on the late surface pressure collapse of the ABA1 triblock copolymers at 25 mN m⁻¹.

Additionally, polymer organization at the air-water interface was investigated by Brewster angle microscopy (BAM). The observed monolayers were smooth and did not show any significant features over the whole compression range (see *Figure 4-2*).

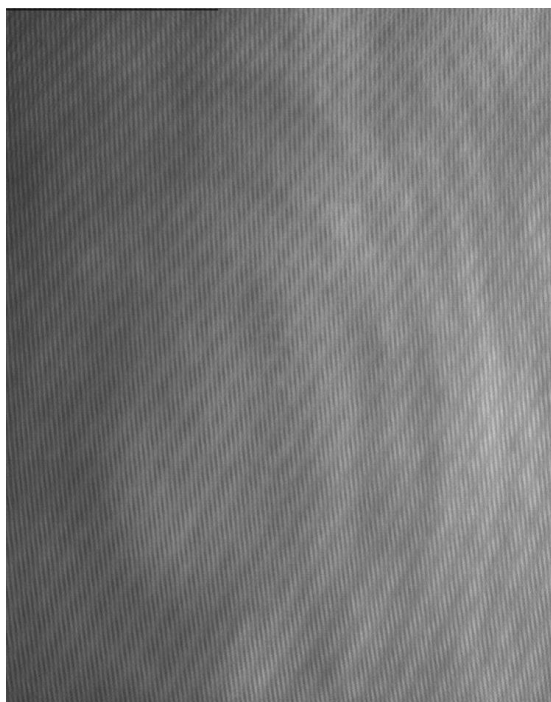


Figure 4-2: BAM image ($220 \times 250 \mu\text{m}^2$) of an ABA1 monolayer at 18 mN m^{-1} .

In order to create bilayers by consecutive Langmuir-Blodgett/-Schaefer film deposition, film stability is crucial. Therefore, the polymer monolayers were compressed to a surface pressure of 22 mN m^{-1} applied in the transfer experiments, which was monitored over time. The compressed monolayers maintained the pressure for longer than 100 min, which was the usual duration for the transfers, indicating high film stability.

4.2.2. Langmuir transfer techniques

4.2.2.1. Monolayers on solid supports

The immobilization of ABA1 was achieved by Langmuir-Blodgett (LB) transfer on different solid supports: silicon wafers for surface characterization, germanium ATR crystal and ultra-smooth gold substrates in order to perform protein insertion experiments after the second monolayer deposition. A major advantage of the LB transfer technique is the ability to produce highly ordered monolayers without major defects on very large scales compared to the size of its components. It has been applied for the controlled fabrication of highly ordered monomolecular films^[37] and successfully employed for lipid bilayer preparation.^[38-40] The procedure is depicted on *Figure 4-3*.

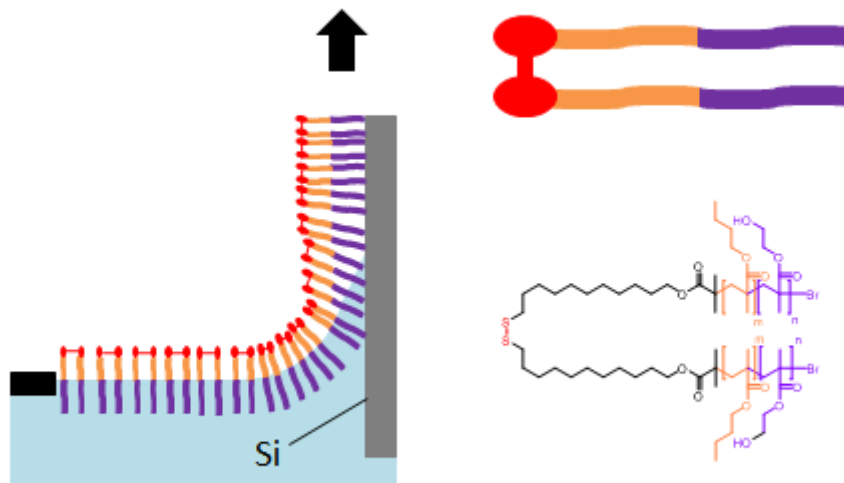


Figure 4-3: Monolayer transfer: the silicon substrate is coated with a monolayer of disulfide-containing polymer on the dipper upstroke.

Film depositions were carried at the surface pressure of 22 mN m^{-1} , which refer to the compressed film at 88% of the collapse pressure. In this phase, the polymer films assume the most densely packed brush-like order. A useful parameter to evaluate the film deposition is the transfer ratio (TR), defined as^[41]:

$$TR = \frac{\text{decrease in Langmuir monolayer surface area}}{\text{total surface area of substrate}}$$

The transfer ratio in this case is approximately 1.4. Since the transfer ratio is an approximate indication of the transfer quality,^[41] our value moderately deviating from unity is acceptable and suggests successful monolayer transfer.

4.2.2.2. Bilayers on solid supports

The Langmuir-Schaefer (LS) technique was applied for the transfer of the second monolayer to the ABA1-covered substrate in order to obtain a complete bilayer membrane. A substrate, which had been previously coated with an ABA1 monolayer, was placed horizontally above an ABA1 Langmuir film and subsequently pressed through the air-water interface. The procedure is depicted in *Figure 4-4*. After transfer, the sample was stored in pure water in a crystallization dish.

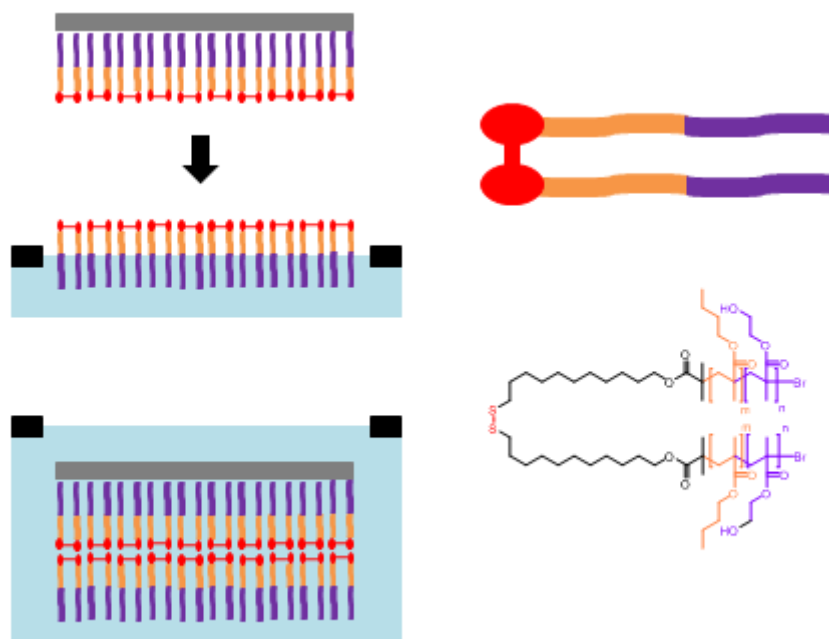


Figure 4-4: Langmuir-Schaefer transfer of an ABAI monolayer to an ABAI-covered substrate.

Depending on the nature of the solid substrate, differences in the film deposition can be observed. When the film transfer occurred on silicon wafers or germanium, the PHEMA blocks are non-covalently attached to the substrate, but they are attracted to the surface because of its hydrophilicity, as depicted in Figure 4-4. However, the behavior of the film deposition on gold cannot be easily predicted. As gold substrate is hydrophobic and the triblock copolymer contains a disulfide bond, we can suppose that the polymer conformation on the surface would lead to a covalently attachment to the gold support by its disulfide group. Contact angles measurements on the monolayer and bilayer films show a difference in wettability. A decrease in contact angle between the monolayer and bilayer film was observed (from 91° to 71°), proving the hydrophilicity of the top layer and therefore the presence of PHEMA brushes.

4.2.3. Characterization of the block copolymer membranes on the surface

All the characterization techniques were performed on the transferred monolayer and bilayer films on silicon wafers in dry state at room temperature.

4.2.3.1. Thickness determination by ellipsometry

Monolayer and bilayer formation were characterized by ellipsometry in order to follow the surface functionalization process. Prior measuring the membrane thicknesses, a thickness of 1.8 ± 0.3 nm was determined for the silicon oxide layer naturally present on silicon wafer. Assuming a refractive index of 1.5 for the block copolymers in monolayer and bilayer membranes, a summary of the overall membrane

thicknesses for the monolayer and the bilayer are presented in *Table 4-1*. The values were measured on three samples as an average of nine different measurements for each sample. The experiments were performed in air.

Table 4-1: Thicknesses on subsequent layers on silicon measured by ellipsometry.

Analyzed layer	Overall membrane thickness (nm)
Monolayer on silicon	3.3 ± 0.4
Bilayer on silicon	8.1 ± 0.6

By comparing the theoretical thickness (based on chemical C-C bonds, 0.154 nm, 109.28°) of the monolayer (3.1 nm) with the obtained experimental thickness, we can assume the formation of an ABA1 monolayer on the solid support. After the bilayer deposition, an increase in thickness was observed, showing the successfulness of the transfer by the Langmuir Schaefer method. The overall thickness for the bilayer is 8.1 nm, meaning that the second layer has a thickness of 4.8 nm. The doubling of the layer thickness suggests a bilayer structure of the type hydrophilic-hydrophobic-hydrophilic. However, the slightly higher thickness of the second layer may suppose either a more extended polymer conformation than in the case of the monolayer transfer, or the formation of nanodomains on the top of the layers.

4.2.3.2. Contact angle

In order to follow the surface functionalization process, contact angle measurements were carried out on the bare silicon wafer surface, and on the transferred LB and LB/LS films. Contact angle values were obtained on three samples from at least nine different individual measurements for the monolayers, and from twelve different measurements for the bilayers. Contact angles increased from 37° for freshly cleaned silicon wafer to $64 \pm 2^\circ$ for the ABA1 monolayer, suggesting the presence of PBMA hydrophobic blocks. From the monolayer to the bilayer membrane, a decrease of 5° was observed, with a contact angle value of $59 \pm 5^\circ$. This slight decrease could suggest the presence of hydrophilic PHEMA layers on the surface. However, the relative large standard deviation in this case indicates a heterogeneous behavior of the bilayer surface.

4.2.3.3. ATR-FTIR characterization

The transfer ratios, the contact angle measurements and the thickness determination by ellipsometry already hint towards successful immobilization of ABA1 monolayers and bilayers on silicon wafer.

Furthermore, attenuated total reflection infrared spectroscopy (ATR-IR) was applied to investigate the presence of monolayer and bilayer samples on the surface. A blank silicon wafer slide was measured as a reference, for which no adsorption bands could be detected. Spectra of ABA1 monolayers and bilayers on silicon wafer were recorded. The measurements were performed immediately after transfer. The spectra in *Figure 4-5* clearly show the ν (C-O) (ester) band at 1110 cm^{-1} for both samples, indicating the successfulness of the two monolayer depositions, forming a bilayer structure on the solid support, which is in accordance with the results reported above.

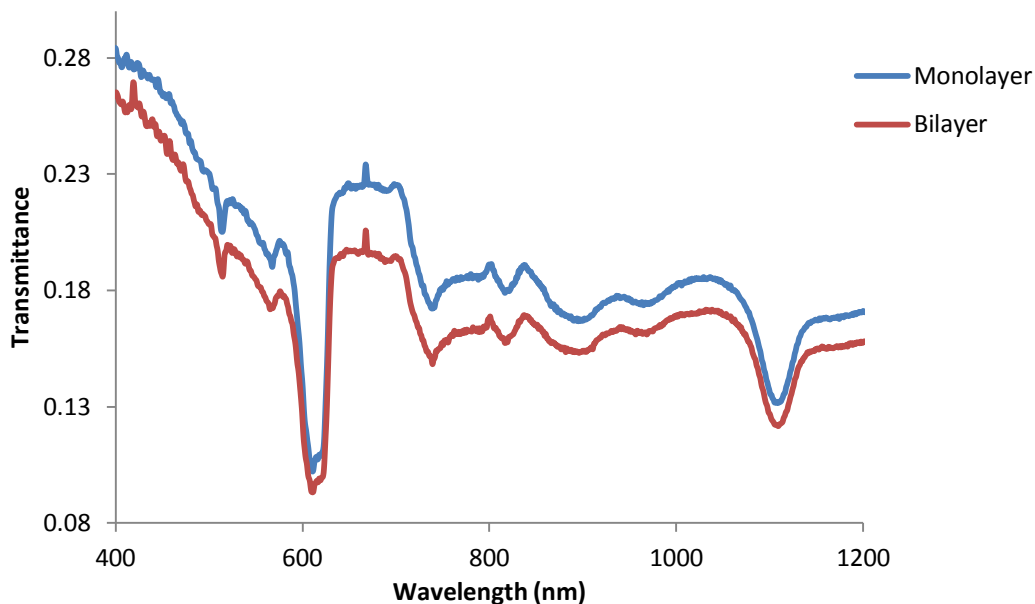
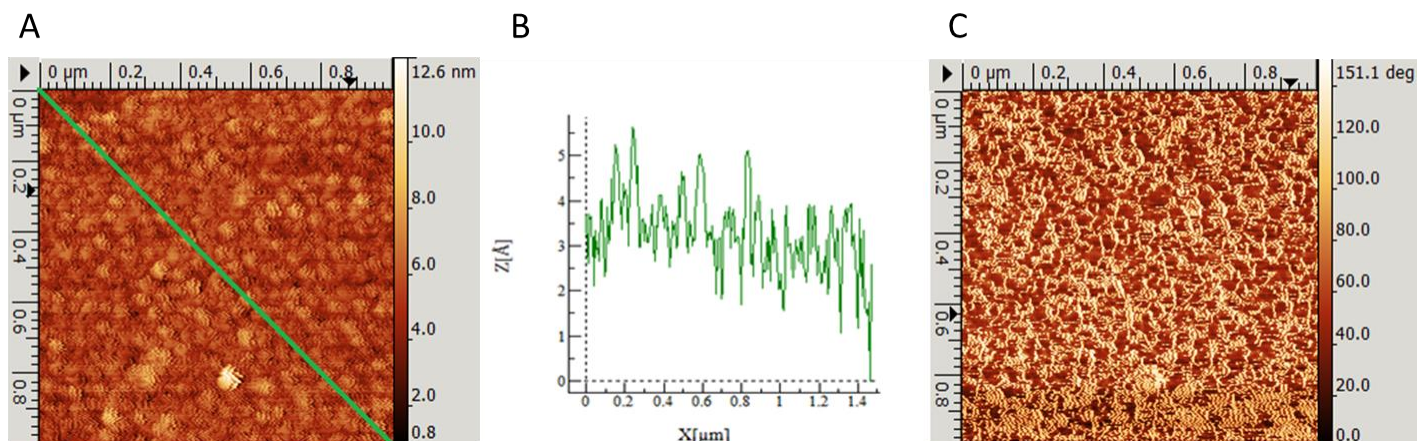


Figure 4-5: Section of an ATR-IR spectrum of ABA1 monolayer and bilayer on silicon wafer.

4.2.3.4. Characterization by AFM

To study local film morphology, atomic force microscopy (AFM) was applied for monolayer and bilayer characterization. Information about homogeneity, structural defects, and roughness of the membranes can be obtained by this method. AFM measurements were performed in air at room temperature. A typical height image, phase image and cross section (with X: distance and Z: height) of a film in dry state for both samples are presented in *Figure 4-6*.



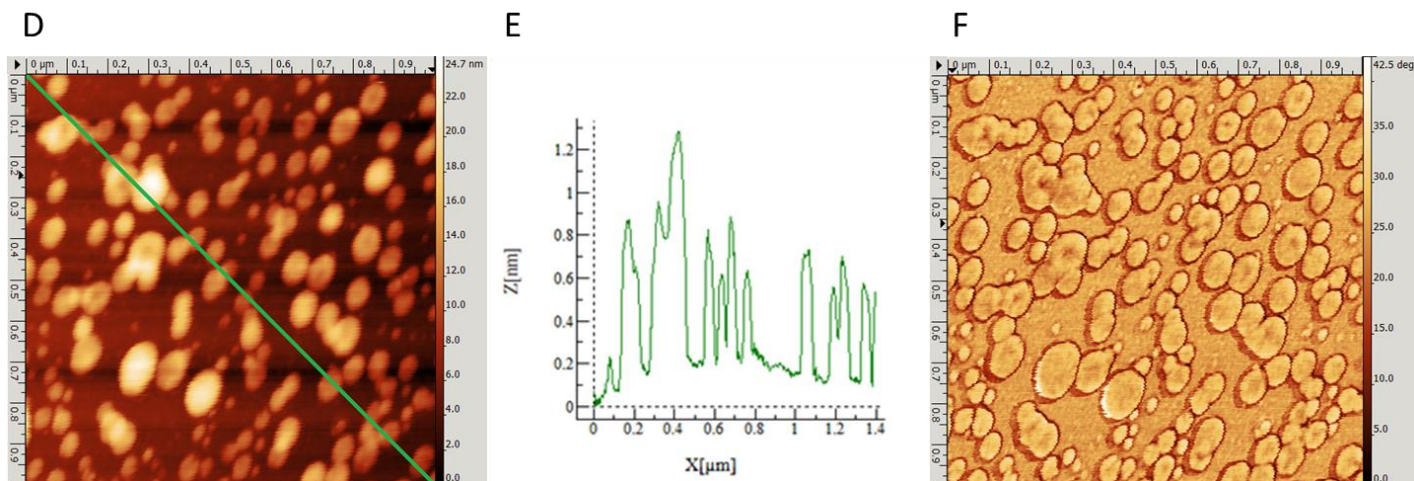


Figure 4-6: AFM images recorded in air of the immobilized ABA1 monolayer (A: height, C: phase image) and ABA1 bilayer (D: height, F: phase image) on silicon wafer; and their corresponding cross sections (Figures B and E).

The monolayer film presents a smooth and defect-free surface on the micrometer scale (Figures 4-6A and 4-6C). Roughness (rootmean-square) does not exceed 0.3 nm over one square micrometer (Figure 4-6B). The polymer monolayer corresponds to the PBMA blocks anchored to disulfide bonds on the top, as previously proved by contact angle. However, the vertical direction shown on the phase image (Figure 4-6C) may suppose that the monolayer film does not cover the whole surface.

The bilayer membrane shows a significant change in morphology, as seen in Figures 4-6D and 4-6F. A heterogeneous surface with formation of nanodomains was observed. Objects of 0.5-1.0 nm in height were present everywhere on the surface (Figure 4-6E), which suggests the disassembly of the architecture. An explanation to this observation could be the formation of PHEMA islands upon compressed surface pressure, as reported previously.^[35] Probably, membrane stability in dry state can be increased by using longer block copolymers. In this case, a higher degree of interaction between the two opposing leaflets, thus enhanced membrane stabilization, is expected. On the other hand, a higher degree of entanglement and an increase in thickness, due to the use of longer polymers, might minimize fluidity and prevent incorporation of proteins.^[42] This is disadvantageous for a prospective purpose of this membrane system, *i.e.* serving as a matrix for protein incorporation. However, surface topography and phases have been performed only in dry state. As protein incorporation experiments were taken place in aqueous media, we expect an extension of the polymer membranes due to the swelling behavior of PHEMA blocks,^[43] that can allow potential protein insertion.

4.2.4. Interaction of channel proteins with the polymeric bilayer

4.2.4.1. ATR in situ studies

In-situ ATR-FTIR spectroscopy is a powerful tool for the assessment of interactions between proteins and surfaces with carefully characterized physicochemical properties. This technique allowed monitoring the processes occurring at the solid-liquid interfaces, such as adsorption and aggregation phenomena.^[44-48] Since ATR-FTIR spectroscopy can work in-situ and does not require protein labeling of some sort, it provides most biologically relevant information about protein adsorption process on solid supports. The aim of this experiment consists in finding out if the bilayer membrane can interact with membrane proteins, prior to further electrical measurements for protein reconstitution. For this purpose, channel protein Outer Membrane Protein F (OmpF) was chosen. The scheme of the experimental setup was described elsewhere.^[48]

OmpF was flowed through ABA1 bilayer membrane attached to a germanium ATR crystal (*Figure 4-7*). Prior to OmpF incubation, an IR spectrum of ABA1 membrane in PBS buffer on solid support was measured (see *Figure 4-7A*).

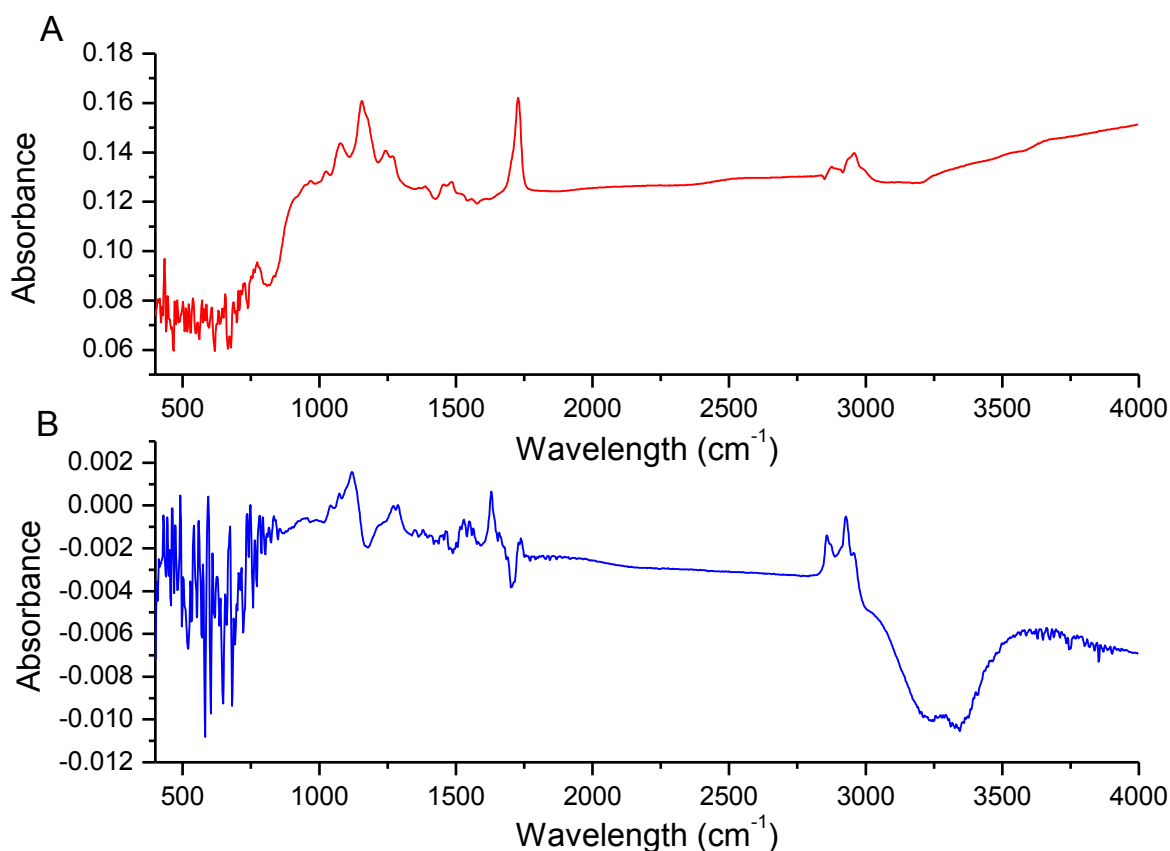


Figure 4-7: ATR-IR spectra of ABA1 bilayer on germanium ATR crystal (A) and of ABA1 bilayer with the presence of OmpF (B).

The spectrum clearly indicates the presence of the membrane with its characteristic ester bands absorption at 1730 cm^{-1} (ν (C=O) (ester)) and at 1150 cm^{-1} (ν (C-O) (ester)). This result is in accordance with previous characterization data on silicon wafers and proves the stability of the bilayer membrane independently from the solid support.

When OmpF solution in PBS flowed over the membrane, scans were taken every 45 seconds to monitor the changes with time. For this purpose, we focused on the changes in absorbance intensity of ν (C=O) (ester) band at 1730 cm^{-1} as well as on the eventual presence of new absorbance peaks. For the ν (C=O) (ester) band at 1730 cm^{-1} , *Figure 4-8* showed an increase in absorbance intensity after 200 seconds, followed by a relative stabilization. It means that OmpF is adsorbing on the polymeric membrane. Moreover, the appearance of new peaks between 1200 and 1700 cm^{-1} along with the more intense peaks between 2800 and 3000 cm^{-1} (*Figure 4-7B*) proved the presence of OmpF on the membrane. After flowing OmpF across the membrane, a washing process with PBS buffer was conducted in order to observe whether the protein still interacts with the polymeric bilayer. In this case, we focused on the peaks between 1200 and 1700 cm^{-1} . The black and the red spectrum looked similar before and after washing with buffer (see *Figure 4-9*), proving that OmpF still stays on or in the polymer membrane even after the washing process.

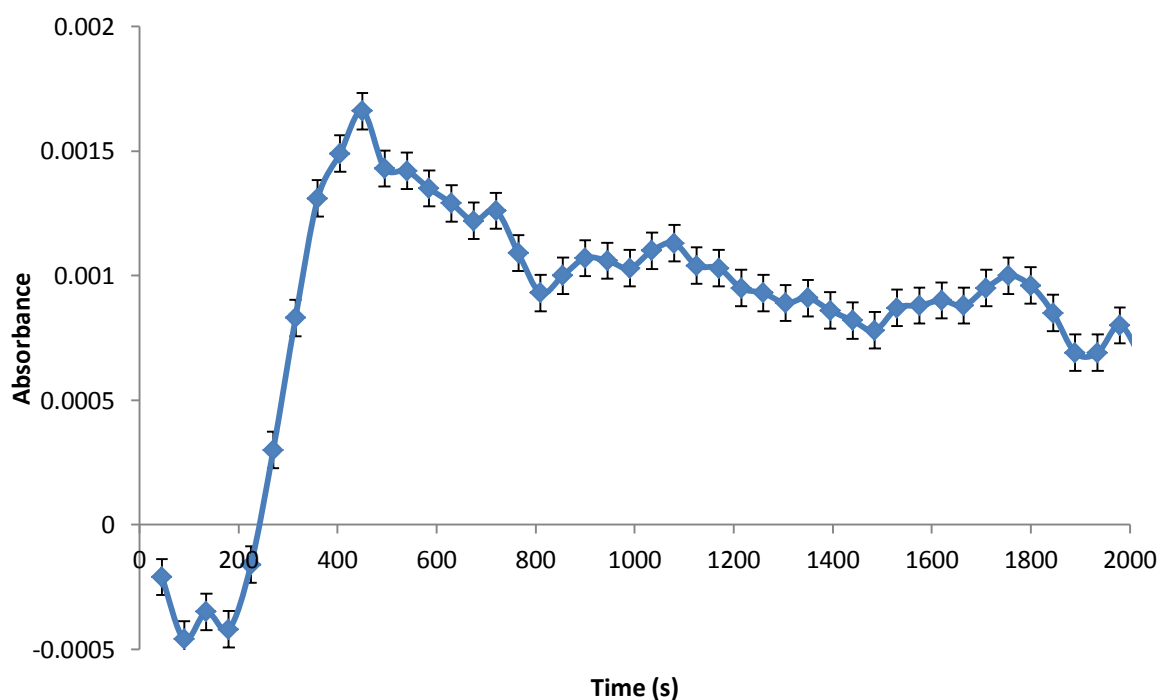


Figure 4-8: Evolution of the ν (C=O) (ester) absorbance intensity at 1730 cm^{-1} in function of time. Spectra were scanned every 45 seconds.

Control experiments consisting in repeating the same experiments as above, but on bare germanium substrate, were carried out. Similar results were observed, *i.e.* no significant changes in the spectra during OmpF incubation and after washing with PBS (see green and blue spectra on *Figure 4-9*). As OmpF can adsorb on the polymeric bilayer as well as on bare Ge surface, we cannot determine if the protein

reconstitution inside the ABA1 membrane occurred by in-situ ATR-FTIR technique. However, we testified the presence of OmpF channel protein on or in the ABA1 membrane. In order to assess whether the proteins have functionally inserted into the membrane, it is necessary to perform further experiments with electrochemical impedance spectroscopy (EIS). Furthermore, the presence of electrical current could help the insertion of channel proteins, as already reported elsewhere.^[29,30]

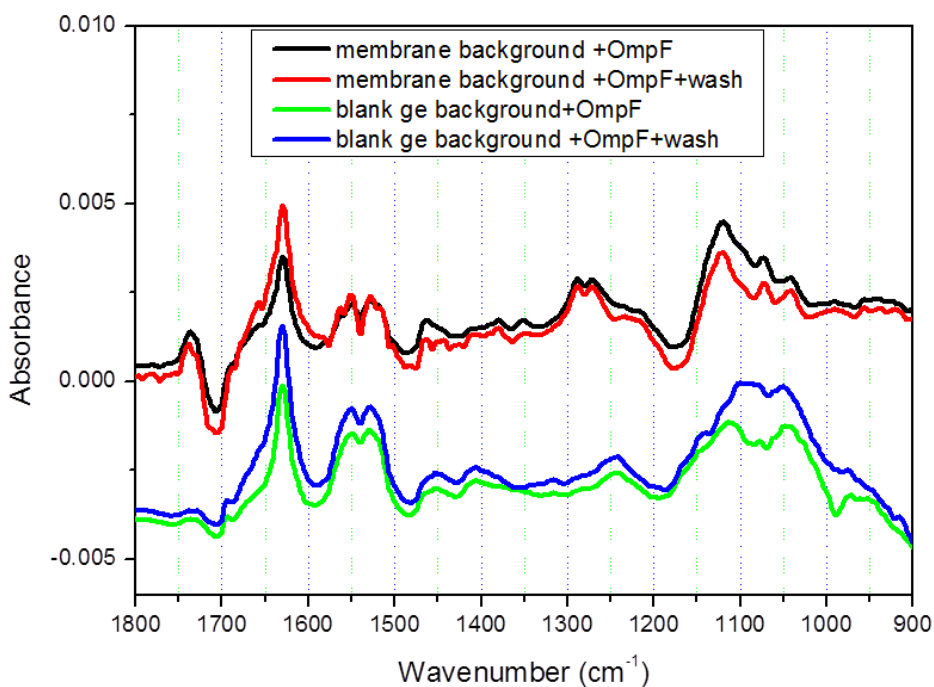


Figure 4-9: ATR-IR spectra of ABA1 bilayer incubated with OmpF and its washing with buffer. Control experiments with incubation with the protein and buffer washing were also performed on bare Ge ATR crystal.

4.2.4.2. Electrical measurements by impedance spectroscopy

Electrochemical impedance spectroscopy (EIS) is a sensitive and non-invasive technique to investigate and characterize the electrochemical properties of materials and their interfaces in contact with electrically conducting electrodes. Among others, the electrochemical properties of artificial membranes, as well as the alterations upon reconstitution of *e.g.* channel proteins, can be probed by EIS.^[29, 30, 38, 49, 50]

The highly reproducible preparation of stable polymer bilayers on gold by sequential Langmuir film transfers was described in sections 4.2.2. and 4.2.3. The aim of this experiment consists of investigating if the ABA1 membrane is a suitable matrix for hosting peptides or proteins by measuring the conductivity through the membrane. If the protein is incorporated into an artificial membrane, the ions flow through the channel protein can be detected. To evaluate if and how biologically relevant species interact with the supported polymer bilayer, two different proteins OmpF and AqpZ were tested. Both proteins were incubated with the bilayer membrane using the Biobeads method in order to remove the detergent used to

stabilize the proteins in aqueous solution.^[51] After an overnight incubation with Biobeads followed by a washing process, electrical measurements were carried out in buffer. The conductance was calculated as $G = I/V$, where I is the electrical current, and V voltage. A constant voltage of 40 mV was applied until a stable current was observed. Control experiments consisting in measuring the electrical current across the polymer membrane in buffer and with Biobeads prior to exposure to proteins, were performed. For a better accuracy of the results, all samples were prepared at least three times separately, and the average values of their conductance were calculated.

Bare gold substrate gave high conductance (138 ± 3 nS), the presence of the polymer membrane resulted in a strong decrease in conductance, with 5.4 ± 0.2 nS, both in buffer and with Biobeads. Moreover, ABA1 polymer membranes incubated with Biobeads and detergent were measured as control experiments and gave a stable conductance of 5.1 ± 0.2 nS (see *Figure 4-10*). This result showed that the Biobeads and detergents did not influence the membrane stability. However, electrical measurements after incubation with OmpF and AqpZ respectively, did not give any reliable results because of unstable conductance over time (*Figure 4-11*). Therefore, these two proteins are not compatible for incorporation inside ABA1 system.

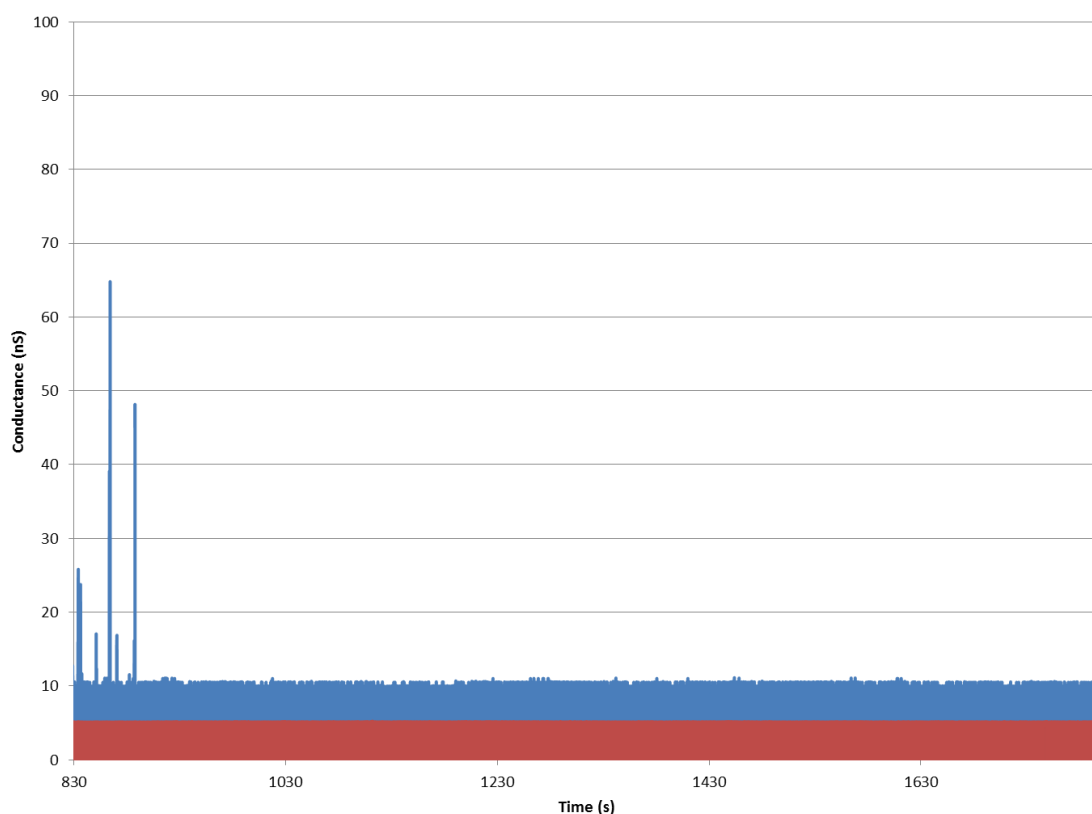


Figure 4-10: Control measurements of electrical conductance across ABA1 polymer in buffer before protein insertion and in buffer with the presence of Biobeads (in blue). The membranes were also incubated in detergent using the Biobeads method (in red).

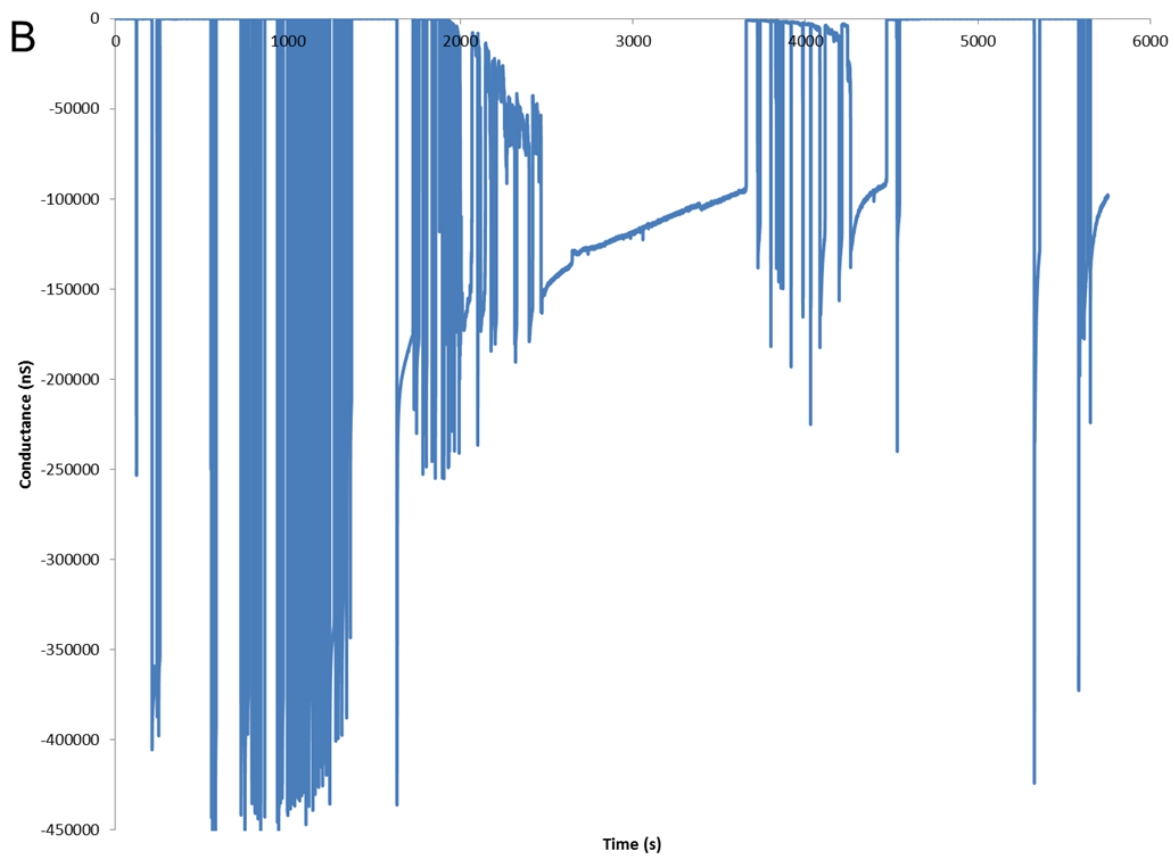
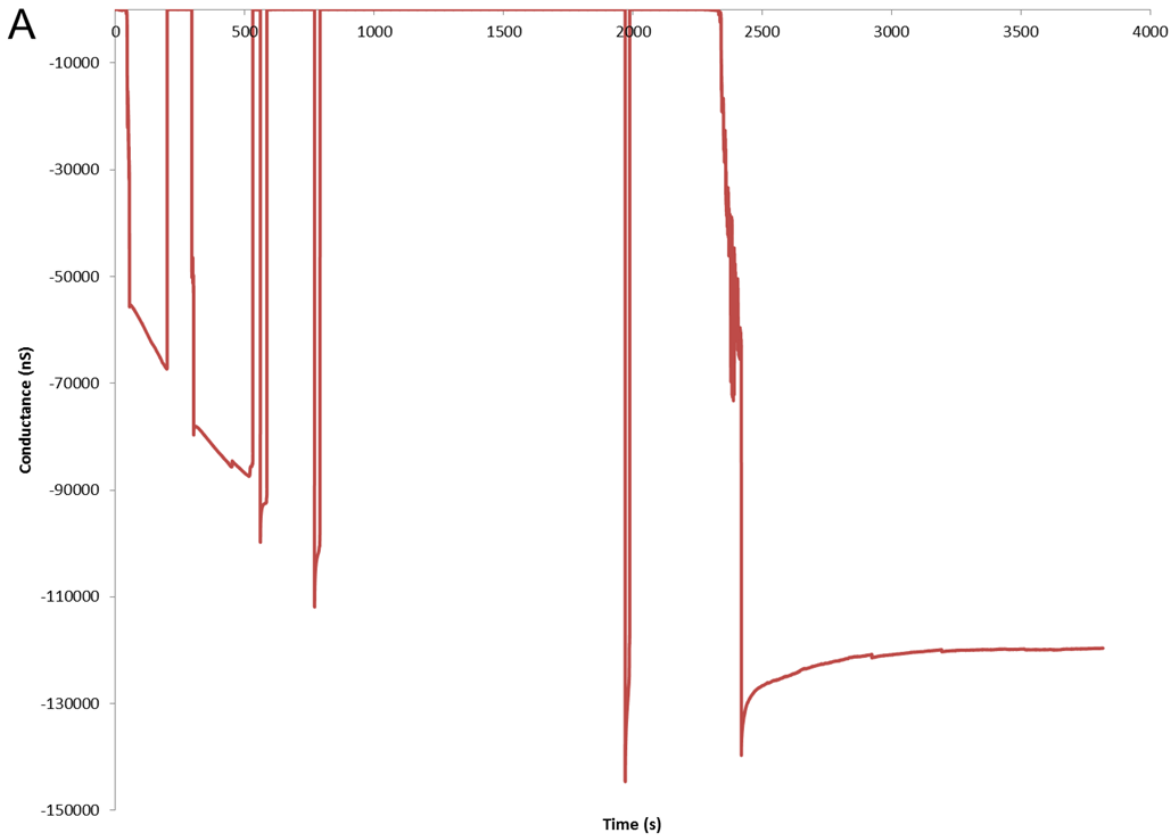


Figure 4-11: Electrical conductance measurements over time of ABA1 membrane after insertion of Outer Membrane Protein F (A) and Aquaporin Z (B).

Consequently, we can deduce that neither OmpF nor AqpZ was inserted into the artificial system. These results could be explained in different ways:

- ABA1 triblock copolymers were not flexible enough to allow the insertion of pore channels OmpF and AqpZ. Moreover, two Langmuir transfers, *i.e.* LB and LS, were performed on a triblock copolymer with a disulfide bond in the middle of the hydrophobic block. The transfer of two triblock copolymers on the gold support in combination with the disulfide bond might have induced the formation of a very complex matrix that cannot allow any protein insertion (see *Figure 4-4* in *section 4.2.2.1*).

- The Biobeads method can lead to some inaccuracies in the results. Actually, the same sample should be used in-situ both for the control measurements and for the protein incubation, as impedance spectroscopy is a sensitive method to any external disturbance that implied changes in conductance and high noise level in the signal. In this case, different samples were used for every control experiment and for protein incubation measurements.

- Conductance measurements could be disturbed either by traces of detergent even with the presence of Biobeads, or by a too rapid detergent removal that can induce protein precipitation.

Also, channel protein alpha-hemolysin (α -HL) was tested for insertion experiments. This peptide from *Staphylococcus aureus* has the advantage of being stable without any detergent.^[38] In this case, the eventual inaccuracies due to the Biobeads method were avoided. Also, the protein insertion with the Biobeads method requires the use of different samples for the control and insertion experiments. In the case of α -HL, the protein incorporation can be measured in-situ on the same sample. Consequently, the inherent errors due to the inhomogeneity of the membrane or defects on the surface could be significantly decreased. Also, previous work already proved the successful incorporation of α -HL into a biomimetic triblock copolymer membrane.^[29, 52] The impedance measurements were performed under the same conditions as above.

Before α -HL insertion, the formation of polymer membranes leads to a strong decrease in conductance, with 5.4 ± 0.2 nS. However, after incubation with α -HL in-situ, the conductance remained stable; with 5.5 ± 0.3 nS (see *Figure 4-12*). As reliable results can be measured after addition of α -HL, studies of protein incorporation without any detergent removal methods proved to be advantageous. But the same conductance before and after peptide incubation was observed, meaning that α -HL was not inserted inside the polymeric membrane. As mentioned previously, this result here might be explained by the very complex matrix of this artificial membrane, which cannot lead to insertion of α -HL.

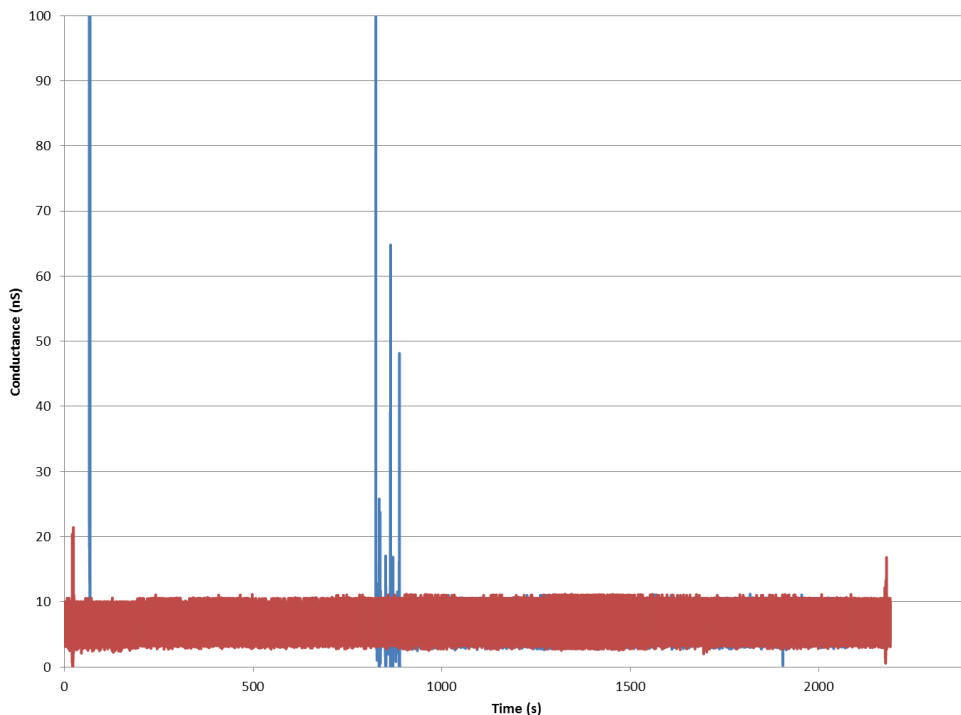


Figure 4-12: Electrical conductance measurements of ABA1 membranes before insertion (in blue) and after insertion (in red) of alpha-hemolysin.

4.3. Conclusions and outlook

In this chapter, novel planar membranes were presented, composed of methacrylate-based amphiphilic triblock copolymer ABA1. This triblock copolymer has been transferred successfully by subsequent Langmuir-Blodgett and Langmuir-Schafer techniques, resulting in a stable bilayer membrane. The characteristic feature of this triblock copolymer, mimicking the hydrophilic-hydrophobic-hydrophilic structure of lipid membranes, consists in its disulfide bond in the middle of the hydrophobic block. Ellipsometry results indicated a bilayer thickness of 8.1 nm and AFM measurements showed the formation of a heterogeneous surface in dry state even though monolayer revealed the presence of a more homogeneous system. However, this matrix is too complex to allow protein insertion. To improve this system as mimics of cell membranes, ABA1 polymer based of PHEMA-*b*-PBMA-S-S-PBMA-*b*-PHEMA could be cleaved after its synthesis by adding a reducing agent to obtain a diblock copolymer. The cleaved polymer PHEMA-*b*-PBMA-SH can be used further for consecutive Langmuir transfers for the formation of an artificial bilayer membrane. By varying the hydrophilic to hydrophobic ratio as well as the chain length of PHEMA-*b*-PBMA-SH diblock copolymers, their self-assembly behavior on solid supports should be systematically investigated in order to find a system that allows protein insertion. However, this diblock copolymer can be covalently attached to a gold substrate with its hydrophobic block. This could disrupt the layer morphology of the amphiphilic block copolymer membranes. Therefore, either the nature of the solid support or the characterization method should be modified to monitor potential protein reconstitution.

4.4. References

- [1] V. Malinova, M. Nallani, W. P. Meier, E.-K. Sinner, *FEBS Letters*, **2012**, 586, 2146-2156.
- [2] X. Zhang, P. Tanner, A. Graff, C. Palivan, W. Meier, *J. Polym. Sci. A: Polymer Chemistry*, **2012**, 50, 2293-2318.
- [3] S. Belegriou, S. Menon, D. Dobrunz, W. Meier, *Soft Matter*, **2011**, 7, 2202-2210.
- [4] O. G. Mouritsen, *Cold Spring Harb. Perspect. Biol.*, **2011**, 3:a004622.
- [5] S. G. Boxer, *Curr. Opin. Chem. Biol.*, **2000**, 4, 704-709.
- [6] W. Knoll, C. W. Frank, C. Heibel, R. Naumann, A. Offenhausser, J. Ruhe, E. K. Schmidt, W. W. Shen, A. Sinner, *Rev. Mol. Biotechnol.*, **2000**, 74, 137-158.
- [7] C. Bieri, O. P. Ernst, S. Heyse, K. P. Hofmann, H. Vogel, *Nat. Biotechnol.*, **1999**, 17, 1105-1108.
- [8] L. Kam, S. G. Boxer, *Langmuir*, **2003**, 19, 1624-1631.
- [9] W. Knoll, H. Park, E.-K. Sinner, D. Yao, F. Yu, *Surf. Sci.*, **2004**, 570, 30-42.
- [10] E. Reimhult, K. Kumar, *Trends Biotechnol.*, **2008**, 26, 82-89.
- [11] P. Lenz, C. M. Ajo-Franklin, S. G. Boxer, *Langmuir*, **2004**, 20, 11092-11099.
- [12] I. Reviakine, A. Brisson, *Langmuir*, **2001**, 17, 8293-8299.
- [13] J. C. Munro, C. W. Frank, *Langmuir*, **2004**, 20, 10567-10575.
- [14] S. Goennenwein, M. Tanaka, B. Hu, L. Moroder, E. Sackmann, *Biophys. J.*, **2003**, 85, 646-655.
- [15] S. Terrettaz, M. Mayer, H. Vogel, *Langmuir*, **2003**, 19, 5567-5569.
- [16] V. I. Silin, H. Wieder, J. T. Woodward, G. Valincius, A. Offenhausser, A. L. Plant, *J. Am. Chem. Soc.*, **2002**, 124, 14676-14683.
- [17] C. A. Naumann, O. Prucker, T. Lehmann, J. R uhe, W. Knoll, C. W. Frank, *Biomacromolecules*, **2002**, 3, 27-35.
- [18] W. Roemer, Y. H. Lam, D. Fischer, A. Watts, W. B. Fischer, P. Goering, R. B. Wehrspohn, U. Goesele, C. Steinem, *J. Am. Chem. Soc.*, **2004**, 126, 16267-16274.
- [19] W. Roemer, C. Steinem, *Biophys. J.*, **2004**, 86, 955-965.
- [20] C. Yoshina-Ishii, S. G. Boxer, *J. Am. Chem. Soc.*, **2003**, 125, 3696-3697.
- [21] A. Janshoff, C. Steinem, *Anal. Bioanal. Chem.*, **2006**, 385, 433-451.
- [22] J. Kowal, X. Zhang, I. A. Dinu, C. G. Palivan, W. Meier, *Macro. Lett.*, **2014**, 3, 59-63.
- [23] H. Bermudez, A. K. Brannan, D. A. Hammer, F. S. Bates, D. E. Discher, *Macromolecules*, **2002**, 35, 8203-8208.
- [24] P. Dalhaimer, F. S. Bates, H. Aranda-Espinoza, D. Discher, *C. R. Phys.*, **2003**, 4, 251-258.
- [25] M. P. Goertz, L. E. Marks, G. A. Monta o, *ACS Nano*, **2012**, 6, 1532-1540.
- [26] J. Dorn, S. Belegriou, M. Kreiter, E.-K. Sinner, W. Meier, *Macromol. Biosci.*, **2011**, 11, 514-525.

- [27] E. Rakhmatullina, W. Meier, *Langmuir*, **2008**, *24*, 6254-6261.
- [28] S. Belegriinou, J. Dorn, M. Kreiter, K. Kita-Tokarczyk, E.-K. Sinner, W. Meier, *Soft Matter*, **2010**, *6*, 179-186.
- [29] X. Zhang, W. Fu, C. Palivan, W. Meier, *Scientific reports* **3**, *2013*, 2196, 1-7.
- [30] J. L. Kowal, J. K. Kowal, D. Wu, H. Stahlberg, C. G. Palivan, W. Meier, *Biomaterials*, **2014**, *35*, 7286-7294.
- [31] S. W. Cowan, R. M. Garavito, J. N. Jansonius, J. A. Jenkins, R. Karlsson, N. König, E. F. Pai, R. A. Pauptit, P. J. Rizkallah, J. P. Rosenbusch, G. Rummel, T. Schirmer, *Structure*, **1995**, *3*, 1041-1050.
- [32] P. Ringler, M. J. Borgnia, H. Stahlberg, P. C. Maloney, P. Agre, *J. Mol. Biology*, **1999**, *291*, 1181-1190.
- [33] L. Song, M. R. Hobaugh, C. Shustak, S. Cheley, H. Baylay, J. E. Gouaux, *Science*, **1996**, *274*, 1859-1866.
- [34] D. J. Crisp, *J. Colloid Sci.*, **1946**, *1*, 161-184.
- [35] N. Nogueira, O. Conde, M. Miñones, J.M. Trillo, J. Miñones Jr., *J. Colloid. And Interface Sci.*, **2012**, *385*, 202-210.
- [36] W-P. Hsu, H-Y. Li, M-S. Chiou, *Colloids and Surfaces A: Physicochem. Eng. Aspects*, **2009**, *335*, 73-79.
- [37] J. A. Zasadzinski, R. Viswanathan, L. Madsen, J. Garnaes, D. K. Schwartz, *Science*, **1994**, *263*, 1726-1733.
- [38] C. Steinem, A. Janshoff, W.-P. Ulrich, M. Sieber, H.-J. Galla, *Biochim. Biophys. Acta. Biomembr.*, **1996**, *1279*, 169-180.
- [39] L. K. Tamm, H. M. McConnell, *Biophys. J.*, **1985**, *47*, 105-113.
- [40] C. L. Brosseau, J. Leitch, X. Bin, M. Chen, S. G. Roscoe, J. Lipkowski, *Langmuir*, **2008**, *24*, 13058-13067.
- [41] D. K. Schwartz, *Surf. Sci. Rep.*, **1997**, *27*, 241-334.
- [42] J. C. M. Lee, M. Santore, F. S. Bates, D. E. Discher, *Macromolecules*, **2002**, *35*, 323-326.
- [43] E. Rakhmatullina, A. Manton, T. Burgi, V. Malinova, W. Meier, *J. Polym. Sci. Part A: Polym. Chem.*, **2008**, *47*, 1-13.
- [44] H. H. Bauer, M. Müller, J. Goette, H. P. Merkle, U. P. Fringeli, *Biochemistry*, **1994**, *33*, 12276-12282.
- [45] R. Barbucci, A. Magnani, *Biomaterials*, **1994**, *15*, 955-962.
- [46] A. Ball, R. A. L. Jones, *Langmuir*, **1995**, *11*, 3542-3548.
- [47] M. Müller, C. Werner, K. Grundke, K.-J. Eichhorn, H. J. Jacobasch, *Microchim. Acta*, **1997**, *14*, 671-674.
- [48] A. Bouhekka, T. Bürgi, *Applied Surface Science*, **2012**, *261*, 369-374.
- [49] I. K. Vockenroth, P. P. Atanasova, J. R. Long, A. T. A. Jenkins, W. Knoll, I. Koeper, *Biochim. Biophys. Acta, Biomembr.*, **2007**, *1768*, 1114-1120.

- [50] V. Atanasov, P. P. Atanasova, I. K. Vockenroth, N. Knorr, I. Koeper, *Bioconjugate Chem.*, **2006**, *17*, 631-637.
- [51] T. M. Allen, A. Y. Romans, H. Kercret, J. P. Segrest, *Biochimica et Biophysica Acta*, **1980**, *601*, 328-342.
- [52] D. Wong, T.-J. Jean, J. Schmidt, *Nanotechnology*, **2006**, *17*, 3710-3717.

5. Functionalization of gold surfaces with amphiphilic block copolymer brushes using surface-initiated ATRP

Parts of this chapter are from: S. Toughraï, C. K. Pandiyarajan, J.-L. Perin, P. Korelis, T. Geue, T. Bürgi, N. Bruns, W. Meier, “Insertion of Natural Channel Protein into a Solid-Supported Artificial Membrane made of Grafted-Amphiphilic Triblock Copolymers”, *in preparation*.

5.1. Introduction

As mentioned previously in this thesis, cell membranes are the most important interface in living organisms. Native biological membranes are fascinating because of their complex composition and functions as well as their amphiphilic structure in which two hydrophilic layers enclose a hydrophobic one.^[1] However, they are not always ideal in the study of specific membrane processes, and their structural complexity limits the scope of their utility in many technological and industrial processes. This is why many efforts have been made over the past decades to mimic cell membranes properties and functions by creating artificial model membranes.^[2-4] Such membrane models offer great potential in fundamental scientific research, especially for investigating the structure and function of membrane proteins. They are also highly relevant for technological applications, including sensor technologies. In particular, block copolymers are regarded as highly promising structures for the development of new biosensors.^[5-8] Polymer synthesis allows for the adjustment of such parameters as block length, molecular weight, chemical composition, hydrophilic/hydrophobic balance, and molecular architecture. This provides new ways to control amphiphilic self-assembly. Moreover, it allows producing structures of defined morphology, molecular packing, and membrane thickness. Previous experiments showed the possibility of mimicking cell membranes with artificial amphiphilic polymer membranes either by consecutive monolayer transfers^[9, 10] or by vesicle^[11, 12] or micelle^[13] spreading. Recently, a “grafting from” approach has been adopted as a well-controlled method for the successful growth of amphiphilic diblock copolymer brushes from silicon and gold surfaces^[14] as well as for the synthesis of triblock copolymer brushes on surfaces.^[15-18] Furthermore, biomimetic polymer membranes based on immobilized amphiphilic triblock copolymers could be particularly interesting structures, since they potentially allow the insertion of membrane proteins.^[19, 20] To be considered as attractive alternative models of biosensors, solid-supported polymer membranes must incorporate membrane proteins as the “active” component.^[21] Successful protein insertion requires a spacer to decouple the membrane from the support, thus minimizing a defect formation, avoiding the denaturation of the protein by contact with the substrate and increasing the mobility (fluidity) of the membrane.^[22]

Here, we demonstrated the potential incorporation of a membrane protein into gold-supported biomimetic membrane based on amphiphilic triblock copolymers. This ABA triblock copolymer with poly (2-hydroxyethyl methacrylate) (PHEMA) as the hydrophilic block and poly (butyl methacrylate) (PBMA) as the hydrophobic part was synthesized by surface-initiated atom transfer radical polymerization (Si-ATRP) from an initiator molecule that forms a self-assembled monolayer (SAM) on the surface.^[18] To determine the most suitable matrix for protein incorporation, polymer brushes were synthesized under variation of the grafting density of the polymer. PHEMA and PBMA are interesting choices for biomedical applications because both polymers are biocompatible.^[23, 24] By varying the grafting density of the brushes, channel proteins could be successfully incorporated inside this artificial membrane. So far the closest achievements in protein insertion into artificial membranes have been solid-supported amphiphilic polymeric bilayers that allow the successful incorporation of membrane proteins with the help of electrical current.^[10, 25] In this case, the deposition of the bilayers was performed using consecutively Langmuir-Blodgett (LB) and Langmuir-Schaefer (LS) techniques. However, polymer bilayers made by monolayer transfers or by vesicle spreading suffer of several drawbacks, mainly the lack of control of the grafting density. The characteristic feature in our present work consists in inserting the membrane protein into an amphiphilic triblock copolymer grafted directly from a solid support. In this case, the grafting-from method offers the advantages of a good surface coverage and a better control of the packing density. Grafting-from involves the synthesis of the triblock copolymer directly from the surface using ATRP technique.^[26-28] Here, grafting density can be controlled by adjusting the surface density of the initiator molecules.

The hydrophilic PHEMA blocks are not fully water-soluble, but take up water and considerably swell in aqueous media. Remarkably, preliminary experiments indicated that the PHEMA-*b*-PBMA-*b*-PHEMA copolymer membranes can reversibly be hydrated and dehydrated without loss of structural integrity,^[18] which is a key importance for successful protein incorporation. Here we will evaluate necessary conditions for a successful insertion of membrane proteins. The insertion process requires a certain flexibility and fluidity of the membrane that should sensitively depend on the length and the grafting density of the polymer chains. The good control over these parameters is of high importance, since thick and very densely packed membranes have a low permeability which affects drastically the protein insertion. The grafting density of the polymer chains depends on the density of the initiator molecules anchored to the surface. The latter can be controlled by diluting the initiator SAM disulfide molecules with similar disulfide molecules which are, however, chemically inert to initiate ATRP. Thus substrates with gradual variation of the grafting density will be studied for protein incorporation. Upon insertion of this channel protein, our polymeric membrane could allow for the preparation of mechanically and chemically stable biosensor devices.

5.2. Results and discussion

5.2.1. Synthesis strategy of the triblock copolymers

Amphiphilic triblock copolymer brushes on gold interfaces were synthesized by the “grafting-from” method. This procedure included the immobilization of initiator molecules 11,11'-dithiobis [1-(2-bromo-2-methylpropionyloxy)undecane] on template stripped gold (TSG) substrates followed by ATRP of 2-hydroxyethyl methacrylate (HEMA) and n-butyl methacrylate (BMA) monomers. In-situ analysis of the initiator monolayer and the copolymer brushes were performed to get a better understanding of the materials behaviour on solid supports in order to investigate a possible protein insertion. A synthesis scheme of the triblock copolymers on gold surfaces is depicted in *Figure 5-1*.

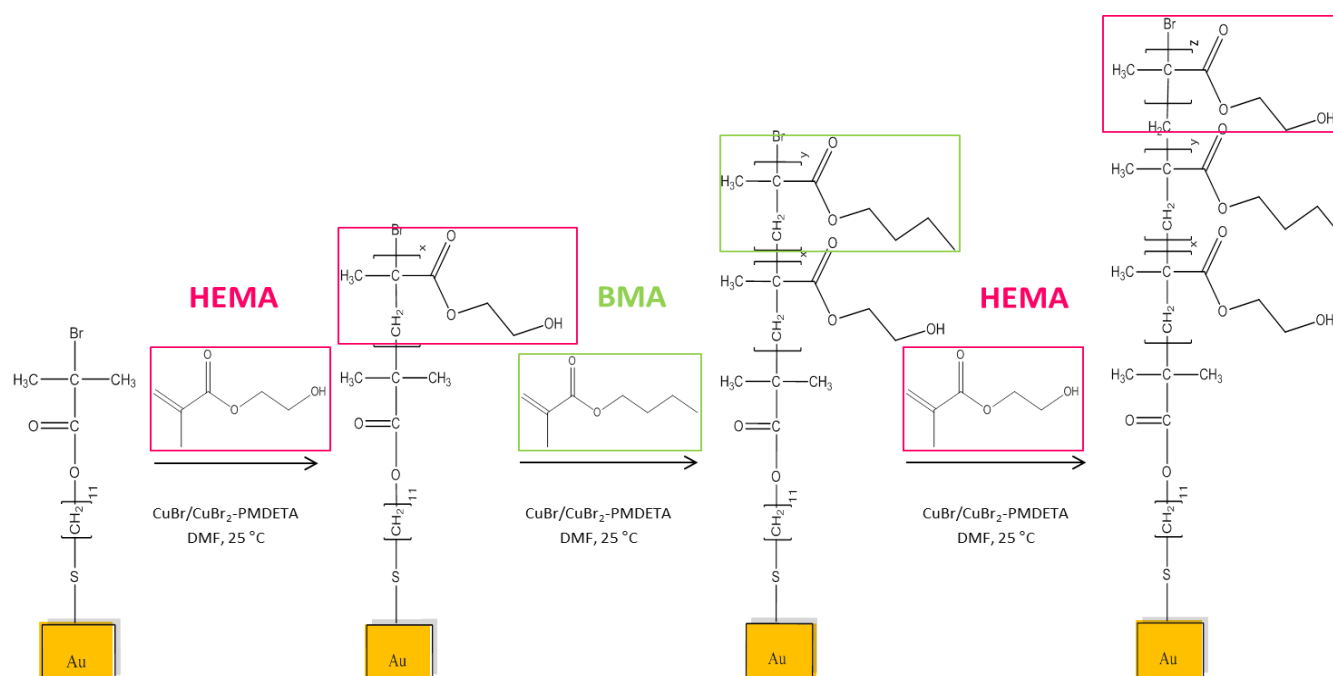


Figure 5-1: Synthesis scheme of PHEMA-b-PBMA-b-PHEMA triblock copolymer grafted from gold supports. The initiator molecule was immobilized on gold surface by its disulfide bond prior to ATRP reactions.

This system was fine-tuned by controlling the chain length in order to allow the insertion of three different membrane proteins: Outer Membrane Protein F (OmpF), Aquaporin Z (AqpZ) and alpha-hemolysin (α -HL). Therefore, taking into account the polymer flexibility, the thickness of the overall ABA polymer could be fixed around 10 nm. Above this value, the probability of protein insertion may decrease, even if both PHEMA and PBMA have flexible properties. Thus, polymerization time and temperature are essential parameters for a better control over the brush thickness. Also, fully packed brushes may be a critical point because of the lack of sufficient space for protein insertion. The grafting density will be therefore systematically varied to give enough space for the incorporation of membrane

proteins. The variation of the grafting density was performed by mixing the initiator molecule with 1-dodecanethiol, inert to ATRP. By decreasing the grafting density, we expect a decrease in brush thickness that can enhance the insertion.^[29, 30] As the channel proteins allow passive diffusion of small solutes (ions, nutrients, antibiotics) across the membrane,^[25, 29, 30] functional incorporation of channel proteins can be monitored directly by conductance measurements across the polymer brushes. Gold was used here as a solid support for its dielectric properties to ease the protein insertion by applying an electrical current.^[25, 31] In addition, the preservation of protein functionality inside the artificial membrane is crucial. For this, the initiator that forms a self-assembled monolayer will serve as a spacer between the substrate and the polymer brushes in order to avoid protein denaturation by contact between the pore channel and the gold substrate.

5.2.2. Initiator self-assembled monolayer on gold surfaces

The formation of self-assembled monolayers (SAMs) of thiolated molecules on gold is well known.^[32] This property of thiol compounds was used to prepare SAMs of ATRP initiator molecules that contain a bromine atom at the other end of the thiol linker. Here we used 11,11'-dithiobis [1-(2-bromo-2-methylpropionyloxy)undecane] as described elsewhere.^[33]

5.2.2.1. Atomic composition determination by XPS

The atomic composition of the self-assembled monolayer (SAM) of initiator was determined by XPS. A bare TSG substrate was used as a reference. The results are displayed in *Figure 5-2*. XPS spectrum of SAM initiator showed an intense oxygen peak (O1s) at 534 eV and an intense carbon signal (C1s) at 286 eV associated with the organic part of the initiator molecules. More specific signals are the sulfur atom (S2s, S2p) peaks and the small bromine signals (Br3d, Br3p, Br3s), which are respectively assigned to the Au-S and C-Br bonds of the SAM initiator. The XPS data qualitatively proved the presence of the initiator layer. However, the presence of a small carbon peak (C1s) was observed on the reference spectrum, due to air contamination.

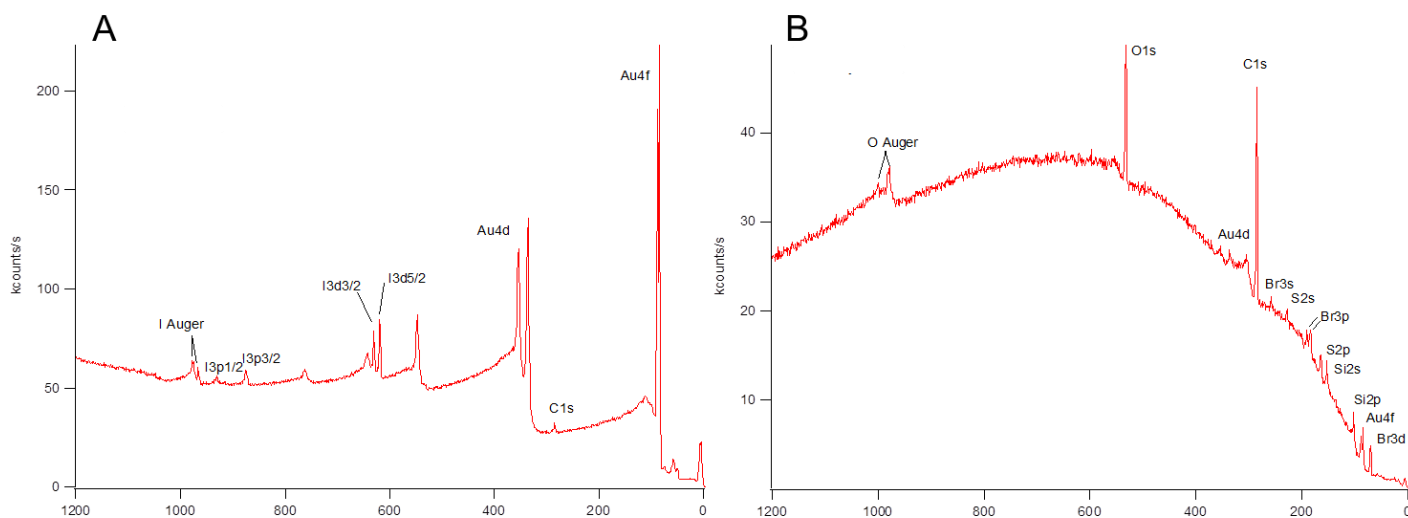


Figure 5-2: XPS spectra of bare TSG substrate as a reference (A) and of SAM initiator on gold surfaces (B).

5.2.2.2. Contact angle measurements

As the coverage of gold substrate with SAM initiator was proven by XPS, contact angles measurements were carried out in order to observe the influence of the SAM initiator on surface wettability. Contact angles increased from 75° for freshly cleaned TSG to $79 \pm 2^\circ$ for the SAM initiator, indicating the monolayer makes the surface slightly more hydrophobic. The small standard deviation can suggest a homogeneous layer with minor defects.

5.2.2.3. Thickness determination by SPR

Thickness measurements of SAM initiator were carried out by SPR in order to follow the surface functionalization process. Prior to the monolayer thickness, the gold layer deposited on glass substrate through the TSG process was determined. The values were measured as an average of three samples. The experiments were performed in air at room temperature. The SPR spectra and their corresponding fits are reported on *Figure 5-3*. A gold layer thickness of 51 ± 2 nm was determined. Assuming a refractive index of 1.4 for the initiator molecule, SAM initiator thickness was found to be 3.4 ± 0.2 nm. Therefore, the increase in this thickness range suggests the successful deposition of the initiator molecules 11,11'-dithiobis [1-(2-bromo-2-methylpropionyloxy)undecane] as a self-assembled monolayer. However, comparing to the theoretical value of 2.5 nm (based on C-C bonds, 0.154 nm, 109.28°), the experimental value may indicate a stretched conformation of the initiator molecules grafted on the surface due to their dense packing in the monolayer.

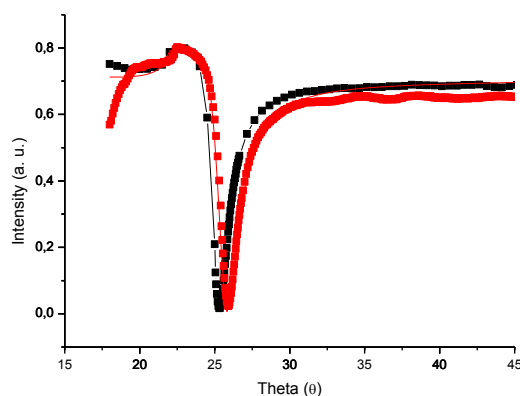


Figure 5-3: Representative angular SPR spectra measured in air at room temperature showing the shift of the reflectivity minimum from blank gold (■) to the covalently attached self-assembled monolayer (■). The solid lines represent the fits.

5.2.2.4. Characterization by AFM

In order to study local topography and roughness, AFM measurements were performed on SAM initiator. AFM measurements were performed in air at room temperature. A typical height image, a phase image and cross section (with X: distance and Z: height) of a SAM in dry state as well as of a bare TSG used as a reference are presented in Figure 5-4.

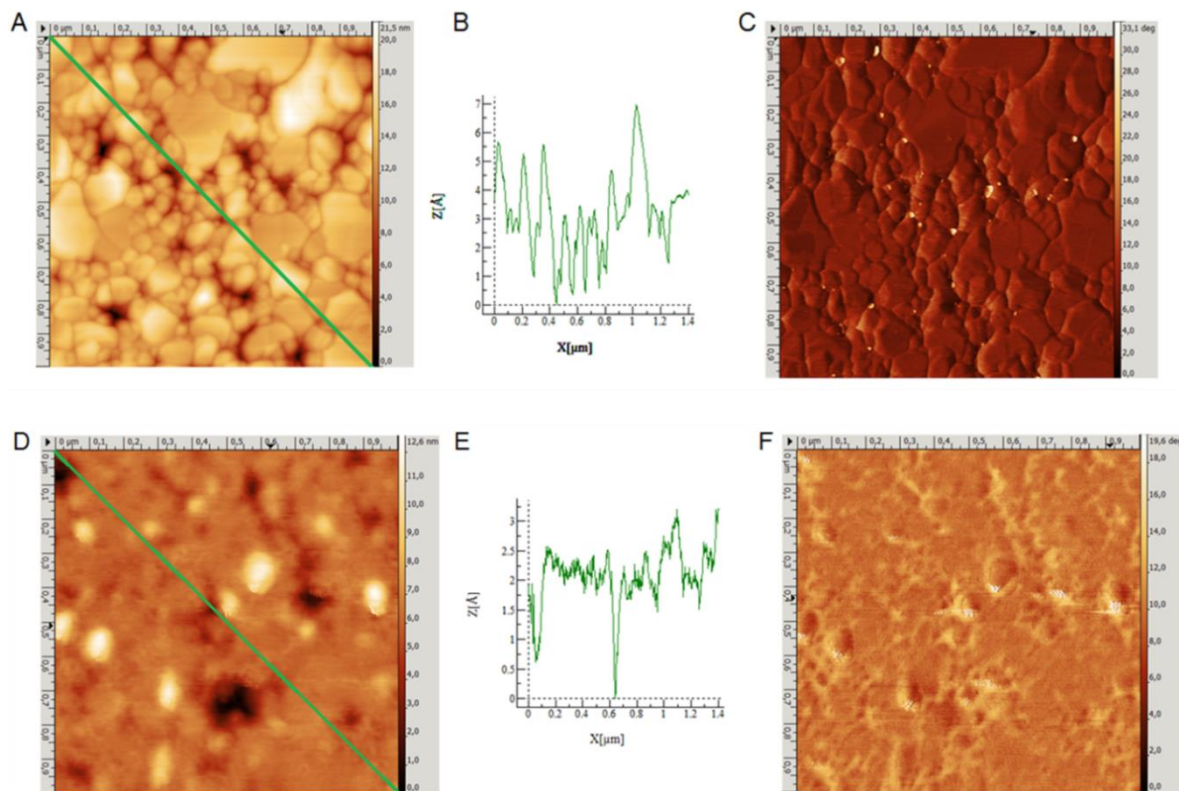


Figure 5-4: AFM images recorded in air of the bare TSG substrate (A: height, C: phase image) and SAM initiator on gold (D: height, F: phase image); and their corresponding cross sections (Figures B and E).

In comparison to the reference AFM image corresponding to the bare gold, topography and phase of SAM initiator shows a coverage of the monolayer on the surface, which is in accordance with results described above. SAM initiator presents a very flat and homogeneous surface on the micrometer range (*Figures 5-4D and 5-4F*). Roughness (rootmean-square) does not exceed 0.2 nm over one square micrometer (*Figure 5-4E*). Therefore, anchoring of the ATRP initiator molecules resulted in a densely packed homogeneous self-assembled monolayer (SAM) on the gold surface. Moreover, AFM measurements also proved the success of the self-made TSG technique, with a maximum roughness of 0.4 nm for the bare gold (*Figure 5-4B*), in accordance with previous results described elsewhere.^[34-36] Here, we have demonstrated the importance of producing very flat metallic layer in order to obtain not only a flat and reproducible SAM initiator, but also to ease further brushes characterization.

5.2.2.5. Orientation of the SAM by PM-IRRAS

Polarization Modulation Infrared Reflection Absorption Spectroscopy (PM-IRRAS) is a powerful surface technique used to determine the orientation of functional groups and molecules,^[37] making use of the polarization of the electric field perpendicular to the surface. This method can be used for the study of the orientation of thin polymeric layers^[38, 39] as well as for single peptide molecules.^[40] Here, we aimed at exploring the orientation of the SAM initiator on gold, as it is covalently attached to the surface. Furthermore, it was previously shown that the initiator forms a densely packed monolayer, suggesting a stretched conformation on the solid substrate.

SAM initiator on gold as well as a drop of the initiator substance 11,11'-dithiobis [1-(2-bromo-2-methylpropionyloxy)undecane] were measured. This bulk sample is isotropic and is used here as a reference. The PM-IRRAS spectra of the initiator molecule in bulk and on the surface are displayed in *Figure 5-5*.

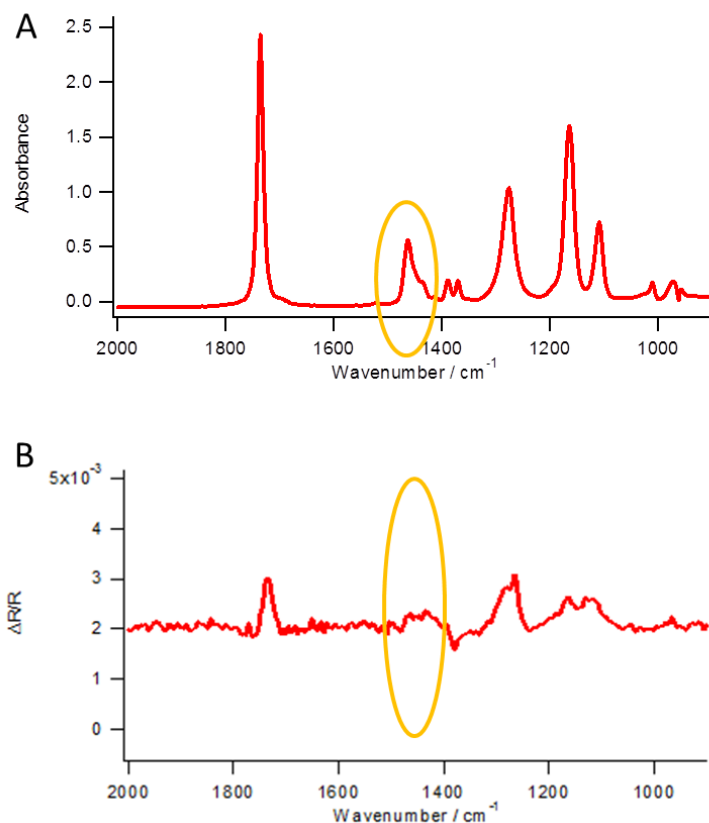


Figure 5-5: PM-IRRAS of 11,11'-dithiobis [1-(2-bromo-2-methylpropionyloxy)undecane] in bulk (A) and as a SAM on 3 different gold surfaces (B).

Both spectra can attest the presence of the initiator molecule by the appearance of the ν (C=O) (ester) band at 1750 cm⁻¹. More importantly, there is a prominent peak at 1450 cm⁻¹ in the bulk spectrum that disappears in the monolayer spectra. This band is associated with a scissoring mode of the CH₂ units of the hydrocarbon chain and is polarized perpendicular to the latter. The disappearance of this band in the SAM spectrum shows the preferential perpendicular orientation of the hydrocarbon chain with respect to the surface. This result confirms that the SAM formed a densely packed and homogeneous monolayer with a stretched conformation.

5.2.3. Characterization of the polymer brushes

5.2.3.1. Following of the polymerization by contact angle

Contact angle measurements were carried out to follow ATRP of the triblock copolymers in-situ. Contact angle values were obtained on three samples from at least nine different individual measurements. A summary of the obtained results for each block is presented in *Table 5-1*.

Table 5-1: Summary of the contact angles of PHEMA-*b*-PBMA-*b*-PHEMA layer by layer for three different gold substrates.

SAM	PHEMA	PHEMA- <i>b</i> -PBMA	PHEMA- <i>b</i> -PBMA- <i>b</i> -PHEMA
81° ± 2°	45° ± 3°	87° ± 6°	83° ± 3°

Contact angles decreased from 81° for the self-assembled monolayer to 43 ± 3° for the first PHEMA layer, suggesting the presence of a hydrophilic surface. From the first to the second layer, an increase of 38° was observed, with a contact angle value of 87 ± 6°. This large increase may suggest the presence of hydrophobic PBMA layer on the surface. The relative large standard deviation in this case indicates a heterogeneous behavior of the second layer on the solid support. A slight decrease of 4° was observed from the second PBMA to the third PHEMA layer, supposing the successful synthesis of the third hydrophilic block. However, this last result also indicates the strong influence of the second hydrophobic block on the contact angle.

5.2.3.2. ATR-FTIR characterization

ATR-FTIR was applied to prove the presence of the amphiphilic polymer on the gold surface. A blank gold slide was measured as a reference, for which no adsorption bands could be detected. Spectra of each layer were recorded immediately after their synthesis. The spectra in *Figure 5-6* clearly show for each layer the ν (C=O) (ester) band at 1725 cm⁻¹, indicating the presence of the polymers on the surface and the successful growth of the brushes.

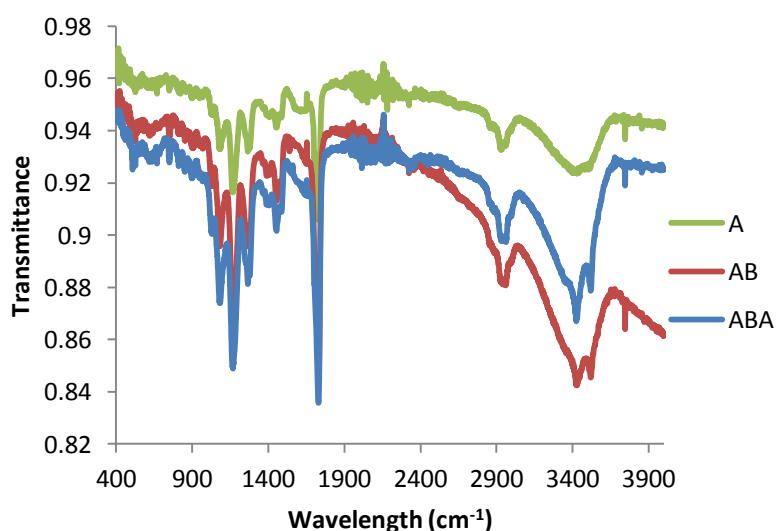


Figure 5-6: ATR-FTIR spectra of PHEMA (A), PHEMA-*b*-PBMA (AB) and PHEMA-*b*-PBMA-*b*-PHEMA (ABA) brushes on a gold substrate.

5.2.3.3. Thickness determination by SPR

Each block of the polymer brushes was characterized by surface plasmon resonance in order to determine their thickness. Assuming a refractive index of 1.512 for the PHEMA blocks and 1.4 for PBMA, a summary of the overall thicknesses of the brushes (without the initiator molecule) were presented in *Table 5-2*. The values were measured on three samples as an average of six different measurements for each sample. The experiments were performed in air at room temperature. For each polymer layer, the SPR spectra and their corresponding fits are displayed in *Figure 5-7*.

Table 5-2: Thicknesses of subsequent layers on gold measured by surface plasmon resonance for fully packed brushes.

Analyzed brush	Overall membrane thickness (nm)
PHEMA	3.8 ± 0.5
PHEMA-<i>b</i>-PBMA	8.4 ± 0.3
PHEMA-<i>b</i>-PBMA-<i>b</i>-PHEMA	10.8 ± 0.3

Each block of the polymer brush revealed a successful growth of the layer by the increase of their thickness. The first PHEMA block got a thickness of 3.8 ± 0.5 nm. The synthesis of the first PHEMA block was fine-tuned to obtain a thickness < 4 nm by controlling the reaction time. Above this value, the probability of increasing termination reactions with bromine groups may occur, and consequently further ATRP reactions with the second and the third block could not be performed efficiently. This assumption was based on previous knowledge from the Meier group in the area of surface-initiated ATRP.^[41] The overall thickness for the diblock brush is 8.4 ± 0.3 nm, meaning that the second layer has a thickness of 4.6 nm. The triblock copolymer presents a hydrophilic-hydrophobic-hydrophilic structure with an overall thickness of 10.8 ± 0.3 nm, meaning the third PHEMA block exhibits a thickness of 2.4 nm. This overall size of 10 nm was targeted based on membrane thickness that allows protein reconstitution.^[4]

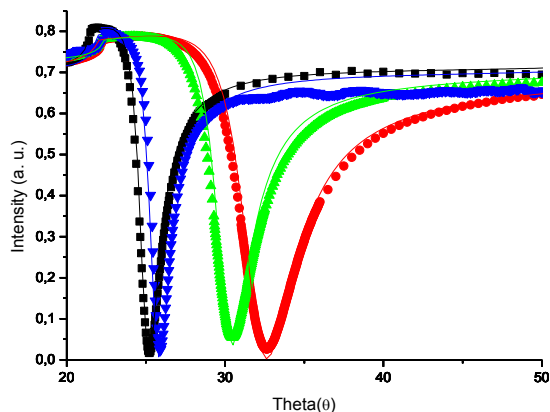
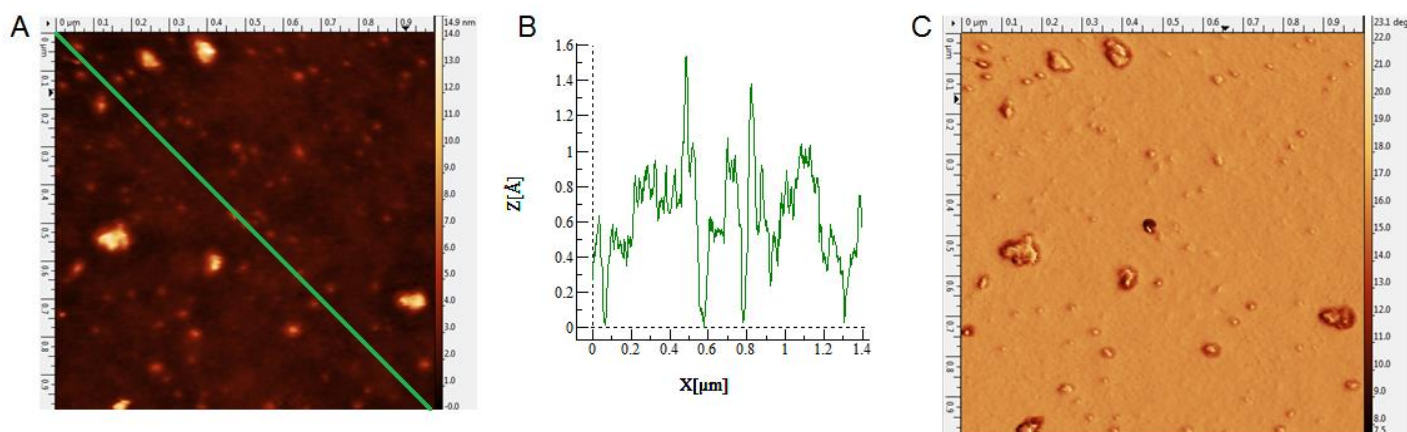


Figure 5-7: Representative angular SPR spectra measured in air at room temperature showing the shift of the reflectivity minimum from initiator SAM (■) to each polymer layer (1st PHEMA: ▼, PHEMA-b-PBMA: ▲, PHEMA-b-PBMA-b-PHEMA: ●). The solid lines represent the fits.

5.2.3.4. Characterization by AFM

To study local film morphology, atomic force microscopy (AFM) was applied for each layer characterization. Information about homogeneity, structural defects, and roughness of the membranes can be obtained by this method. AFM measurements were performed in air at room temperature. A typical height image, phase image and cross section (with X: distance and Z: height) of a film in dry state for the three samples are presented in Figure 5-8.



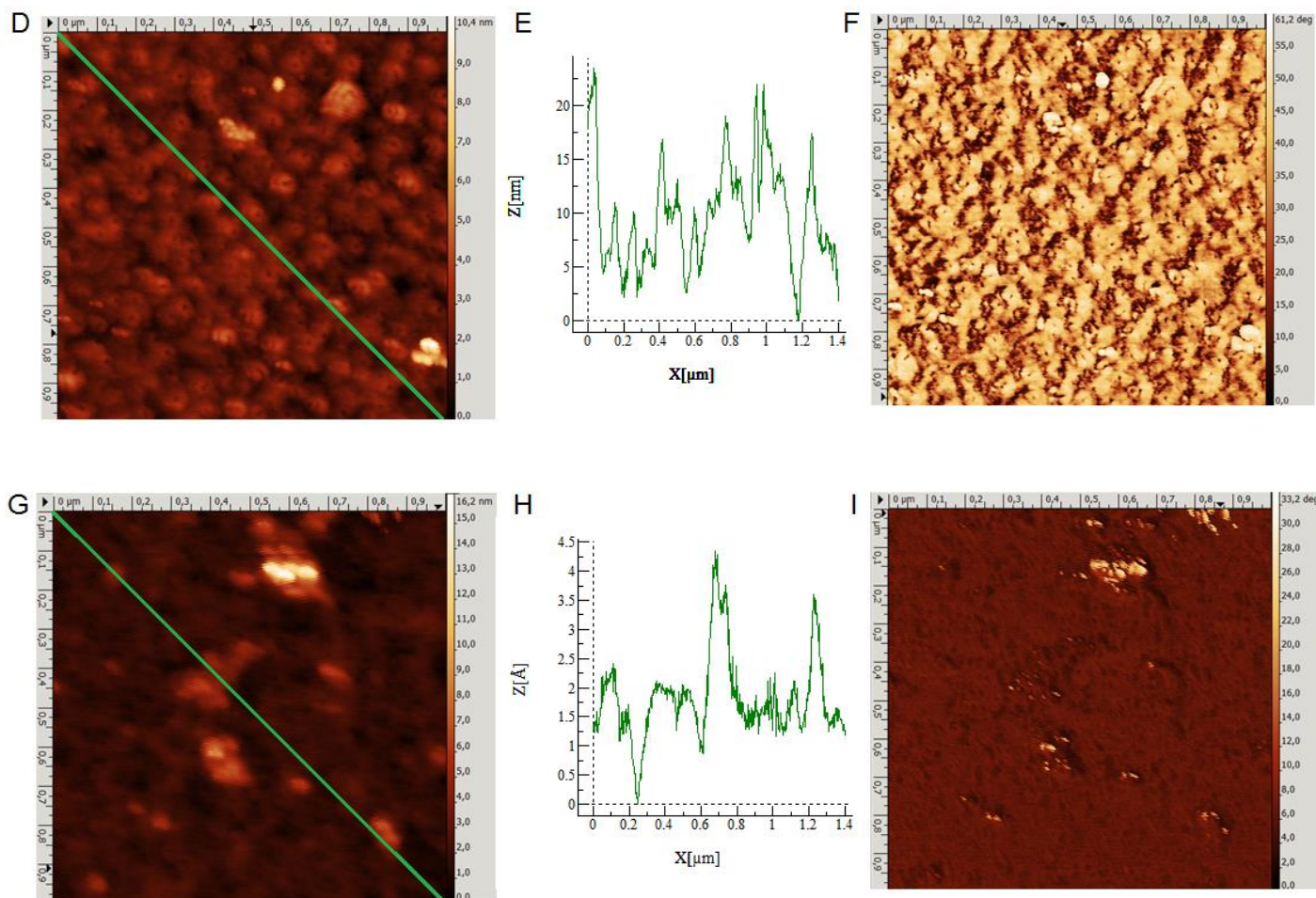


Figure 5-8: AFM images recorded in air of the PHEMA layer (A: height, C: phase), diblock (D: height, F: phase) and triblock (G: height, I: phase) copolymers on gold; and their corresponding cross sections (Figures B, E and H).

The first PHEMA film presents a smooth and homogeneous surface with minor defects, with a well-ordered structure on the micrometer scale (Figures 5-8A and 5-8C). Roughness (rootmean-square) does not exceed 0.16 nm over one square micrometer (Figure 5-8B). This proves the presence of a hydrophilic polymer monolayer. The second polymer block shows a significant change in morphology, as seen in Figures 5-8D and 5-8F. A heterogeneous and rough surface was observed, with objects of 5-20 nm in height (Figure 5-8E), showing the presence of the hydrophobic block on the surface. This is in accordance with the contact angle results described above. The third block revealed a more homogeneous layer, with fewer defects on the surface due to the hydrophilic behavior of the PHEMA layer (Figures 5-8G and 5-8I). Roughness of 0.10-0.35 nm over one square micrometer was determined. However, this roughness was higher than the one from the first PHEMA layer. ATRP reaction was initiated by the bromine group at the end of the brushes. After each block, the probability to initiate new ATRP reaction decreased due to the termination reactions that could occur between the polymer radicals. In the case of the third polymerization, some of the end groups will be not initiated because they are terminated from previous reactions.^[41] Therefore, we get less PHEMA brushes in the third layer than in the first one. This hypothesis could also explain the less pronounced decrease in contact angle for the third block than for

the first one. To conclude this part, the overall ABA polymer brushes present a homogeneous surface with minor defects, which is a key importance for electrical characterization during the functional incorporation of channel proteins.

5.2.3.5. Orientation of the brushes by PM-IRRAS

PM-IRRAS was applied to detect orientation changes of the methacrylate ester group with respect to the surface during chain growth. The ester group is directly connected to the main polymer chain, thus the results obtained in the PM-IRRAS experiment provide a qualitative indication of the chain tilt toward the gold surface. The analysis is based on the fact that for metal surfaces a PM-IRRAS signal is only observed for molecular vibrations polarized in the z -direction, *i.e.* perpendicular to the surface. This means that only the projection of the dynamic dipole moment on the z -direction gives rise to signal. One way to make use of this fact is to choose two modes, which are orthogonally polarized and to compare their relative intensity for an isotropic sample and for the adsorbed (oriented) sample. We chose the ester functionality for this purpose. The signals due to ν (C=O) at 1732 cm^{-1} and ν (C-C-O) at 1080 cm^{-1} were assigned before for similar systems.^[42, 43] The two bands are orthogonally polarized. We have performed similar analysis on a similar system before and more details can be found elsewhere.^[18]

Qualitatively one can observe that the relative intensity of the ester carbonyl ν (C=O) vibration with respect to the ν (C-C-O) is larger for the PHEMA block when compared to the isotropic polymer reference (see *Figure 5-9*). This means that the carbonyl group is oriented preferentially perpendicular to the surface. The situation then changes when growing the PBMA and the second PHEMA block. Here the relative intensity of the carbonyl band decreases, meaning that the carbonyl is now more inclined towards the surface. By applying a quantitative approach^[44] one can determine an average angle θ between the carbonyl bond and the surface normal of 38° , 51° and 54° , for PHEMA, PHEMA-*b*-PBMA and PHEMA-*b*-PBMA-*b*-PHEMA, respectively. Note that these are averages that rely on assumptions^[45] and therefore the absolute values are to be taken with care. However, the trend is clear and a similar behavior was found before.^[35] Because the methacrylate ester group is connected to the main polymer chain, its increasing tilt to the surface upon addition of polymer blocks might be also related to the change of polymer chain orientation. Therefore the PM-IRRAS measurements indicate that the polymer chain, on average, is tilted more away from the surface normal when the PBMA block is added.

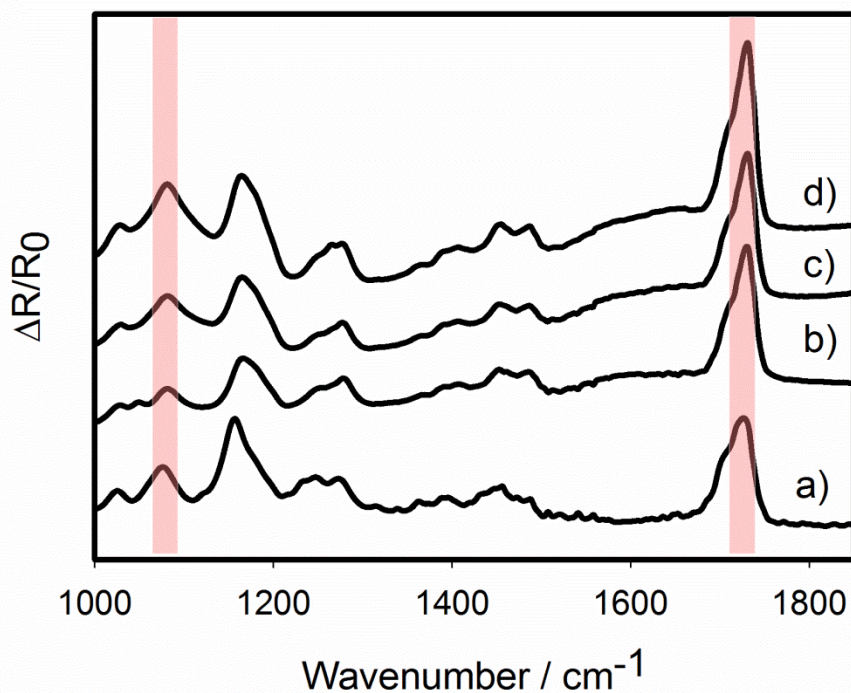


Figure 5-9: PM-IRRAS spectra on gold substrate of a) PHEMA reference polymer sample (isotropic), b) PHEMA brush, c) PHEMA-*b*-PBMA brush, d) PHEMA-*b*-PBMA-*b*-PHEMA brush. The neat gold surface was used as the reference. Spectra were scaled for clarity and the bands used for the analysis (see text) are highlighted.

5.2.4. Influence of the grafting density on the block copolymer brushes

5.2.4.1. Thickness and roughness determination by neutron scattering

To determine the potential suitable matrix for protein incorporation, experiments with variation of the packing density were performed. The grafting density was varied by mixing the initiator used for the surface-initiated ATRP with a molecule inert to ATRP reaction that can be still attached to the gold substrate. In this case, 1-dodecanethiol was used. The grafting densities were expressed as the volume percentage of the ATRP initiator in the mixture. The thickness of each layer depending on the grafting density was measured by neutron reflectivity, as it is a powerful technique to characterize ultra-thin polymers films down to the nanoscale.^[46] The experimental data of the ABA triblock copolymer at different grafting densities and their corresponding fits^[47, 48] are depicted in *Figure 5-10*. The fits for the determination of ABA thicknesses took into account the thicknesses of initiator, PHEMA and AB block copolymers measured separately by neutron reflectivity. Also, for the fits, we assumed that the layer roughnesses for each block at every grafting density were similar to the ones determined by AFM for fully packed brushes. A summary of the obtained overall membrane thicknesses for each block and different grafting densities is presented in *Table 5-3*.

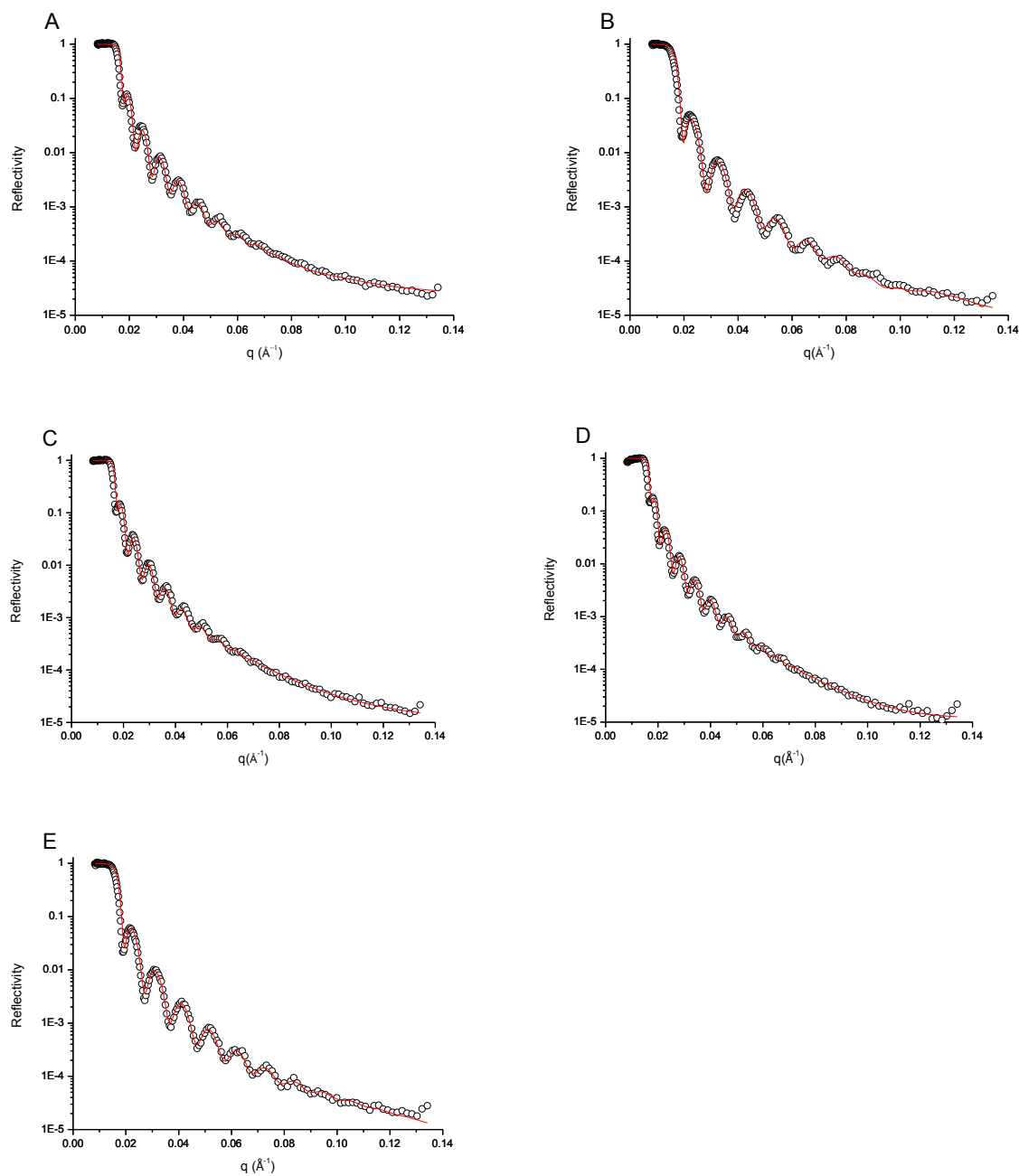


Figure 5-10: Experimental reflectivity data and their corresponding fits (red solid lines) of triblock copolymer PHEMA-*b*-PBMA-*b*-PHEMA at different grafting densities (A: 100% grafted SAM initiator, B: 90%, C: 70%, D: 50%, E: 30%).

Table 5-3: Overall membrane thicknesses on subsequent layers on gold at different grafting densities measured by neutron reflectivity.

% grafted initiator	Initiator thickness (nm)	Overall PHEMA thickness (nm)	Overall AB thickness (nm)	Overall ABA thickness (nm)
100	3.1	5.9	10.2	12.7
90	2.3	5.0	9.9	10.9
70	1.6	3.9	8.9	9.9
50	1.3	3.0	5.7	6.7
30	1.3	3.1	5.4	6.6

For fully packed brushes, the thicknesses obtained for SAM, first, second and third block copolymer were 3.1 nm, 2.8 nm, 4.3 nm and 2.5 nm respectively; in accordance with SPR results presented above. However, for all layers, a decrease in grafting density implied a decrease in brush thicknesses (*see Figure 5-11*). Therefore, we can conclude that the grafting density has an effect on the thickness of the brushes, in accordance with previous results described elsewhere.^[29, 30, 49-51] In particular, the thickness dropped markedly from 9.9 nm to 6.7 nm when the grafting density changed from 70% to 50%. This effect could be explained by the “mushroom” behavior of the brushes on the surface when a decrease of the grafting density occurred (*see Figure 5-12*). Therefore, taking into account the overall ABA thicknesses and with respect of the membrane protein dimensions, the samples at 100%, 90% and 70% will be tested as suitable matrix for the insertion of channel proteins.

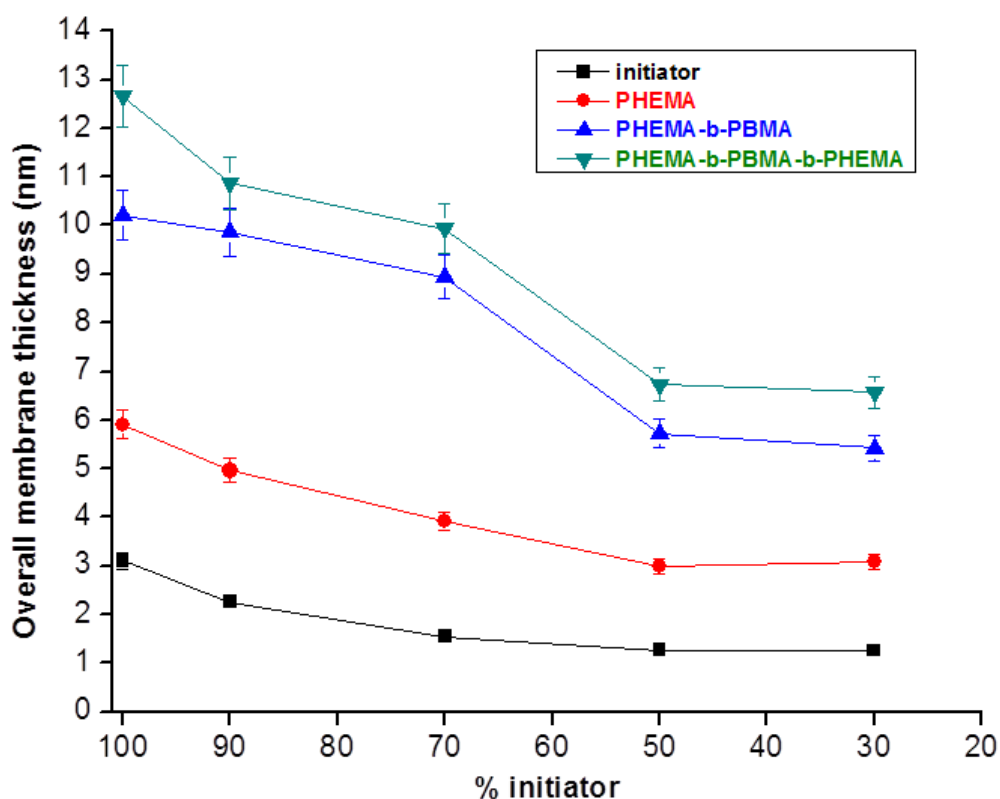


Figure 5-11: Relationship between the percentage of grafted initiator on the gold substrate and the overall thickness of the layers. A decrease in brushes thickness was observed while decreasing the grafting density.

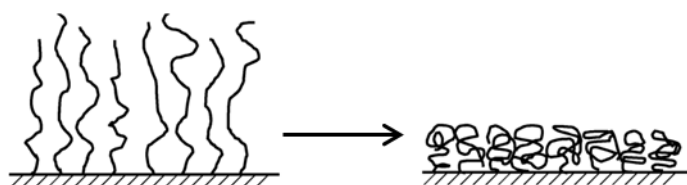


Figure 5-12: Scheme of brushes behavior while decreasing the grafting density.

5.2.4.2. Orientation of the brushes by PM-IRRAS

The samples with various grafting densities were also investigated by PM-IRRAS to evaluate the brushes orientation. Like previously, ester groups at 1730 cm^{-1} were chosen for this purpose. However, except for the fully packed brushes (see *Section 5.2.3.5*), reliable signals could not be obtained for lower grafting densities (see *Figure 5-13*). As noticed in previous *section 5.2.4.1.*, brushes thickness decreased by lower packing densities because of their mushroom behavior in dry state. In these conditions, the brushes orientation could not be determined.

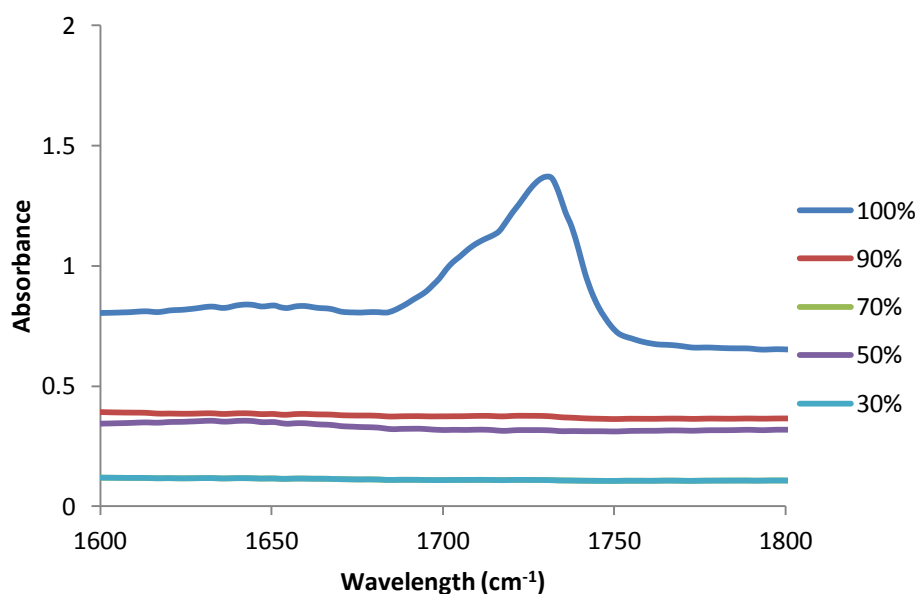


Figure 5-13: PM-IRRAS spectra on gold surfaces of ABA triblock copolymers at different grafting densities.

5.2.5. Influence of channel proteins on the block copolymer brushes

5.2.5.1. Protein insertion with the Biobeads method

First, the protein insertion experiments were tested with channel proteins Outer Membrane Protein F (OmpF) and Aquaporin Z (AqpZ). Both proteins were incubated in the triblock copolymer membranes at 100%, 90% and 70% packing density using the Biobeads method to remove the detergent used to stabilize the proteins in aqueous solution.^[52] After washing, the protein incorporation was monitored in buffer by electrical measurements.^[53] A constant voltage of 40 mV was applied until a stable current was observed. Prior incubating the membrane with channel proteins, control experiments consisting in measuring the electrical current across the polymer membrane in buffer and with Biobeads, were

performed. For a better accuracy of the results, all samples were prepared at least three times separately, and the average values of their conductance were calculated.

Bare gold substrate gave high conductance (138 ± 3 nS), and formation of the polymer membrane resulted in a strong decrease in conductance, with 5.2 ± 0.2 nS for the fully packed brushes and 17.1 ± 0.3 nS for the 90% grafted brushes (see *Figures 5-14A and 5-14B*). The same results as previously were obtained for polymer membranes in buffer with the presence of Biobeads. Also, polymer membranes incubated with Biobeads and detergent were also measured as control experiments and gave stable conductance: 5.3 ± 0.2 nS for the fully packed brushes and 15.4 ± 0.3 nS for the 90% grafted brushes (see *Figures 5-14C and 5-14D*). Systems at 70% of grafted brushes also gave an average stable conductance of 62 ± 2 nS from 1840 seconds (see *Figure 5-15 blue*). Therefore, an increase of conductance was observed with the decrease of packing density, as lower grafting density allows more space for the circulation of electric current. The 70% grafted brushes were also incubated with Biobeads and detergent, and gave a stable conductance of 61 ± 2 nS, showing that the Biobeads and detergents did not affect the membrane stability. However, for the 90% and 70% grafted brushes, artefacts and noise were noticed at the beginning of the measurements (*Figures 5-14B and 5-15 blue*), as impedance spectroscopy technique is highly sensitive to external disturbance.

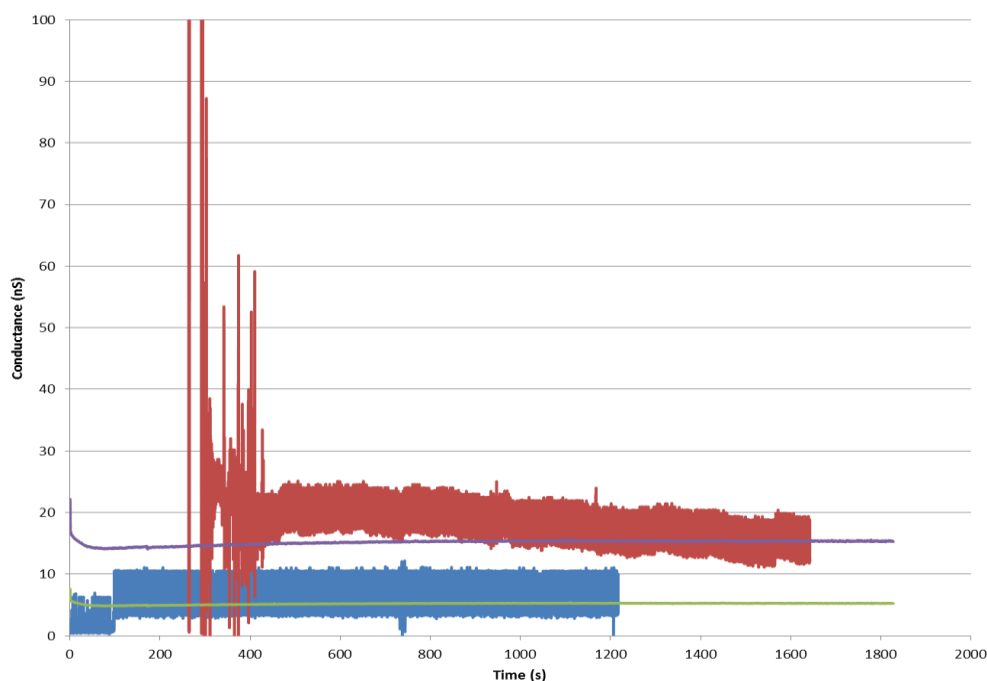


Figure 5-14: Control measurements of electrical conductance in buffer before protein insertion at 100% grafted brushes (A) and at 90% grafted brushes (B). The membranes were also incubated in detergent and Biobeads at 100% brushes (C) and at 90% of grafted brushes (D).

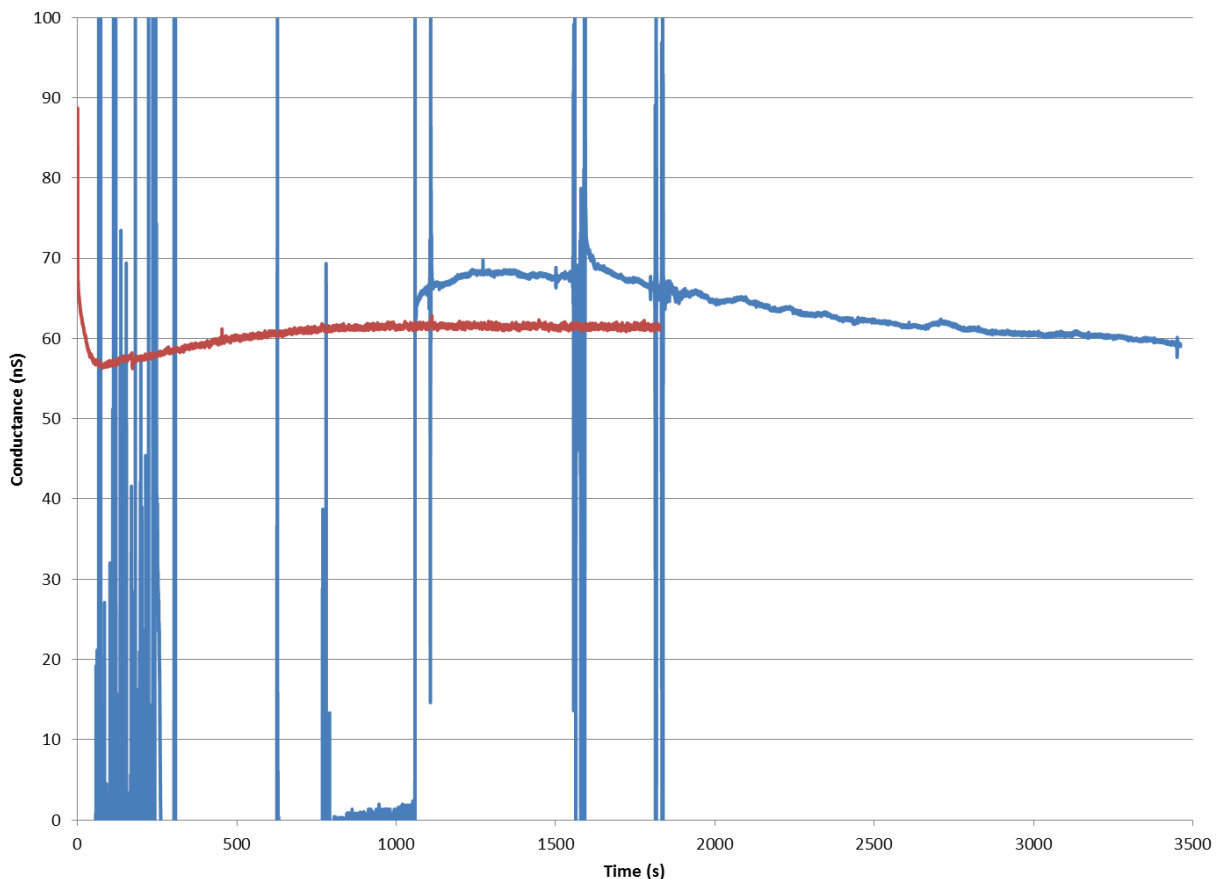


Figure 5-15: Control measurements of electrical conductance across membrane at 70% grafted brushes in buffer before protein insertion (blue spectrum). The membranes were also incubated in detergent and Biobeads (red spectrum).

Electrical impedance spectroscopy measurements after incubation of proteins for the polymer brushes at different grafting density lead to either unstable conductance or unreliable results in conductance (see *Figure 5-16*). Systems composed of 100% grafted brushes and of 70% grafted brushes gave conductance with at least 10^4 times higher than expected for conductance across artificial membranes (*Figures 5-16A, 5-16C, 5-16D and 5-16F*).^[25] Also, unstable conductance was observed for 90% grafted brushes (*Figures 5-16B and 5-16E*). It means that neither OmpF nor AqpZ was inserted into systems with fully packed brushes, 90% and 70% packing density.

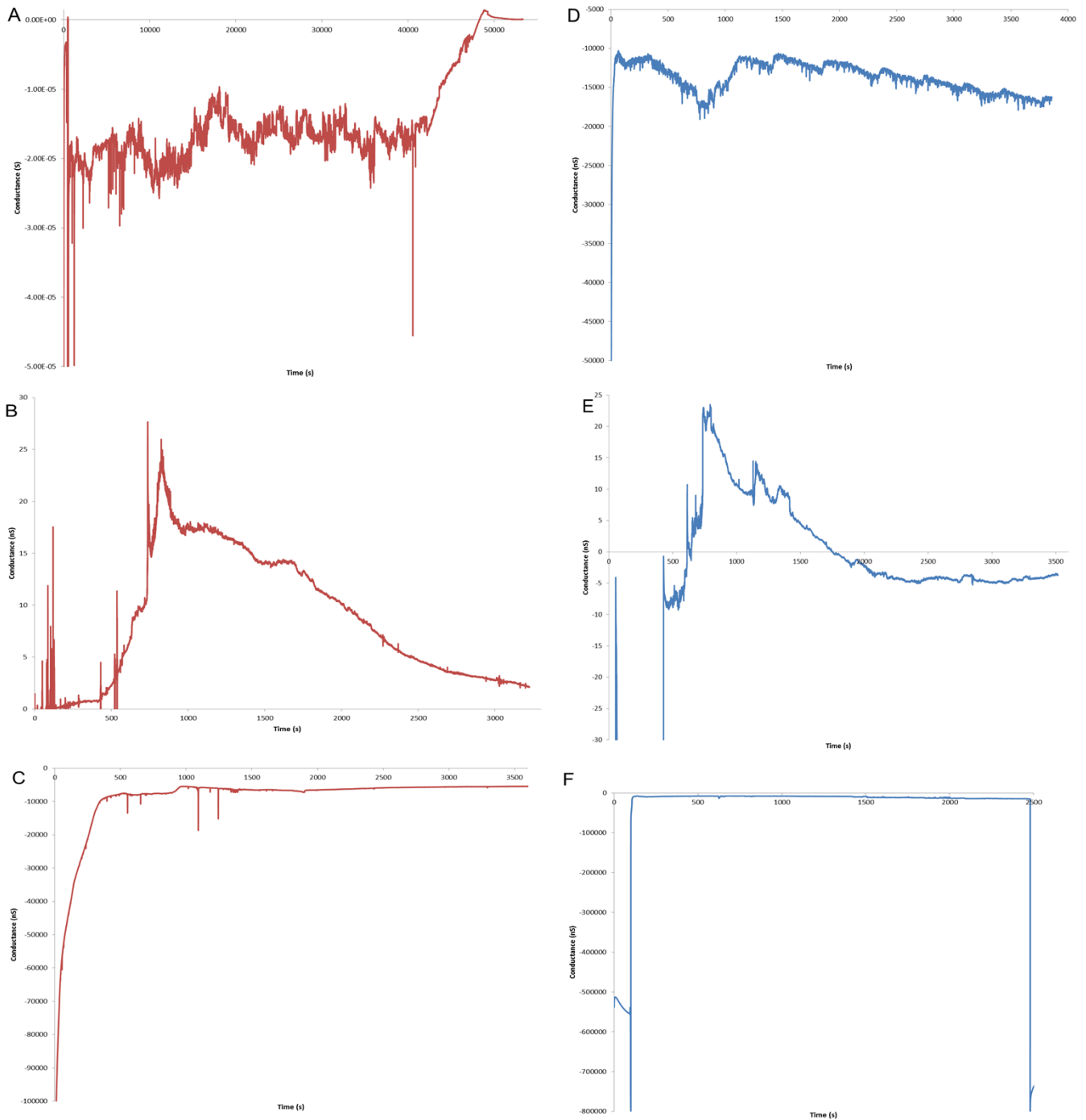


Figure 5-16: Electrical conductance measurements of polymeric membranes after incubation of OmpF (in red) and AqpZ (in blue) for 100% grafted brushes (A, D), 90% grafted brushes (B, E) and 70% grafted brushes (C, F) on gold support.

Therefore, with all these combined results, we can deduce that neither OmpF nor AqpZ was completely inserted into the artificial system. Other possible reasons, similar as for the transferred ABA1 polymer (see section 4.2.4.2. on Chapter 4) can also explain those results:

- ABA triblock copolymers were too rigid to allow the incorporation of pore channels OmpF and AqpZ.
- Impedance spectroscopy is a sensitive method to any external disturbance that can imply changes in conductance as well as noise in the signals.

- Therefore the Biobeads methods can give inaccurate results, as for the same grafting density, the same sample should be measured in-situ both for the control measurements and for the protein incubation. Also, the differences in the noise level in the measurements as well as the observed artefacts in the signals can be explained by the sensitivity of electrical impedance spectroscopy.
- Conductance measurements could be disturbed either by traces of detergent even with the presence of Biobeads, or by a too rapid detergent removal that can induce protein precipitation.

5.2.5.2. Protein insertion with alpha-hemolysin

Performing experiments with α -HL present many advantages, as it does not require any detergent for stabilization in aqueous media. Therefore, using Biobeads to remove the detergent is not needed. Also, the protein insertion with the Biobeads method requires the use of different samples for the control and insertion experiments.^[10] In our case, the protein incorporation can be measured in-situ on the same sample. Consequently, the inherent errors due to the inhomogeneity of the membrane or defects on the surface could be significantly decreased.

The incorporation of the channel protein into the polymeric membrane was evaluated by measuring the electrical conductance across the artificial membrane. We measured the current across the membrane as a function of time for a constant applied voltage of 40 mV. This voltage was applied until a stable conductance was obtained. The conductance was calculated as $G = I/V$, where I is the electrical current, and V voltage. Also, previous work already proved the successful incorporation of α -HL into a biomimetic triblock copolymer membrane.^[54] We tested the insertion for the following grafting densities: 100%, 90% and 70% (see raw data in *Figure 5-17*). For a better accuracy of the results, all samples were prepared at least three times separately, and the average values of their conductance were calculated.

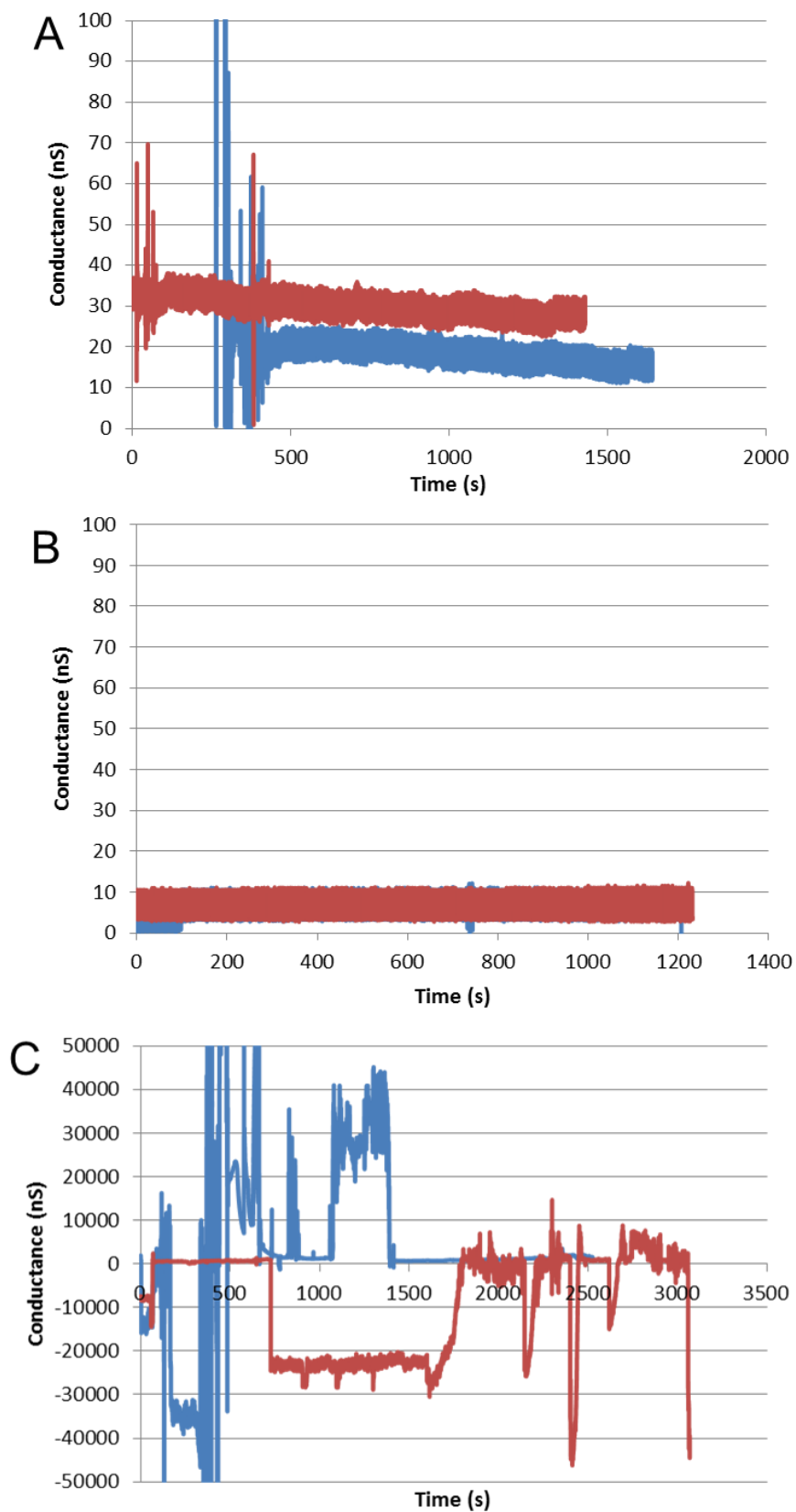


Figure 5-17: Electrical conductance measurements of polymeric membranes before insertion (in blue) and after insertion (in red) of alpha-hemolysin for 90% grafted brushes (A), 100% grafted brushes (B) and 70% grafted brushes (C) on gold support.

Bare gold substrate gave high conductance (138 ± 2 nS), and as expected, presence of the polymer membrane resulted in a strong decrease in conductance. A summary of the obtained conductance before and after the protein insertion are presented in *Table 5-4*.

Table 5-4: Conductance measured by electrochemical impedance spectroscopy at different grafting densities before and after the incorporation of membrane protein alpha-hemolysin.

% grafted initiator	Membrane conductance before insertion of α-HL (nS)	Membrane conductance after insertion of α-HL (nS)
100	5.2 ± 0.2	5.7 ± 0.2
90	17.1 ± 0.3	28.8 ± 0.3
70	62 ± 2	unstable

After adding in-situ the α -HL solution in PBS, conductance increased from 17.1 ± 0.3 nS to 28.8 ± 0.3 nS for the brushes grafted at 90% (*Figure 5-17A* and *Table 5-4*), whereas the conductance did not change and remained stable for the fully packed polymer brushes (*Figure 5-17B* and *Table 5-4*). 100% grafted polymer brushes are too densely packed to let the protein incorporation happen. Also, the tilted orientation of the 100% grafted brushes observed by PM-IRRAS could have prevented the insertion of alpha-hemolysin, even if the brushes orientation plays here a minor role. The conductance results obtained for the 90% grafted brushes is close to conductance obtained for polymer bilayers^[30, 43] and for natural lipid membranes^[55, 56] after protein insertion, which indicates a successful insertion of the protein into the amphiphilic triblock copolymer membrane. At 90% polymer grafting density, there may be enough space to allow protein insertion. Also, the slight decrease in grafting density implied a decrease in polymer thickness that could enhance the insertion. As the buffer and temperature conditions were similar to the work of Zhang *et al.*, the insertion of a single α -HL corresponds to a conductance of 0.8 nS.^[43] Due to protein insertion, a conductance increase of 11.7 nS was observed. Therefore at least 15 α -HL proteins were inserted in the “measuring window”, which covered a membrane surface area of 12.5 mm². This corresponds to approximately 1.2 α -HL per mm² of the membrane. In addition, the conductance after the α -HL insertion remained stable for at least 1400 seconds (see raw data on *Figure 5-17A*), which proved the preservation of the channel protein’s functionality in the artificial membrane. However, we were not able to obtain reliable results with the 70% grafted brushes after protein insertion, as unstable conductance was observed (*Figure 5-17C*). Most probably, the packing density is not dense enough. This system is therefore not suitable as a matrix for protein insertion.

5.3. Conclusions and outlook

In conclusion, amphiphilic triblock copolymers were synthesized from a self-assembled initiator monolayer that initiated a surface ATRP reaction. The obtained polymer brushes were fully characterized layer by layer using a broad range of surface characterization techniques in order to investigate the behavior of the polymer brushes on the surface (wettability, covalent attachment, thickness, roughness, orientation). By varying the grafting density, a potential matrix for the functional incorporation of alpha-hemolysin was found. Electrochemical impedance spectroscopy showed an increase in conductance during the insertion of α -HL in systems made of 90% grafted PHEMA-*b*-PBMA-*b*-PHEMA brushes. The stable conductance observed after incorporation proved the full preservation of protein functionality. We demonstrate a successful reconstitution of membrane proteins into a system made of amphiphilic triblock copolymers synthesized with a grafting-from approach. Further insertion experiments with alpha-hemolysin at grafting densities between 90% and 100% should be conducted in order to investigate the changes in the amount of inserted proteins, and therefore confirm the biomimetic potential of this artificial system. Upon insertion of membrane proteins these systems could allow for the preparation of mechanically and chemically robust and, potentially, air-stable biosensor devices.

5.4. References

- [1] S. J. Singer, G. L. Nicolson, *Science*, **1972**, *175*, 720-731.
- [2] V. Malinova, S. Belegriou, D. d. B. Ouboter, W. P. Meier, *Adv. Polym. Sci.*, **2010**, *224*, 113-165.
- [3] S. Belegriou, S. Menon, D. Dobrunz, W. Meier, *Soft Matter*, **2011**, *7*, 2202-2210.
- [4] X. Zhang, P. Tanner, A. Graff, C. G. Palivan, W. Meier, *J. of Polymer Science Part A : Polymer Chemistry*, **2012**, *50*, 2293-2318.
- [5] I. Tokarev, S. Minko, *Soft Matter*, **2009**, *5*, 511-524.
- [6] I. Tokarev, S. Minko, *Adv. Mater. (Weinheim, Ger.)*, **2009**, *21*, 241-247.
- [7] H. Ma, J. He, X. Liu, J. Gan, G. Jin, J. Zhou, *ACS Appl. Mater. and Interfaces*, **2010**, *2*, 3223-3230.
- [8] N. Schüwer, R. Barbey, H.-A. Klok, *Chimia*, **2011**, *65*, 276.
- [9] S. Belegriou, J. Dorn, M. Kreiter, K. Kita-Tokarczyk, E.-K. Sinner, W. Meier, *Soft Matter*, **2010**, *6*, 179-186.
- [10] J. L. Kowal, J. K. Kowal, D. Wu, H. Stahlberg, C. G. Palivan, W. Meier, *Biomaterials*, **2014**, *35*, 7286-7294.
- [11] J. Dorn, S. Belegriou, M. Kreiter, E.-K. Sinner, W. Meier, *Macromolecular Bioscience*, **2011**, *11*, 514-525.
- [12] E. Rakhmatullina, W. Meier, *Langmuir*, **2008**, *24*, 6254-6261.
- [13] M. P. Goertz, L. E. Marks, G. A. Montaña, *J. Am. Chem. Soc.*, **2012**, *6*, 1532-1540.
- [14] E. Rakhmatullina, T. Braun, T. Kaufmann, H. Spillmann, V. Malinova, W. Meier, *Macromol. Chem. Phys.*, **2007**, *208*, 1283-1293.
- [15] A. M. Boyes, Granville, M. Baum, B. Akgun, B. K. Mirous, W. J. Brittain, *Surf. Sci.*, **2004**, *570*, 1-12.
- [16] W. Huang, J.-B. Kim, G. L. Baker, M. L. Bruening, *Nanotechnology*, **2003**, *14*, 1075-1080.
- [17] J.-B. Kim, W. Huang, M. L. Bruening, G. L. Baker, *Macromolecules*, **2002**, *35*, 5410-5416.
- [18] E. Rakhmatullina, A. Manton, T. Burgi, V. Malinova, W. Meier, *J. Polym. Sci. Part A: Polym. Chem.*, **2008**, *47*, 1-13.
- [19] W. Meier, C. Nardin, M. Winterhalter, *Angew. Chem. Int. Ed.*, **2000**, *39*, 4599-4602.
- [20] M. Kumar, J. E. O. Habel, Y.-X. Shen, W. P. Meier, T. Walz, *J. Am. Chem. Soc.*, **2012**, *134*, 18631-18637.
- [21] A. Kocer, L. Tauk, P. Déjardin, *Biosensors and Bioelectronics*, **2012**, *38*, 1-10.
- [22] M. Tanaka, E. Sackmann, *Nature*, **2005**, *437*, 656-663.
- [23] B. D. Ratner, T. Horbett, A. S. Hoffmann, S. D. Hauschka, *Journal of Biomedical Materials Research*, **1975**, *9*, 407-422.
- [24] S. M. Derkaoui, A. Labbé, A. Purnama, V. Gueguen, C. Barbaud, T. Avramoglu, D. Letourneur, *Acta Biomaterialia*, **2010**, *6*, 3506-3513.

- [25] X. Zhang, W. Fu, C. Palivan, W. Meier, *Scientific reports* 3, **2013**, 2196, 1-7.
- [26] J. Pyun, T. Kowalewski, K. Matyjaszewski, *Macromol. Rapid Commun.*, **2003**, 24, 1043-1059.
- [27] S. Edmondson, V. L. Osborne, W. T. S. Huck, *Chem. Soc. Rev.*, **2004**, 33, 14-22.
- [28] W. A. Braunecker, K. Matyjaszewski, *Prog. Polym. Sci.*, **2007**, 32, 93-146.
- [29] K. N. Plunkett, X. Zhu, J. S. Moore, D. E. Leckband, *Langmuir*, **2006**, 22, 4259-4266.
- [30] T. Alonso Garcia, C. A. Gervasi, M. J. Rodriguez Presa, J. Irogoyen Otamendi, S. E. Moya, O. Azzaroni, *J. Phys. Chem. C.*, **2012**, 116, 13944-13953.
- [31] S. A. Glazier, D. J. Vanderah, A. L. Plant, H. Baylay, G. Valincius, J. J. Kasianowicz, *Langmuir*, **2000**, 16, 10428-10435.
- [32] A. Ulman, *Chem. Rev.*, **1996**, 96, 1533-1554.
- [33] S. Belegriou, V. Malinova, R. Masciadri, W. Meier, *Synth. Comm*, **2010**, 40, 3000-3007.
- [34] R. Naumann, S. M. Schiller, F. Giess, B. Grohe, K. B. Hartman, I. Kaercher, I. Koeper, J. Luebben, K. Vasilev, W. Knoll, *Langmuir*, **2003**, 19, 5435-5443.
- [35] M. Hegner, P. Wagner, G. Semenza, *Surface Sci.*, **1993**, 291, 39-46.
- [36] P. Wagner, M. Hegner, H. J. Güntherodt, G. Semenza, *Langmuir*, **1995**, 11, 3867-3875.
- [37] P. R. Griffiths, J. A. de Haseth, *Fourier Transformation Infrared Spectroscopy*, in *Chemical Analysis volume 83*, ed. Wiley and Sons, New-York, U.S.A., **1986**, p. 656.
- [38] M. C. Fauré, P. Bassereau, B. Desbat, *Eur. Phys. J. E*, **2000**, 2, 145-151.
- [39] T. Elzein, M. Brogly, J. Schulz, *Polymer*, **2003**, 44, 3649-3660.
- [40] M. Bieri, T. Bürgi, *J. Phys. Chem. B*, **2005**, 109, 22476-22485.
- [41] Ekaterina Rakhmatullina's personal comment.
- [42] N. B. Colthup, L. H. Dely, C. H. J. Wells, *Introduction to Molecular Spectroscopy*; Academic Press: New York, **1970**, 248-253.
- [43] H. W. Thompson, P. Torkington, *J. Chem. Soc.*, **1945**, 171, 640-645.
- [44] M. K. Debe, *J. Appl. Phys.*, **1984**, 55, 3354-3366.
- [45] R. Arnold, A. Terfort, C. Wöll, *Langmuir*, **2001**, 17, 4980-4989.
- [46] F. Ott, F. Cousin, A. Menelle, *J. of Alloys and Compounds*, **2004**, 382, 29-38.
- [47] L. G. Parratt, *Physical Review*, **1954**, 95, 359-369.
- [48] C. Braun, *Parratt32 or the reflectometry tool.*, **1997-1999**: HMI, Berlin.
- [49] T. Elzein, M. Brogly, J. Schultz, *Surf. And Interfaces Analysis*, **2003**, 35, 231-236.
- [50] Z. Bao, M. L. Bruening, G. L. Baker, *Macromolecules*, **2006**, 39, 5251-5258.
- [51] N. Singh, X. Cui, T. Boland, S. M. Husson, *Biomaterials*, **2007**, 28, 763-771.
- [52] T. M. Allen, A. Y. Romans, H. Kercret, J. P. Segrest, *Biochimica et Biophysica Acta*, **1980**, 601, 328-342.

- [53] C. Steinem, A. Janshoff, W. P. Ulrich, M. Sieber, H.-J. Galla, *Biochimica and Biophysica Acta*, **1996**, *1279*, 169-180.
- [54] D. Wong, T.-J. Jean, J. Schmidt, *Nanotechnology*, **2006**, *17*, 3710-3717.
- [55] W. Knoll, I. Koeper, R. Naumann, E.-K. Sinner, *Electrochim. Acta*, **2008**, *53*, 6680-6689.
- [56] D. K. Shenoy, W. R. Barger, A. Singh, R. G. Panchal, M. Misakian, V. M. Stanford, *et al.*, *Nano Lett.*, **2005**, *5*, 1181-1185.

6. General conclusions and outlook

In this thesis, the synthesis and characterization of methacrylate-based amphiphilic triblock copolymer membranes and nanoparticles in solution and on solid supports have been described. This study started with the synthesis of different polymer amphiphiles in solution, followed by the characterization of their self-assembly behavior. Further, the research shifted from solution to surfaces to take another step towards the development of solid-supported biomimetic block polymer membranes.

Reduction-sensitive amphiphilic triblock copolymers with different hydrophilic to hydrophobic ratios and chain length were synthesized using ATRP. We showed the influence of these two parameters on their macromolecular self-organization. The first polymer PHEMA₂₅-*b*-(PBMA₂₅-S-S-PBMA₂₅)-*b*-PHEMA₂₅, with a hydrophilic to hydrophobic ratio of 0.83, self-assembled into micelles of 40-60 nm in diameter. The second structure PHEMA₁₃-*b*-(PBMA₂₀-S-S-PBMA₂₀)-*b*-PHEMA₁₃, with a hydrophilic to hydrophobic ratio of 0.47, favored the formation of hard spheres nanoparticles with diameters ranging from 130 nm to 140 nm. The self-assembled nanostructures disintegrated upon reduction of the disulfide bond with the reducing agents tris (2-carboxyethyl) phosphine (TCEP) and glutathione, yielding amphiphilic diblock copolymers that self-assembled into smaller micellar-like structures. Micelles were further able to encapsulate hydrophobic dyes molecules (Nile Red, BodiPy 630/650) as model payloads. Upon reduction of the disulfide bond, fluorescence spectroscopy and fluorescence correlation spectroscopy showed a burst release of payload within the first 15 minutes, followed by a constant release over several hours. The release of hydrophobic model substances from the micelles show that these self-assembled nanostructures could serve as efficient reduction-responsive intracellular drug delivery systems.

Polymer brushes obtained through the synthesis of block copolymers on a solid support were investigated as potential biosensing systems. These brushes were synthesized via a “grafting-from” approach to give an amphiphilic triblock copolymer anchored to a gold substrate. Therefore, a hydrophilic-hydrophobic-hydrophilic artificial membrane that mimics the lipid bilayer structure can be formed. PHEMA-*b*-PBMA-*b*-PHEMA triblock copolymer brushes were synthesized by surface-initiated ATRP. By systematically varying the grafting density of the polymer brushes and measuring their corresponding thicknesses by neutron reflectivity and SPR, we found a potential matrix for the incorporation of alpha-hemolysin, a membrane protein from *Staphylococcus aureus*. Electrochemical impedance spectroscopy showed during the protein insertion an increase in conductance from 17.1 nS to 28.8 nS for systems with 90% of grafted brushes, with preservation of protein’s functionality. Here, we demonstrated a successful protein reconstitution into an artificial membrane made of amphiphilic triblock copolymers synthesized with a grafting-from approach. This system could be potentially used for further applications in biosensing or in local drug delivery systems. As a comparison, planar membranes using the “grafting-to” approach were

prepared using PHEMA₂₅-*b*-(PBMA₂₅-S-S-PBMA₂₅)-*b*-PHEMA₂₅ triblock copolymer. But the consecutive Langmuir transfers with this polymer lead to a membrane with a complex structure that did not allow any protein insertion.

Nevertheless, some improvements need to be achieved in the membranes preparation. Using copper catalysts for ATRP can be an issue for membranes that can find their potential application as biomedical devices. For both systems in solution and on solid supports, ATRP catalysts containing transition metals can be substituted by natural catalysts such as enzymes. Sigg *et al.*^[1] as well as Silva *et al.*^[2] reported the development of new ATRP catalysts based on horseradish peroxidase and hemoglobin respectively. Also, nanostructures containing a disulfide bond in the middle of the hydrophobic block implied a complex self-assembly on gold supports. The possibility of protein insertion in this complex matrix was limited, probably due to steric hindrance of the polymer chains. Therefore, the cleavage of the disulfide bond before Langmuir transfers on the surface should be performed. With a novel structure such as PHEMA-*b*-PBMA-SH, consecutive monolayer transfers could lead to less steric hindrance and more flexible amphiphilic bilayer that can be investigated as a new matrix for protein incorporation. Finally, the self-assembly studies of systems composed of diblock PHEMA-*b*-PBMA or triblock PHEMA-*b*-PBMA-*b*-PHEMA are quite recent. Consequently, their macromolecular architecture should be investigated by varying the hydrophilic to hydrophobic ratio as well as the chain length in order to study their self-assembly behavior in solution and on surfaces.

References

- [1] S. J. Sigg, F. Seidi, K. Renggli, T. B. Silva, G. Kali, N. Bruns, *Macromol. Rapid. Commun.*, **2011**, *32*, 1710-1715.
- [2] T. B. Silva, M. Spulber, M. K. Kocik, F. Seidi, H. Charan, M. Rother, S. J. Sigg, K. Renggli, G. Kali, N. Bruns, *Biomacromolecules*, **2013**, *14*, 2703-2712.

7. Experimental Part

7.1. Materials

Dimethylformamide (DMF; Sigma-Aldrich, > 99.8 %), acetone (Sigma-Aldrich, > 99.9 %), tetrahydrofuran (THF; J. T. Baker, > 99.5 %), methanol (MeOH; J. T. Baker, > 99.8 %), diethylether (DEE; J. T. Baker, > 99.0 %), acetonitrile (Sigma-Aldrich, > 99.5 %), ethanol (EtOH; Sigma-Aldrich, > 99.8 %), chloroform (CHCl₃; Sigma-Aldrich, > 99.8 %), tris (2-carboxyethyl) phosphine (TCEP; Alfa Aesar, 98 %), glutathione (Alfa Aesar, 97 %), methyl 9-maleimido-8-methoxy-2-oxo-2H-naphtho[2,3-b]pyran-3-carboxylate (ThioGlo-5; Covalent Associates Inc.), Nile Red (Sigma), BodiPy 630/650 (Invitrogen), Biobeads (SM-2 adsorbents, BioRad) and alpha-hemolysin (α -HL; Sigma-Aldrich, lyophilized powder, protein ~ 60 % by Lowry, > 10 000 units/mg) were used as received.

2-Hydroxyethyl methacrylate (HEMA; Sigma-Aldrich, 99.0 %), n-butyl methacrylate (BMA; Sigma-Aldrich, 99.0 %), N,N,N',N'',N'''-pentamethyldiethylenetriamine (PMDETA; Sigma-Aldrich, 99.0 %) were distilled before use. Copper (I) bromide (CuBr; Sigma-Aldrich, > 98.0 %) and copper (II) bromide (CuBr₂; Fluka, > 99.0 %) were dried overnight under vacuum at 80°C.

11,11'-Dithiobis [1-(2-bromo-2-methylpropionyloxy)undecane] was synthesized according to a protocol described elsewhere.^[1] Phosphate Buffered Saline (PBS) was prepared by dissolving 8.0 g of NaCl, 0.2 g of KCl, 1.44 g of Na₂HPO₄ and 0.24 g of KH₂PO₄ in 1 L H₂O, the pH was adjusted to 7.4. Outer Membrane Protein F channel (OmpF) was extracted and purified according to a procedure described previously.^[2] Aquaporin Z (AqpZ) was purified as described by Borgnia *et al.*^[3]

7.2. Self-organization behavior of methacrylate-based redox-sensitive amphiphilic triblock copolymers in solution

7.2.1. Synthesis and characterization of block copolymers

Atom Transfer Radical Polymerization (ATRP) was carried out under inert argon atmosphere and oxygen- and water-free conditions using standard Schlenk techniques.

7.2.1.1. Synthesis of the macroinitiators Br-(PBMA_m-S-S-PBMA_m)-Br

Macroinitiator 1 (B1): 11,11'-Dithiobis [1-(2-bromo-2-methylpropionyloxy)undecane] (443 mg, 0.629 mmol) and freshly distilled BMA (20 mL, 126 mmol) were dissolved in a 100 mL Schlenk flask in dry acetone (15 mL) and degassed by three freeze-evacuate-thaw cycles. CuBr (90 mg, 0.63 mmol), and CuBr₂ (14 mg, 0.063 mmol) were dissolved in dry acetone (6 mL) under argon in a 50 mL Schlenk flask and degassed as described above. PMDETA (0.144 mL, 0.692 mmol) was added under stirring for 30 min to produce a dark green solution. One-tenth of this catalyst solution was transferred with an argon-flushed syringe to the monomer/initiator solution. The reaction mixture was stirred for one hour. Quenching of the reaction was achieved by exposure to air; subsequently the mixture was diluted in non-degassed acetone. The polymer solution was passed through a basic aluminum oxide column and rinsed with acetone to remove copper impurities. The liquids (acetone, BMA) were evaporated under vacuum for 3 h. The crude product was dissolved in THF, passed through a small column of basic aluminum oxide and rinsed with THF to remove residual copper salts. The filtrate was evaporated to dryness, the crude polymer was dissolved in THF and added slowly to cold (-80 °C) MeOH (200 mL) under stirring. While MeOH was still cold, the precipitate was filtered off through a porcelain funnel with filter paper and the polymer was collected, dissolved in THF and precipitated in cold MeOH (60 mL) a second time in the same manner. The polymer was dried overnight at room temperature under high vacuum.

Macroinitiator 2 (B2): The second macroinitiator was synthesized following the above described procedure, but using different reagents amounts: 11,11'-Dithiobis [1-(2-bromo-2-methylpropionyloxy)undecane] (466 mg, 0.662 mmol), CuBr (101 mg, 0.703 mmol), CuBr₂ (18 mg, 0.08 mmol), PMDETA (0.144 mL, 0.690 mmol), with ratios for initiator : CuBr : CuBr₂ : PMDETA of 1 : 1 : 0.1 : 1.1. The reaction was performed for 30 minutes.

7.2.1.2. Synthesis of the triblock copolymers PHEMA_n-b-(PBMA_m-S-S-PBMA_m)-b-PHEMA_n

Polymer 1 (ABA1): Macroinitiator 1 Br-(PBMA_m-S-S-PBMA_m)-Br (1.32 g, 0.182 mmol) and HEMA (4.42 mL, 36.4 mmol) were dissolved in dry DMF (4.42 mL) in a 50 mL Schlenk flask and the solution was degassed by three freeze-evacuate-thaw cycles. CuBr (260 mg, 1.82 mmol) and CuBr₂ (40 mg, 0.18 mmol) were dissolved under stirring in dry DMF (44.2 mL) in a second argon-filled 50 mL Schlenk flask, and degassed as described above. Then, PMDETA (0.42 mL, 2.0 mmol) was added and stirred at room temperature for 30 min. One-tenth of this catalyst solution was added with an argon-flushed syringe to the HEMA/macroinitiator solution. The reaction mixture was stirred for two hours. Then the reaction mixture was exposed to air and directly added into water (100 mL). The precipitate was filtered off on a

paper filter as a thin film and was then washed with bidistilled water. Thereby the HEMA, the copper salts and the DMF were mostly removed. The obtained crude copolymer was dissolved in THF and further purified by filtering through a basic aluminum oxide column. After drying, the polymer was dissolved in a minimal amount of THF and was added into 100 mL of cold DEE (-20°C). A turbid mixture was obtained and centrifuged at 4000 rpm until the polymer was separated from the solvent. The final product was dried at room temperature under high vacuum overnight.

Polymer 2 (ABA2): The second polymer was synthesized following the above described procedure, but using different reagents amounts: macroinitiator 2 Br-(PBMA_m-S-S-PBMA_m)-Br (566 mg, 0.075 mmol) and HEMA (2.1 mL, 15 mmol) were dissolved in DMF (1.1 mL), CuBr (70 mg, 0.48 mmol), CuBr₂ (12 mg, 0.05 mmol), PMDETA (0.10 mL, 0.52 mmol) were dissolved under stirring in dry DMF (12.8 mL). The reaction was performed for 30 minutes.

7.2.1.3. Methods

7.2.1.3.1. Characterization of the macroinitiators

The molecular weight of the macroinitiator was determined by GPC (Viscotek GPCmax; column: PLgel 5 μ m mixed C, Varian) and ¹H NMR (Bruker DPX-400 in CDCl₃; calibration: tetramethylsilane; processing: MestReNova software). Samples were analyzed by GPC with THF as eluent (flow rate: 1 ml min⁻¹; temperature: 30 °C; detection: refractive index). Narrow poly (methyl methacrylate) standards (Agilent Technologies) were used to calculate number average molecular weight M_n and polydispersity index PDI of the macroinitiator block. The number of the butyl methacrylate repeating units (the molecular weight, respectively), was calculated as a ratio of the integral corresponding to the 4 protons of the initiator at $\delta = 2.6$ ppm to the 4 protons of the poly (butyl methacrylate) from the side chains at $\delta = 4.0$ ppm in the ¹H NMR spectrum of the block copolymer (see *figures 2, 3, 17, 18* and *tables 1 and 2* in *Chapter 3*).

7.2.1.3.2. Characterization of the triblock copolymers

The triblock copolymers were also characterized by ¹H NMR and GPC. HEMA polymerization is evidenced with the appearance of the characteristic signals belonging to the protons of the methylene groups of HEMA residues at $\delta = 3.8$ ppm and $\delta = 4.0$ ppm (see the corresponding *figures* above in *Chapter 3*). The number of the 2-hydroxyethyl methacrylate repeating units, thus the molecular weight, was calculated as a ratio of the integral corresponding to the 4 protons of the initiator at $\delta = 2.6$ ppm to

the 4 protons of the poly (2-hydroxyethyl methacrylate) from the side chains at $\delta = 3.8$ ppm in the ^1H NMR spectrum of the block copolymer (see *figures 2, 3, 17, 18* and *tables 1 and 2* in *Chapter 3*).

7.2.2. Preparation of self-assembled structures

Triblock copolymers were dissolved in 1 mL of THF. Bidistilled water was added dropwise under stirring until a THF:water ratio of 1:9 was reached. Solutions with final polymer concentration from 0.1 to 1.0 mg mL⁻¹ were prepared. The solutions were allowed to equilibrate overnight, and then extruded three times through 1.0 μm and 0.4 μm PTFE filters (Nucleopore Track-Etched membrane, Whatman). The encapsulation of small dye molecules was conducted as follows:

7.2.2.1. Nile Red and BodiPy 630/650 encapsulation into micelles

0.1 mL of a 1 mg mL⁻¹ Nile Red solution in THF, or 0.1 mL of a 72 $\mu\text{g mL}^{-1}$ BodiPy 630/650 solution in pure water were mixed to a polymer solution in THF. Bidistilled water was added dropwise under stirring until a THF:water ratio of 1:9 was reached. The mixture was allowed to equilibrate overnight. Then it was extruded first through 1.0 μm and 0.4 μm PTFE filters (Nucleopore Track-Etched membrane, Whatman). No further removal of free dye was performed.

7.2.2.2. Characterization of the self-assemblies

Transmission electron microscopy (TEM) was used to visualize the self-assembled copolymer structures. 0.1 to 1.0 mg mL⁻¹ solutions of polymer were placed on parlodium-coated copper grids (400 mesh), treated with glow discharge to make them hydrophilic. Then the grids were rinsed with water and stained (2% uranyl acetate). TEM micrographs were acquired with a Philips CM 100 instrument, operated at 80 kV. The hydrodynamic radii and size distribution of the self-assembled copolymer structures were measured at 20°C by dynamic light scattering (DLS; scattering angle: 90°) with a goniometer (ALV/CGS-8F, ALV Langen) equipped with a He:Ne linear polarized laser (JDS Uniphase, wavelength = 632.8 nm). An ALV/LSE-5004 v. 1.7.4 correlator was used to calculate the correlation function of the scattered light intensity, which was analyzed using the CONTIN algorithm. Hydrodynamic radii for DLS measurements were determined with its standard deviation as an average of 12 measurements. For static light scattering measurements (SLS), we used solutions with different polymer concentrations (from 0.1 to 1.0 mg mL⁻¹), at scattering angles from 30 to 150° with 10° angular steps. For each angle, three measurements of 100 s were performed. For DLS and SLS data processing, we used the ALV static &

dynamic fit and plot software (version 4.31 10/01). SLS data were processed according to the Zimm model and cumulant analysis.

7.2.3. Reduction of the disulfide bond

The reduction of the disulfide bond was performed with two reducing agents: TCEP and glutathione. 0.5 mL polymer solution (self-assemblies in water, concentration 0.05 mg mL^{-1}) was mixed with 0.5 mL of 35 mM reducing agent solution in pure water. After mixing, the behavior of the polymer aggregates was followed by DLS and TEM up to 24 hours. Experiments were conducted at room temperature.

7.2.4. Thiol quantification using ThioGlo-5

A 2.6 mM stock solution of ThioGlo-5 was prepared by dissolving 1.00 mg of ThioGlo-5 in 1 mL anhydrous acetonitrile. The solution was stored at 4°C and protected from light. The stock solution was diluted in bidistilled water to obtain a $9 \mu\text{M}$ ThioGlo-5 solution and the pH was adjusted to 7.4 with concentrated HCl.

0.2 mL reduced polymer solution was mixed with 1 mL of a $9 \mu\text{M}$ ThioGlo-5 solution. Free thiols were determined by fluorescence on a LS55 spectrometer (Perkin Elmer). The excitation wavelength was set at 365 nm, and the emission spectra were recorded from 450 to 700 nm. The instrument was used in scan mode, with excitation and emission slits set to 10 nm. Experiments were conducted at room temperature.

7.2.5. Fluorescence kinetics

The release of fluorescent dyes was followed at room temperature using fluorescence spectroscopy on a LS55 spectrometer (Perkin Elmer). 0.5 mL of loaded self-assembled structures were mixed in quartz cuvettes with 0.5 mL of 35 mM reducing agent solution in pure water and directly analyzed. For Nile Red and BodiPy 630/650, the excitation wavelength was set at 530 nm and 630 nm, respectively. The emission spectra were recorded from 550 to 690 nm and from 610 nm to 670 nm, respectively. The instrument was used in scan mode, with excitation and emission slits set to 10 nm for Nile Red; with excitation and emission slits set to 5 nm for BodiPy 630/650. For the release of Nile Red, spectra were recorded after 45 minutes and after 24 hours; for the release of BodiPy 630/650, every 5 minutes during the first hour, then every 2 hours over a time of 8 hours.

7.2.6. Encapsulation efficiency

The encapsulation efficiency was determined by UV-vis spectroscopy, using a Specord 210 plus spectrometer (Analytik Jena). After separating micelles from free dye by simple decantation, 1 mL of a polymer solution with encapsulated BodiPy 630/650 was measured, with a slit width of 4 nm in 1 cm quartz cuvettes (Hellma). In order to determine the concentration of the encapsulated dye in the sample, a dilution series of the dye in bidistilled water was measured in order to establish a calibration curve. The absorbance was set at 630 nm, and the spectra were recorded from 550 to 700 nm. Experiments were conducted at room temperature.

7.2.7. Fluorescence correlation spectroscopy

Fluorescence correlation spectroscopy (FCS) measurements were performed in special chambered quartz glass holders (Lab-Tek; 8-well, NUNC A/S) at an air-conditioned room (23°C) using a Zeiss LSM 510-META/ConfoCor2 laser-scanning microscope with a Helium/Neon laser (633 nm) and a 40x-water-immersion objective (Zeiss C/Apochromat 40x, NA 1.2). The pinhole was adjusted to 90 μm for the measurements. The He/Ne laser had an excitation power of $P_L = 5$ mW, and the excitation transmission at 633 nm was set to 5%. Spectra were recorded over 10 s, and the measurement was repeated 10 times. The diffusion time and the structural parameters for the free dye (BodiPy) were independently determined and fixed in the fitting procedure and used for the analysis of further dye-release measurements. The fitting parameters were processed using a single component auto-correlation function for the free BodiPy, two-component auto-correlation function for the encapsulated micelles and three-component auto-correlation function for the release of BodiPy from micelles.

7.3. Solid-supported amphiphilic block copolymer membranes using Langmuir techniques

7.3.1. Gold substrates preparation

Ultrasoother template stripped gold (TSG) surfaces were prepared according to a procedure previously described by Naumann *et al.*^[4] where 50 nm thin gold films were deposited by electrothermal evaporation (0.8-1 \AA s^{-1} ; 5×10^{-6} mbar) on clean silicon wafers (CrysTec, Germany) and glued with epoxy glue

(EPO-TEK 353ND4, USA) to clean microcrown LaSFN9 glass slides (Menzel, Germany). The glued slides were cured for 2 h at 120 °C and stored until further use.

7.3.2. Bilayer preparation using Langmuir-Blodgett/Langmuir-Schaefer transfers

PHEMA₂₅-*b*-(PBMA₂₅-S-S-PBMA₂₅)-*b*-PHEMA₂₅ (ABA1) triblock copolymer was prepared following the procedure in *section 7.2.1.2*. A CHCl₃/MeOH solution (4:1 by volume) of ABA1 (concentration 0.5 mg mL⁻¹) was used for the film spreading. First, ABA1 monolayers were transferred onto various solid supports by the Langmuir-Blodgett technique, using a KSV 5000 (KSV Instruments, Finland) Langmuir Teflon™ trough (area 1860 cm²), placed on an antivibrational table in a plastic cabinet. Prior to film spreading, one freshly cleaved TSG substrate, 3 freshly cleaned silicon wafers and one freshly cleaned Ge substrate (internal reflection element, 50 mm × 20 mm × 1 mm, treated by diamond paste polishing, ethanol, acetone and ethanol rinsing, and UV cleaning) were immersed in the subphase using a dipper. After compressing a film to the pressure of 22 mN m⁻¹, it was left for 15 min in order for the polymer chains to establish their most favorable orientation. Afterwards, a monolayer film was transferred at constant speed (0.3 mm min⁻¹) on dipper upstroke. The polymer coated slide was then used for a second monolayer transfer by the Langmuir-Schaefer technique in order to obtain the bilayer membrane. For that, the ABA1 coated slide was placed in the dipper horizontally above the floating monolayer. A compressed ABA1 film (target pressure 22 mN m⁻¹) was produced at the air-water interface. At constant dipper speed (51 mm min⁻¹), the substrate was lowered through the interface. The water was cleaned and the obtained bilayers deposited on the solid supports were stored under water in a crystallization dish for further in-situ ATR-FTIR experiments on the Ge surface, and for electrical measurements on the TSG substrate. Bilayers transferred on silicon surfaces were immediately used for membrane characterization.

7.3.3. Measurement methods of the bilayer

7.3.3.1. Characterization at the air-water interface

Monolayers measurements were investigated with a KSV 2000 Langmuir Teflon™ trough (KSV Instruments, Finland), area 420 cm², equipped with two symmetric, hydrophilic barriers (Delrin™) and a Wilhelmy plate (ashless filter paper strips; width: 10 mm; accuracy: 0.1 mN m⁻¹) to monitor the surface pressure. The trough was placed in a plastic cabinet to prevent dust contaminations. All experiments were carried out in an air-conditioned lab (20 °C). Monolayers (concentration 0.5 mg mL⁻¹) were spread drop-wise on bidistilled water surface from CHCl₃/MeOH solutions (4:1 by volume). The solvent was allowed

to evaporate for 15 min, and the monolayers were compressed at the rate of 10 mm min⁻¹. The compression was monitored together with the Brewster angle microscopy (BAM) setup (EP 3 SW system, Accurion, Göttingen, Germany).

7.3.3.2. Ellipsometry

Film thickness was determined using a spectroscopic multi-angle ellipsometer Nanofilm_ep3 (Accurion GmbH, Germany) measuring between 55° and 75°, increments of 2°. Measurements were carried out on three samples in dry state and at 20°C. The values were measured as an average of nine measurements for each sample. The refractive index of the films at all angles was fitted to 1.5.

7.3.3.3. Contact angle

All the contact angle measurements were performed applying the static sessile drop method with a fully computer-controlled instrument (DSA 10, Krüss, Germany). The measurements were carried out under constant ambient temperature (20°C) and constant drop size (3 µL). Bidistilled water was applied for the analysis. The presented results were taken as average values from at least nine different individual measurements for the monolayers, and from twelve different measurements for the bilayers. The errors were defined by the standard deviations.

7.3.3.4. Attenuated Total Reflectance Fourier Transform Infrared Spectroscopy (ATR-FTIR)

ATR-FTIR measurements were performed using an Alpha Platinum ATR single reflection diamond ATR module spectrophotometer (Bruker Optics GmbH). Spectra were recorded with 128 scans repetition for the blank gold surface and the sample, with 2 cm⁻¹ resolution.

7.3.3.5. Atomic force spectroscopy (AFM)

Tapping mode AFM was performed using PycoLE System, Molecular Imaging, and aluminum coated silicon cantilevers (k=10-350 N/m). Images were recorded at a scan speed of 1.2 lines s⁻¹, a force set point of 6.5 V, in topography and friction modes with a pixel number of 512 x 512. All the measurements were run in an air-conditioned lab (23°C).

7.3.4. Bilayer incubation with channel proteins analyzed by in-situ ATR-FTIR

To study the influence of channel proteins on ABA1 membranes, we used attenuated total reflection infrared (ATR-IR) spectroscopy. The cell was mounted on an attachment for ATR measurements within the sample compartment of a Bruker Vertex 80 V FTIR spectrometer, equipped with a narrow-band MCT detector. Spectra were recorded at room temperature with a resolution of 4 cm^{-1} by co-adding 200 scans and the whole spectrometer (optical bench and sample compartment) was under vacuum of 1 hpa. $20\mu\text{g mL}^{-1}$ of an OmpF solution in PBS was passed through the cell and over the Ge ATR crystal by means of peristaltic pump located before the cell. A constant flow rate of about 0.2 ml min^{-1} was used and the spectra were recorded every 45 seconds. Bidistilled water and PBS were flowed through the sample before and after incubation with OmpF solution. Control experiments consist in following the same procedure with bare Ge surface.

7.3.5. Incubation of bilayers with channel protein using Biobeads

Channel proteins were incubated into the bilayer membranes using the Biobeads method.^[5] Freshly transferred bilayer membranes on gold supports were immersed either in OmpF or AqpZ solutions in PBS (concentration $20\text{ }\mu\text{M}$). Biobeads were added into the protein solutions containing the immersed substrates following this rule of thumb (1 g Biobeads remove 0.07 g detergent at room temperature within 6 h),^[6] and the slides were incubated in the protein solutions overnight. After that, both protein solutions and Biobeads were removed and exchanged with fresh PBS solution. The surfaces were cleaned 3 times with PBS and stored in buffer prior to electrical measurements. Control experiments with immersing polymer membranes in PBS and detergent solutions were performed with addition of Biobeads.

7.3.6. Electrical measurements with channel proteins

Electrical measurements were performed according to a procedure previously described by Zhang *et al.*,^[7] where micro-sized gold electrodes prepared by using a standard photolithography process were used together with a PDMS liquid chamber. The gold wires were first attached to the bilayer surface with silver paint, and the samples left for 10 min to stabilize. After that, the bilayer membrane on the surface was immersed with a PBS solution in the PDMS liquid chamber and a constant voltage of 40 mV was

applied across the bilayer membrane for several minutes before measurement in order to initialize the system until stable conductance of the membrane was achieved. The current was measured by a source-meter (Keithley 2636A) at a constantly applied 40 mV. All devices were automatically controlled by a self-made LabView program.

7.4. Functionalization of gold surfaces with amphiphilic block copolymer brushes using surface-initiated ATRP

7.4.1. Preparation of initiator functionalized substrates

In order to form self-assembled monolayers (SAM) of the initiator molecules on the gold surface, freshly stripped gold substrates were immersed into a 1 mM ethanol solution of 11,11'-Dithiobis [1-(2-bromo-2-methylpropionyloxy)undecane] during 24 h at room temperature under oxygen- and water-free conditions in a glovebox. After that, the samples were washed 3 times with ethanol and dried in an argon stream. To create SAMs with lower grafting densities, 11,11'-Dithiobis [1-(2-bromo-2-methylpropionyloxy)undecane] was mixed with 1-dodecanethiol in ethanol solution, the gold substrates were immersed in those solutions following the same procedure as above.

7.4.2. Growth of polymer brushes from immobilized initiator SAMs

7.4.2.1. Synthesis of the first PHEMA block

In a dry box under inert atmosphere, water- and oxygen-free reaction conditions, HEMA (2 mL, 17 mmol) was dissolved in dry DMF (1 mL) in a Petri dish. Freshly SAMs on TSG were immersed in this solution. CuBr (592 mg, 4.13 mmol) and CuBr₂ (92 mg, 0.41 mmol) were dissolved under stirring in dry DMF (25 mL) in an argon-filled 50 mL round-bottom flask. Then, PMDETA (0.95 mL, 4.5 mmol) was added and stirred at room temperature for 30 min to allow the complex formation. One-twenty-fifth of this catalyst solution was transferred with a syringe to the HEMA solution containing immersed TSG and the reaction was carried out at room temperature for 30 min. Quenching of the reaction was achieved by injecting an ethanol/water solution of CuBr₂ and PMDETA (molar ratio 1 : 1, 0.04 M CuBr₂) in order to preserve the end functionality of the PHEMA block. The substrates were consecutively cleaned with ethanol, water, ethanol, and dried under an argon stream.

7.4.2.2. Synthesis of the second PBMA block

The same procedure as above was applied for BMA polymerization. 2.6 mL of BMA were dissolved in 1.6 mL dry DMF. The reaction was carried out for 60 minutes and quenched by addition of a CuBr₂/PMDETA solution. The substrates were cleaned with DMF, water, DMF and dried under an argon stream.

7.4.2.3. Synthesis of the third PHEMA block

The same procedure as for *section 7.4.2.1.* was applied for the polymerization of the third PHEMA block, with a 30-min reaction time, with a quenching by a CuBr₂/PMDETA solution and with the same cleaning process as previously.

7.4.3. Measurement methods of initiator SAMs and the polymer brushes

7.4.3.1. Contact angle

All the contact angle measurements were performed applying the same procedure as for *section 7.3.3.3.* The presented results were taken as average values from nine measurements.

7.4.3.2. AFM

Tapping mode AFM was performed using the same method as for *section 7.3.3.5.*, with a set point force of 7.2 V and a scan speed of 1 line/s for the images recording.

7.4.3.3. Surface Plasmon Resonance (SPR)

Surface Plasmon Resonance (SPR) is an optical method used to measure the film thickness and refractive index of a film deposited on a metal surface. The technique is based on the fact that at a certain condition, the surface plasmons are excited on a metallic film (typically gold surface) at a specific resonance frequency.^[8] Such measurements were performed using an instrument constructed with the Kretschmann configuration from RES-TEC (Germany), where, Helium-Neon laser was used as a light source ($\lambda = 632.8$ nm).^[9] In SPR, angular scan was run to determine the optical components where, the reflected

intensity is measured as a function of incident angle. Upon fitting the obtained data using Fresnel calculations with the software Winspall 3.02 (Max Planck Institute for Polymer Research, Mainz, Germany), the optical components of a deposited film can be determined.^[8] The real (ϵ') and imaginary (ϵ'') permittivity constants of the layers are presented in the following table.

Layer	Thickness (d) nm	ϵ'	ϵ''
LaSFN9 (glass)	--	3.4036	0
Au	50	-12.3	1.29
Initiator	--	1.992	0
PHEMA	--	2.286	0
PBMA	--	1.939	0
PHEMA	--	2.286	0
Nitrogen air	0	1	0

Spectra were analyzed using a seven layer model including the LaSFN9 glass, gold, initiator, each block of the triblock copolymer, and air. A refractive index of $n = 1.4$ was assumed for the initiator, $n = 1.512$ for the PHEMA and $n = 1.40$ for the PBMA.^[10] All the measurements were performed using dried samples in a nitrogen atmosphere.

7.4.3.4. X-Ray Photoelectron Spectroscopy (XPS)

The photoemission spectroscopy measurements were performed with a VG ESCALAB 210 spectrometer using monochromatic Al $K\alpha$ radiation (1486.6 eV) without breaking the vacuum. The Gaussian broadening of the spectrometer (convolution of the spectral resolution (which itself is a convolution of the analyzer resolution and the source resolution) and thermal broadening) was calibrated as 0.55 eV for the 20 V analyzer pass energy used in this thesis. Normal electron escape angle and a step size of (maximum) 0.05 eV were used. Initially, wide scan XPS spectra from 0 to 1200 eV were taken in order to specify all the species present on the sample surface. The base pressure in the chamber was around 1×10^{-7} Pa during acquisition. The binding energy scale was calibrated using a clean gold sample and positioning the Au $4f_{7/2}$ line at 84.0 eV binding energy. As all the samples were verified to be stable in UHV and under X-ray irradiation, longer integration times could be used to optimize the signal to noise ratio.

7.4.3.5. ATR-FTIR

ATR-FTIR measurements were performed using a FTIR-8400S spectrophotometer applying a Golden Gate ATR setup (Shimadzu). Spectra were recorded with 128 scans repetition for the blank gold surface and the sample, with 2 cm^{-1} resolution.

7.4.3.6. Polarization Modulation Infrared Reflection Absorption Spectroscopy (PM-IRRAS)

The sample was mounted in the complementary setup for PM-IRRAS measurements within the compartment of a Bruker PM 50 accessory, connected to an external beam port of a Bruker Tensor 27 Fourier Transform Infrared spectrometer. The detector was a photovoltaic MCT element cooled with liquid nitrogen. Polarization was modulated with a photoelastic modulator (Hinds, PEM 90) at a frequency of 50 kHz. Demodulation was performed with a lock-in amplifier (Stanford Research, SR830 DSP). All spectra were recorded with a resolution of 2 cm^{-1} . Bare cleaned gold surface served as a reference for the PM-IRRAS spectra. Reference spectra for PBMA and PHEMA were recorded using commercial non crystalline polymers. Orientation measurements were performed using the Debe method.^[11] The azimuthal factor was taken into the relative concentration factor and was further ignored.^[12] We selected vibrations from the ester functionality $\nu(\text{C}=\text{O})$ at 1732 cm^{-1} and $\nu(\text{C}-\text{C}-\text{O})$ at 1080 cm^{-1} for the analysis.^[13]

7.4.3.7. Neutron Reflectivity

Experiments were carried out in Time-of-Flight (ToF) mode at the neutron reflectometer instrument AMOR at SINQ, Paul Scherrer Institute, Villigen, Switzerland at three angles of incidence.^[14, 15] The experimentally obtained reflectivity curves were analyzed by applying a standard fitting routine using Parratt's recursive method^[16] by the corresponding software program package Parratt32.^[17] The measurements were performed with dried samples at room temperature.

7.4.4. Influence of the channel proteins on block copolymer brushes

7.4.4.1. Incubation of polymer brushes with channel protein

The incubation process of channel protein for the triblock copolymer brushes was performed in the same manner as in *section 7.3.5*.

7.4.4.2. Electrochemical Impedance Spectroscopy (EIS)

EIS measurements were performed by using the same procedure as in *section 7.3.6*.

7.5. References

- [1] S. Belegriou, V. Malinova, R. Masciadri, W. Meier, *Synth. Comm*, **2010**, *40*, 3000-3007.
- [2] A. Zabara, R. Negrini, O. Onaca-Fischer, R. Mezzenga, *Small*, **2013**, *9*, 3602-3609.
- [3] M. J. Borgnia, D. Kozono, G. Calamita, P. C. Maloney, P. Agre, *J. Mol. Biol.*, **1999**, *291*, 1169-1179.
- [4] R. Naumann, S. M. Schiller, F. Giess, B. Grohe, K. B. Hartman, I. Kaercher, I. Koeper, J. Luebben, K. Vasilev, W. Knoll, *Langmuir*, **2003**, *19*, 5435-5443.
- [5] T. M. Allen, A. Y. Romans, H. Kercret, J. P. Segrest, *Biochimica et Biophysica Acta*, **1980**, *601*, 328-342.
- [6] J.-L. Rigaud, G. Mosser, J.-J. Lacapere, A. Olofsson, D. Levy, J.-L. Ranck, *Journal of Structural Biology*, **1997**, *118*, 226-235.
- [7] X. Zhang, W. Fu, C. Palivan, W. Meier, *Scientific reports* *3*, **2013**, *2196*, 1-7.
- [8] C. K. Pandiyarajan, *The interaction of blood proteins and platelets on surface-attached poly (alkylacrylamide) networks*, PhD thesis, **2013**, University of Freiburg, Freiburg, Germany.
- [9] J. R. Sambles, G. W. Bradbery, F. Yang, *Contemp. Phys.*, **1991**, *32*, 173-183.
- [10] J. Brandrup, E. H. Immergut, *Polymer Handbook*, John Wiley & Sons, New York, **1975**.
- [11] M. K. Debe, *J. Appl. Phys.*, **1984**, *55*, 3354-3366.
- [12] R. Arnold, A. Terfort, C. Wöll, *Langmuir*, **2001**, *17*, 4980-4989.
- [13] H. W. Thompson, P. Torkington, *J. Chem. Soc.*, **1945**, *171*, 640-645.
- [14] D. Clemens, P. Gross, P. Keller, N. Schlumpf, M. Konnecke, *Physica B*, **2000**, *276*, 140-141.
- [15] <http://www.psi.ch/sinq/amor/>, accessed on November 23, **2014**.
- [16] L. G. Parratt, *Physical Review*, **1954**, *95*, 359-369.
- [17] C. Braun, *Parratt32 or the reflectometry tool.*, **1997-1999**: HMI, Berlin.

8. Curriculum Vitae and list of publications

Personal Data

Name **Smahan Toughraï**

Date and place of birth 22.08.1984 in Villeurbanne (France)

Nationality French, Moroccan

Education

11/2009 – 12/2014 **PhD** in polymer and physical chemistry, **University of Basel, Switzerland**, supervised by Prof. Dr. Wolfgang Meier and Prof. Dr. Nico Bruns.
“Functional surfaces through biomimetic block copolymer membranes”.

2002 - 2009 **Msc. Engineering** in chemistry and process engineering, **CPE-Lyon, France**, with majors in analytical chemistry and formulation.

Working Experience

11/2009 – 08/2014 **Research assistant at University of Basel (Switzerland):**

- Synthesis and characterization of redox-sensitive block copolymers in solution and on solid supports. Study of the self-assembly behavior of the polymers and their potential in the field of sensing technology and functional transmembrane protein analysis.
- Work published in peer review journals and presented at different international congresses.
- Laboratory teaching assistant in physical chemistry for bachelor students in chemistry, pharmacy, biology and nanosciences.
- Supervision of project works for bachelor and master students in chemistry and nanosciences.

02-09/2009 **Development assistant at Kolb AG (Switzerland):** development of new dispersing agents and new defoamers for waterborne pigments concentrates for paints and inks.

07/2007 – 06/2008 **Lab technician at AQura Evonik GmbH (Germany):** quality control of pharmaceutical active substances by various organic analysis, chromatography and electrophoresis.

07/2006 **Lab technician at Celliose Coatings (France):** analysis of different components of paints and varnishes (pigments, binding agent, mineral compounds) by IR-spectroscopy.

07/2005 **Visiting scientist at INSERM-Lyon** (Institut National de la Santé Et de la Recherche Médicale, Lyon) : dosing of proteins and immunological compounds, cell cultures.

07/2004 **Visiting scientist at INSERM-Lyon:** cell cultures, RNA extraction, Polymerase Chain Reaction (PCR).

Relevant Skills

Scientific and technical skills

- Synthesis of small organic molecules and polymers (ATRP).
- Self-assembly methods for amphiphilic copolymers, encapsulation techniques.
- Characterization of polymers and small organic molecules in solution: separation techniques (GPC, SEC, HPLC, GC, electrophoresis), spectroscopy (NMR, MS, FT-IR, UV-Vis, Fluorescence), particle number, size and shape analysis (light scattering, turbidity), morphology analysis (TEM, cryo-TEM).
- Surface chemistry: preparation of substrates, synthesis of amphiphilic block copolymer brushes on surfaces (grafting-from approach and Langmuir transfer techniques), channel protein insertion, characterization

techniques (AFM, SPR, ellipsometry, contact angle, ATR-FTIR, XPS, neutron reflectometry, PM-IRRAS, surface tension, Brewster Angle Microscopy, electrochemical impedance spectroscopy).

- Quantitative chemical analysis: elemental analysis, Karl-Fischer, loss of drying.
- Formulation chemistry and experimental design.
- Data analysis and statistics.
- Scientific writing of peer review publications.
- Scientific writing of progress reports for the Swiss National Foundation (SNF).
- Scientific writing of research proposals for the Commission for Technology and Innovation (CTI).

Social and organizational skills

- Establishing scientific collaborations in Europe for various research projects.
- Conference organization: Polycoll (Basel, 2013), Swiss Soft Days (Basel, 2011 and 2014).
- Communication, adaptation, self-organization and team work skills.
- Autonomy, initiative taking, project management, will of continuous learning.

Teaching

- Supervision of bachelor and master students in various project works and laboratory classes.
- Lectures in chemistry and engineering for high schools classes.
- Private tuition in maths, physics and chemistry for high school level.
- Training collaborators on instruments and software.

Languages

- French und Moroccan Arabic Mother tongue.
- German and English Fluent (C1).
- Italian and Spanish Basic (A2).

IT skills

- Good knowledge of MS Office, Origin, ChemDraw, MestReNova, NemrodW, Scifinder, Matlab, Maple and various instrument softwares.
- Notions of programming (Java, C language).

Personal Interests

Theater (member of “La Compagnie du Lys” troupe since 2010), travelling, learning languages, sport (biking, running and swimming), listening to music, reading books, watching movies, crosswords/arrow puzzles.

Participation to different universities events: Science Slam Basel (2011-2013), Year of Chemistry (2011), 550-year anniversary of University of Basel (2010), Junior Entreprises CPE-Lyon (2008).

Honor and Awards

- | | |
|-----------|---|
| 2012 | Poster Prize Givaudan AG – Swiss Soft Days VIII, Geneva, Switzerland. |
| 2010-2011 | WIN Program: Women into industry. A combined program between University of Basel and Novartis AG for promoting young women to high responsibilities positions. |
| 2006 | Dow Chemicals Prize for the best company creation project, CPE Lyon, France. |

List of publications

S. Toughrai, V. Malinova, R. Masciadri, S. Menon, P. Tanner, C. G. Palivan, N. Bruns, W. Meier, “Reduction-Sensitive Amphiphilic Triblock Copolymers Self-Assemble into Stimuli-Responsive Micelles for Drug Delivery”, *Macromolecular Bioscience*, **2014**, DOI: 10.1002/mabi.201400400.

S. Toughrai, C. K. Pandiyarajan, J.-L. Perin, P. Korelis, T. Geue, T. Bürgi, N. Bruns, W. Meier, “Insertion of Natural Channel Protein into a Solid-Supported Artificial Membrane made of Grafted-Amphiphilic Triblock Copolymers”, *in preparation*.

M. G. Nussbaumer, M. Rother, F. Itel, S. Toughraï, K. Renggli, M. Delcea, W. Meier, N. Bruns, "Polymer-Protein Hybrid Materials", *in preparation*.

Oral presentations

S. Toughraï, J.L. Perin, C.K. Pandiyarajan, T. Bürgi, T. Geue, N. Bruns, W. Meier, "Functionalized surfaces through biomimetic block copolymer membranes"

- *Swiss Chemical Society Fall Meeting*, Zürich, Switzerland, September 13, 2012.
- *4th EuChemS*, Prague, Czech Republic, August 26-30, 2012.
- *NRP 62 nanocontainers meeting*, Fribourg, Switzerland, August 22, 2011.
- *NRP 62 Kick-off meeting*, Murten, Switzerland, April 22, 2010.

Poster presentations

S. Toughraï, J.-L. Perin, H. Ghosh, T. Bürgi, P. Korelis, T. Geue, N. Bruns, W. Meier, "Immobilization of Biomimetic Block Copolymer Membranes on Solid Supports"

- *Swiss Chemical Society Fall Meeting*, Zürich, Switzerland, September 11, 2014.
- *Swiss Soft Days XIV*, Basel, Switzerland, June 06, 2014.

S. Toughraï, H. Ghosh, T. Bürgi, N. Bruns, W. Meier, "Functional surfaces through biomimetic block copolymer membranes"

- *Swiss Chemical Society Fall Meeting*, Lausanne, Switzerland, September 06, 2013.
- *Swiss Soft Days XI*, Fribourg, Switzerland, June 04, 2013.

S. Toughraï, V. Malinova, R. Masciadri, S. Menon, P. Tanner, C. G. Palivan, N. Bruns, W. Meier, "Synthesis and Self-assembly of Methacrylate-based Amphiphilic, Redox-Sensitive Block Copolymers"

- *PolyColl*, Basel, Switzerland, June 07, 2013.
- *Swiss Soft Days VIII*, Geneva, Switzerland, June 01, 2012: **Poster Prize Givaudan AG**.

S. Toughraï, N. Bruns, W. Meier, "Biomimetic Block Copolymer Membranes for Functionalized Surfaces"

- *Swiss Chemical Society Meeting*, Lausanne, Switzerland, September 09, 2011.
- *EPF 2011 – European Polymer Congress*, Granada, Spain, June 26 - July 1, 2011.

S. Toughraï, N. Bruns, W. Meier, "Solid-Supported Biomimetic Block Copolymer Membranes"

- *1st P2M Networking Conference- Precision Polymer Materials (European Science Foundation)*, Obernai, France, December 11-14, 2011.
- *Swiss Soft Days V*, Basel, Switzerland, June 08, 2011.
- *Swiss Soft Days IV*, Fribourg, Switzerland, October 20, 2010.
- *3rd International NanoBio Conference, ETH Zürich*, Switzerland, August 24-28, 2010.

References

Prof. Dr. Wolfgang Meier

✉ wolfgang.meier@unibas.ch

☎ +41 (0) 61 267 38 02

Department of Chemistry

University of Basel

Klingelbergstrasse 80

CH-4056 Basel, Switzerland

Prof. Dr. Nico Bruns

✉ nico.bruns@unifr.ch

☎ +41 (0) 26 300 94 25

Adolphe Merkle Institute

University of Fribourg

Chemin des Verdiers 4

CH-1700 Fribourg, Switzerland

